Studies on Electric and Magnetic Properties of Cobalt Ferrite and its Modified Systems

A thesis submitted in partial fulfillment
of the requirements for the degree of

Doctor of philosophy

in

Department of Physics and Astronomy

by

Ranjit Kumar Panda

Under the supervision of

Dr. Dhrubananda Behera

National Institute of Technology, Rourkela
Rourkela-769008, Odisha
India
August-2015

It’s my fortune to have my parents from the land of God-Deva Bhoomi

Department of Physics and Astronomy
National Institute of Technology Rourkela
Rourkela-769 008, Orissa, India

This is to certify that thesis entitled **“Studies on electric and magnetic properties of cobalt ferrite and its modified systems”** submitted by Mr. Ranjit Kumar Panda to the Department of Physics and Astronomy, National Institute of Technology, Rourkela for the award of doctor of philosophy is a bonafide record of research work carried out by him under my supervision. The contents embodied in this thesis have not been submitted to any Institute for the award of any degree.

Date (D. Behera)

Rourkela

ACKNOWLEDGEMENT

I avail this opportunity to extend my hearty indebtedness to my supervisor **Prof. D. Behera** for his invaluable guidance, untiring efforts and meticulous attention at all stages during my research work.

I am grateful to **Prof. Sunil Kumar Sarangi**, Director, National Institute of Technology, Rourkela who has been a constant source of inspiration for me. I express my sincere thanks to **Prof. D.K. Bisoyi,** Head of the Department of Physics and Astronomy, NIT Rourkela for providing me the necessary facilities in the department.

I thank to all my D.Sc members **Prof. S.C. Mishra, Prof. B.B. Nayak and Prof. P.N. Viswakarma** for their suggestions and keen interest on my work.

I would like to express my gratitude to all the faculty members of the department for their suggestions. I also thank staffs of the Department of Physics and Astronomy, for their cooperation.

My sincere thanks to Subrat Bhai, Naresh, Senthil, Satya, Krutika, Bibek, Achyuta, Sourav, Sweta, Jyoti, Jayarao, Ranjit, Tapobrata, Chandra, Laxman, Binu, Somu, Subhajit, Hari, Bamadev, Prakash, Surya, Kailash, Nila, Ram, Satya, Vineesh, Priyambada, Kadambini, Sridevi, Arpana, Mousumi, Jashashree, and Rakesh Bhai for being so supportive and helpful in every possible way.

(Ranjit Kumar Panda)

Abstract

Electric and magnetic properties of bulk and nano cobalt ferrite and modified with Bi^{3+}, Cr^{3+} and K_2CrO_4 in nano level have been investigated. Bulk cobalt ferrite ($CoFe_2O_4$) system was prepared by conventional solid state route and nano $CoFe_2O_4$ system was prepared by auto combustion method of the chemical route. The contribution of microstructures (intrinsic grain and extrinsic grain boundary, sample surface-electrode contact) to the conduction mechanism was investigated by complex impedance spectroscopic analysis. Both the intrinsic and extrinsic conductions were observed in the bulk cobalt ferrite system whereas intrinsic grain conduction is found absent in its nano system. It is observed that though the room temperature resistivity of the nano system is higher than bulk one but the rate of decrease in resistance with elevated temperature is higher in former case. Perhaps, this may be the reason behind the early surface-conduction in nano system. The high resistance of nano system at room temperature (RT) is due to the increase in density of high resistive grain boundaries. The high dielectric loss in nano system may be due to the early conduction of charge carriers in high resistive regions in comparison to bulk system. It is observed that the saturation magnetization of bulk cobalt ferrite was found to be higher than nano system. However, coercivity is higher in nano-cobalt ferrite which can be related to the surface spin effects.

Bismuth substituted nano cobalt ferrite ($CoFe_{2-x}Bi_xO_4$, x= 0, 0.05, 0.1, 0.15) samples were prepared by auto combustion technique. The single phase XRD pattern confirmed the successful substitution of the larger cation. Surface morphology from FESEM image indicated the control average particle growth (50 nm – 160 nm) as an effect of bismuth substitution. The increased particle size has effectively modified the electrical properties of the system in three major ways: (a) increase in resistivity, (b) evolution of grain relaxation and (c) reduction in dielectric loss and surface conduction. Additionally, magnetic behavior is also affected due to control particle growth. Magnetic hysteresis study at room temperature confirmed the rise in saturation magnetization (M_S = 74.5 to 86.5 emu/g.) and reduction in coercivity (H_C = 1633 to 1524 Oe).

The samples of $CoFe_{2-x}Cr_xO4$ (x = 0, 0.15, 0.3) series were prepared by auto combustion route. X-ray diffraction technique was used to confirm the phase formation and structure analysis. The surface morphology of samples was imaged by the field emission scanning electron microscope. The average particle size was found to be ~55, ~43 and ~35 nm for x= 0, 0.15, 0.3 respectively. The substitution of Cr^{3+} in the parent systems caused a significant reduction in particle size. The samples were subjected to magnetic characterization and also studied with Mossbauer spectroscopy at room temperature. Analysis of extracted parameters from Mossbauer spectroscopy concluded that Cr^{3+} has replaced the Fe^{3+} at B-site (octahedral). The decrease in magnetization at B-site was responsible for the observed reduced saturation magnetization and coercivity. The Cole-Cole plots of impedance showed the growth of semicircle describing the effect of grain boundary and the suppression of semicircle describing the electrode-sample surface conduction effect. The increasing radius of Cole-Cole semicircles indicated the enhancement of the material resistivity which was also confirmed by the dc resistivity measurement. All these results were explained on the basis of occupancy of Cr^{3+} at B-site, surface anisotropy potential and reduced particle size. The parent cobalt ferrite system further modified with K_2CrO_4 in which chromium exists in its highest oxidation state (6^+). The samples were synthesized by the auto-combustion method with different dopant concentration. The modified systems contain all the characteristic XRD peaks of cobalt ferrite and no peaks related to secondary phases are observed. The effect of dopant further reduces the particle size and at its higher percentage, the particle size is reduced to ~15 nm. An interesting result of metallic to semiconducting transition behavior is observed in the modified cobalt ferrite system of higher dopant concentration. From the impedance spectroscopic analysis it is revealed that grain conduction was active in the temperature belt of metallic region. The variations of magnetic moment along with coercivity with addition of K_2CrO_4 were explained on the basis of particle size.

CONTENTS

CHAPTER 1

INTRODUCTION AND LITERATURE REVIEW

CHAPTER 2

EXPERIMENTAL TECHNIQUES

CHAPTER 3

ELECTRIC AND MAGNETIC INVESTIGATIONS ON BULK COBALT FERRITE

CHAPTER 4

INVESTIGATIONS ON CONDUCTION MECHANISM AND MAGNETIC PROPERTIES OF COBALT FERRITE NANOPARTICLES

CHAPTER 5

ELECTRIC AND MAGNETIC PROPERTIES OF Bi^{3+} SUBSTITUTED COBALT FERRITE NANOPARTICLES

CHAPTER 6

ELECTRIC AND MAGNETIC PROPERTIES OF Cr^{3+} SUBSTITUTED COBALT FERRITE NANOPARTICLES

List of figures

List of tables

List of Abbreviations and Notations

CFO	Cobalt ferrite
SEM	Scanning electron microscopy
FESEM	Field emission scanning electron microscopy
XRD	X-ray diffraction
H	Applied field
H_C	Coercivity
M	Magnetization
M_r	Remnant magnetization
M_S	Saturation magnetization
Z	Impedance
Z'	Real impedance
Z''	Imaginary impedance
M	Electric modulus
M'	Real modulus
M''	Imaginary modulus
τ	Relaxation time
ε	Dielectric constant
σ	Electrical conductivity
ρ	Electrical resistivity
$\tan \delta$	dielectric loss
T	Temperature
eV	electron volt

K	Kelvin
g	gram
Hz	Hertz
nm	nanometer
Å	angstrom
d	Inter planner spacing
ɵ	Bragg angle

CHAPTER 1

Introduction and literature review

This chapter describes spinel ferrite materials and important aspects of cobalt ferrite which is selected for the present investigation. It explains the basic structure of the spinel ferrites and its relation to the electric and magnetic properties and briefly discussed recent related literatures about cobalt ferrite. At the end of this chapter, motivation and objective of the present thesis is discussed.

1.1. Introduction

Transition metal oxides have a rare combination of electric and magnetic properties among which ferrites show comparably good properties. Ferrite materials are insulating/semiconductor metal oxides that exhibit moderate saturation magnetization, high coercivity, high electrical resistance, low eddy current and dielectric loss with moderate permittivity [1-5]. No other material has such a wide range of properties and therefore these materials are exploited for vast applications in various fields like transducers, activators, recording media, permanent magnets, phase shifters, electrode material for Lithium ion batteries, solid oxygen fuel cells and computer technology [6-9]. In addition with, the ferrite nanoparticles are used in magnetic fluids, humidity and gas sensors, drug delivery etc. [10,11]. In 12th century, the Chinese have used Iron oxide Fe_3O_4 (lodestone) as compass for navigation but the studies on electric and magnetic properties of ferrites started in 1930. The ferrites exhibit dielectric properties and do not conduct electricity easily therefore ferrites became an alternative for the metal magnets like iron, nickel which conduct electricity readily [12]. Therefore, the processing of these materials is important to modify its properties as per the desired applications.

Ferrites are classified into three types depending on the structure namely spinel, garnets and hexagonal ferrites. Garnets have the general formula $M^{3+}Fe_5O_{12}$ where M = Y, Sm, Eu, Gd, Tb etc. and have applications in microwave systems [13]. The hexagonal ferrites represented by the formula $Me^{2+}Fe_{12}O_{19}$ where M = Ba, Sr, Ca, …. are important in permanent applications [14]. The spinel ferrites are represented by the general formula MFe_2O_4 where M is the divalent cation M = Co, Mn, Zn, Ni, Cd…. etc [15]. This research work deals with the spinel ferrites and we shall discuss the ferrite family in detail.

1.2. Spinel structure

The spinel ferrites are a large group of oxides which possess the structure of the natural spinel $MgAl_2O_4$. Many of the commercially important spinels are synthetic, one of the most important and probably the oldest magnetic material with practical applications, magnetite Fe_3O_4 ($FeFe_2O_4$), is a natural oxide. Their great abundance points to a very stable crystal structure. Spinels are predominately Ionics. The particular sites occupied by cations are however, influenced by several other factors, including covalent bonding effects and crystal field stabilization energies of the transition metal cations [13-15].

The ideal spinel structure is formed by a cubic closed packed array of O atoms, in which one-eighth of the tetrahedral and one-half of the octahedral interstitial sites are occupied by cations. The tetrahedral coordinated sites and octahedral coordinated sites are referred to as the A and B sites respectively. The unit cell contains eight formula units AB_2O_3, with eight A sites, 16 B sites and 32 Oxygen. It can be described by taking an A site as the origin of the unit cell. It is convenient to drive the unit cell into eight cubes of edge a/2 to show the arrangement of the A and B sites as shown in figure 1.1. The space group is Fd3m. The Oxygen atom has fourfold coordination, formed by three B cations and one A cations as shown in the figure 1.2 [13,15-17].

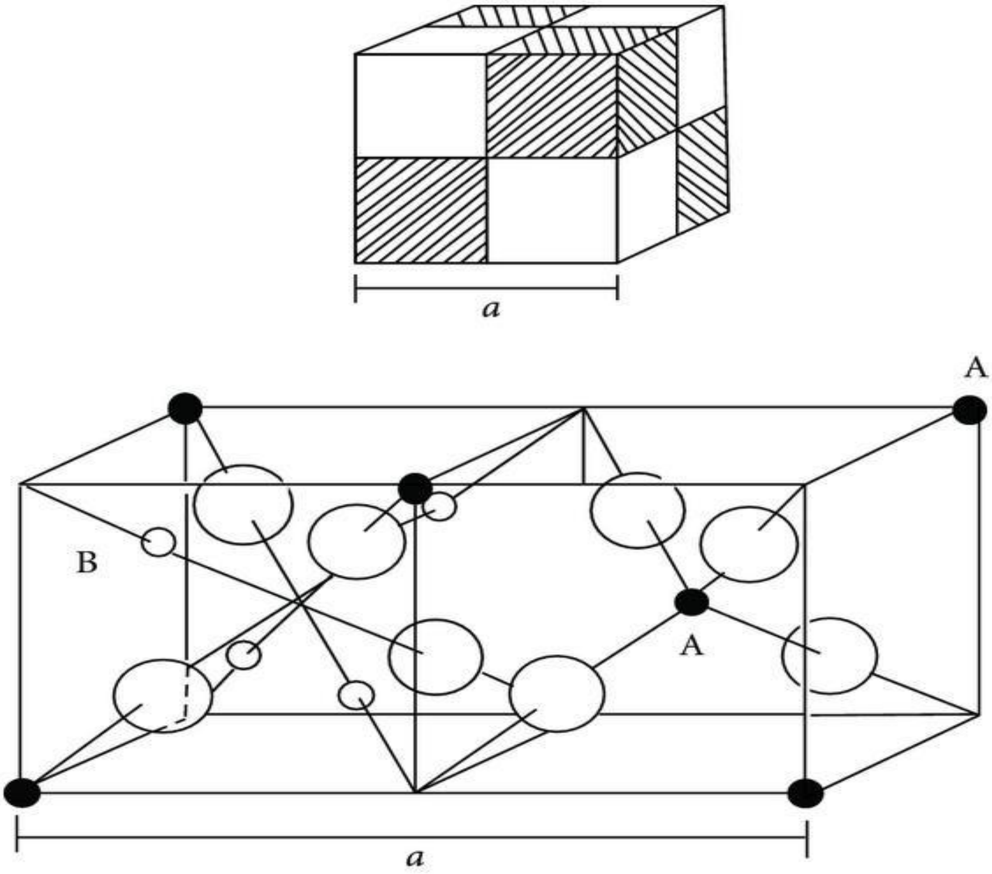

Fig1.1. The spinel structure. The unit cell divided into octants; tetrahedral cations A and octahedral cations B and O atoms are shown in two octants [13].

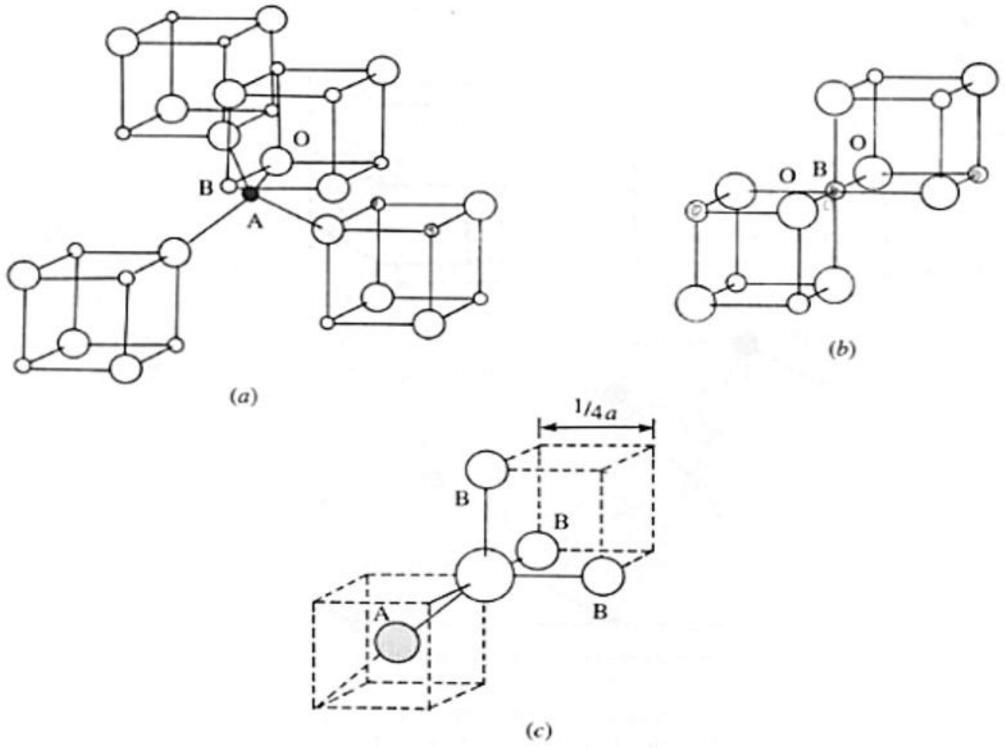

Fig1.2. Nearest neighbors of (a) a tetrahedral site (b) an octahedral site (c) an anion site [13]

The O atoms in the spinel structure are not generally located at the exact position of the sub-lattice. Their details position is determined by a parameter u, which reflects adjustment of the structure to accommodate differences in the radius ratio of the cations in the tetrahedral and octahedral sites. The u parameter is a value of 0.375 for an ideal close packed arrangement of O atoms, taking as a unit cell. The ideal situation is almost never realized, and the u value of the vast majority of the known spinels, ranges between 0.375 and 0.385. Interatomic distances are given as a function of the unit cell parameter a and the u parameter in table 1.1 [13-15, 18, 19].

The average radii of the cations affect primarily the cell parameter a, while the ratio between the tetrahedral and octahedral cation radii determines mainly the u value. If the lattice parameter is taken as a weighted average of the projections of the octahedral and tetrahedral bond lengths in the unit cell, the lattice parameter can be expressed.

$$a = \frac{8(Tet\ bond)}{3\sqrt{3}} + \frac{8(oct\ bond)}{3} \qquad 1.1$$

This expression accounts for 96.7 % of the variation in the lattice parameter of 149 spinel oxides [13].

Table 1.1. Interatomic distances and site radii in spinels AB_2O_4 as a function of unit cell edge 'a' and deformation factor u.

tetra-tetra separation A-A	$a\sqrt{\frac{3}{4}}$
tetra-octa separation A-B	$a\sqrt{\frac{11}{8}}$
octa-octa separation B-B	$a\sqrt{\frac{2}{4}}$
tetra- O separation A-O	$a\sqrt{3(u-0.25)}$
Octa- O separation B-O	$a\left[3u^2-2.75u+\frac{43}{64}\right]^{1/2}$
tetrahedral radius	$a\sqrt{3(u-0.25)}-R_O$
octahedral radius	$a\left[3u^2-2.75u+\frac{43}{64}\right]^{1/2}-R_O$

1.3. Physical properties

Physical properties of the spinel ferrites not only depend on the kinds of cation present on the lattice but also their distribution over the crystal sites. So it is important to know the factors influence the site occupancy. Understanding and predicting the cation distribution in spinels have been among the more interesting and persistent problem in crystal chemistry. According to the crystal field theory the charge density of the d orbitals shown in figure 1.3 interacts with the charge distribution of the environment in which the transition ion placed. The five d orbitals d_{xy}, d_{yz}, d_{zx}, d_{z^2} and $d_{x^2-y^2}$ split according to the symmetry of the electrostatic field produced by the anions of the particular lattice site. The physical basis for the splitting of 'd' orbitals is the electrostatic repulsion between the d electrons and the electrons of the orbitals of the surrounding anions [13-15].

The energy level of the d orbital splits into two groups in an octahedral field. The lower triplet formed by the d_{xy}, d_{yz}, and d_{zx} orbitals, and a higher doublet with the d_{z^2} and $d_{x^2-y^2}$ shown in figure 1.5. The energy of the doublet is increased as these orbitals points directly to the anions while the triplet energy decreases, because the orbitals point to regions of low electron density. The energy difference between the triplet and the doublet is given as Δ. In case of tetrahedral sites the splitting is reversed so the doublet has the lower energy than the triplet. The energy difference in tetrahedral coordinated cations is a fraction (4/9) of that for the octahedral coordination [13-15].

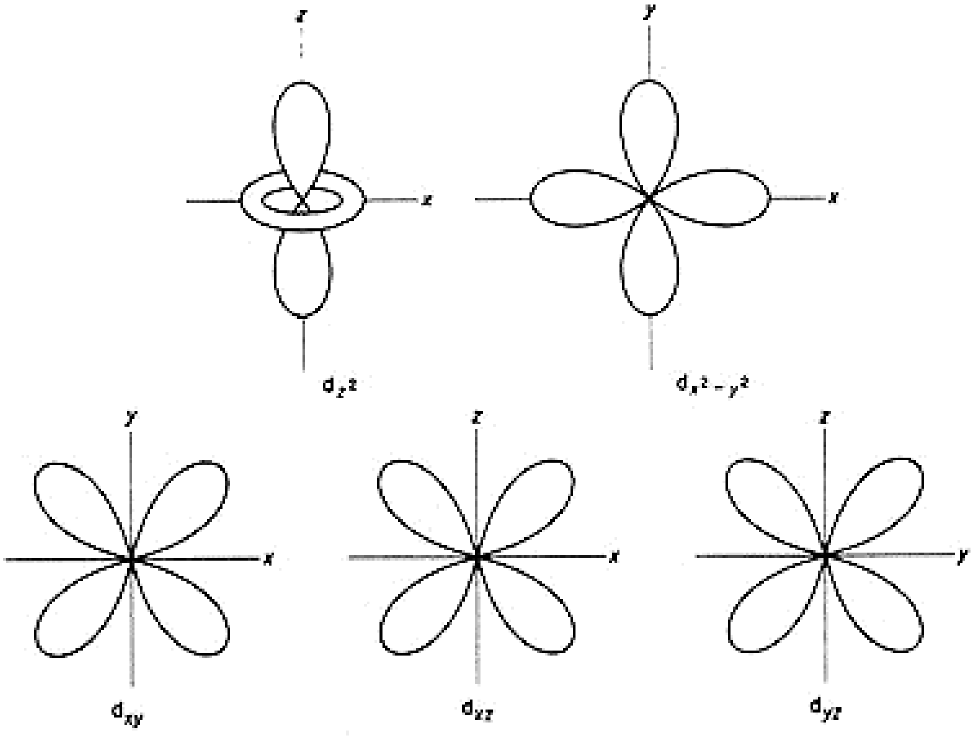

Fig 1.3. Spatial geometry of d orbitals of spinels [13].

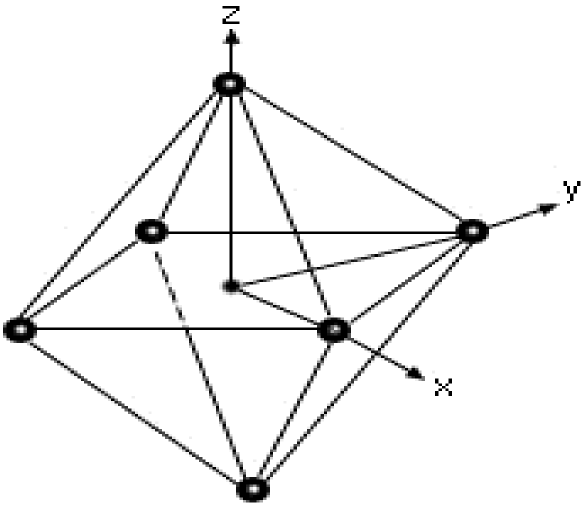

Fig 1.4. Transition metal cation in an octahedral field [13].

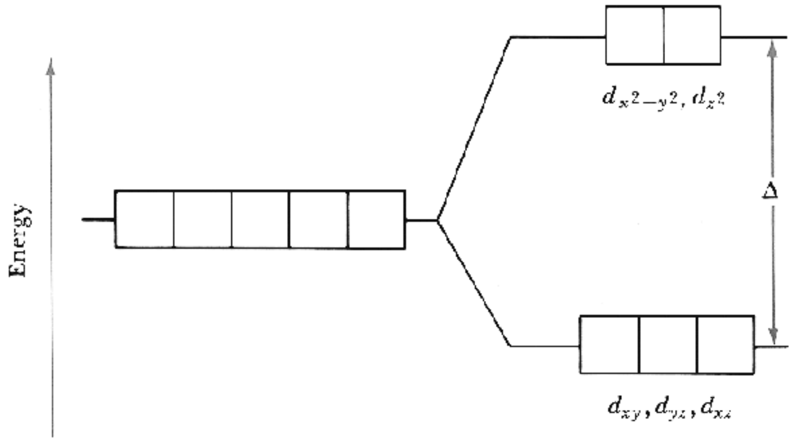

Fig 1.5. Energy level diagram for 'd' level splitting [13].

In ferrites the arrangement is dependent on the divalent cation because Fe^{3+} has no crystal field stabilization energy. When the divalent cation has also no clear preference, then δ value takes in between the zero and one. According to Hund's law, electronic state with higher spin state are the most stable so the high spin states like d^1, d^2, d^3 especially d^3 (Cr^{3+}, Mn^{4+}, V^{2+}) occupy octahedral site. The half-filled d orbitals (Mn^{2+}, Fe^{3+}) in the high spin state have d^5 spherical configuration with no particular preference for either coordination. The degree of inversion δ is not exactly zero for many ferrites. The mechanism of cation redistribution is more complex and can be significantly affected by the presence of Fe^{2+} [13].

1.4.Types of spinel ferrites

Spinels can be broadly classified in to three types depending on the distribution of the cations between the octahedral and the tetrahedral sites [13-15].

1.4.1. Normal spinel

First one is normal spinel where all the divalent cations occupy tetrahedral site and trivalent cations occupy the octahedral sites. The general formula is

$$[M^{2+}]_T [M^{3+}{}_2]_O O_4$$

Where letter 'O' indicates octahedral site occupancy and the 'T' indicates tetrahedral site occupancy. Here octahedral sites are occupied by only one kind of cations [13-15, 20].

1.4.2. Inverse spinel

Second one is inverse spinel where trivalent cations occupy both the octahedral and tetrahedral sites and divalent cations occupy only octahedral sites. The general formula is [13-15, 20].

$$[M^{3+}]_T\,[M^{2+}M^{3+}]_O\,O_4$$

1.4.3. Partial inversion

Third one is partial spinel where divalent and trivalent cations randomly distributed among the tetrahedral and octahedral sites. It is intermediate cation distribution between the normal spinel and inverse spinel. The cation distribution is given by the general formula

$$(M^{3+}{}_{\delta}M^{2+}{}_{1-\delta})[M^{3+}{}_{2-\delta}M^{2+}{}_{\delta}]\,O_4$$

where δ is the degree of inversion with a value of zero for the normal and one for the inverse distribution. Degree of inversion depends on the synthesis techniques, calcination and sintering temperature [13-15, 20].

With all the above, spinel ferrites are the derivatives of the naturally occurred mineral $FeFe_2O_4$ (Fe_3O_4) which has the inverse spinel structure. General formula for spinel ferrites is MFe_2O_4 where M is the divalent cation M = Co, Mn, Zn, Ni, Cd…. etc. Comparison of magnetic properties among some of the important ferrites is given in table 1.2.

Table 1.2. Comparison of magnetic properties of different spinel ferrites

S.No	Ferrite	Saturation magnetisation (kAm^{-1})	Net magnetic moment per formula unit $\mu=(x)\mu m+10(1-x)$
1	Fe_2O_3	360	4 μ_B
2	$CoFe_2O_4$	422	3 μ_B (bulk)
3	$MnFe_2O_4$	386	5μ_B
4	$NiFe_2O_4$	270	2 μ_B
5	$CuFe_2O_4$	135	1 μ_B
6	$ZnFe_2O_4$	122	0 μ_B

1.5. Cobalt ferrite

Among all the ferrites, cobalt ferrite is one of the potential candidates which exhibit moderate saturation magnetization, high coercivity, electrical insulation with low eddy current loss, and chemical stability etc. Therefore it has been extensively used in high density storage, transformer core, high quality filters, phase shifters etc. [7, 21]. Cobalt ferrite is selected as representative for the spinel ferrites to study the electric and magnetic properties and relate its structural modifications. Bulk cobalt ferrite has inverse spinel structure that shifts to partial inversion for nano ferrites. In inverse spinel eight of the tetrahedral sites occupied by the octahedral Fe^{3+} ions and half of the octahedral sites occupied by $Co^{2+}$and Fe^{3+}. When the size reduced to nano-level some of the Co^{2+} ions in the octahedral site shifts to tetrahedral site leads to partial inversion structure. Cobalt ferrite belongs to Fd3m space group [22] and lattice parameter typically ~ 8.39 A^{o}. In cobalt ferrite, oxygen anions form cubic structure resulting 64 tetrahedral sites and 32 octahedral sites. Each unit cell contains 8 chemical formulas [23] so that eight ferric ions occupy tetrahedral sites and eight cobalt ions and iron ions occupy octahedral ions in ideal inverse spinel structure. Unit cell of the cobalt ferrite is shown in figure 1.7. Axis [100] is the easy axis of magnetization of cobalt ferrite over the whole temperature range [10]. Cobalt ferrite exhibits high anisotropy constant (K_1) which is in the range of 2.1-3.9×10^6ergs/cm^3(for bulk) and for nano materials it is around 6.5×10^6 ergs/cm^3 and is increased with decreasing temperature [24,25]. The origin of the magneto-crystalline anisotropy in the cobalt ferrite is due to the L-S coupling in the presence of lattice [26, 27]. Both cobalt ions and ferric ions contribute to the magnetic anisotropy but major contribution comes from cobalt ions. The magnetic crystalline anisotropies of $CoFe_2O_4$materials are closely related to the distribution of magnetic ions in the tetrahedral and octahedral sites. So that any change in the site occupation (both sites) will change the magnetic properties.

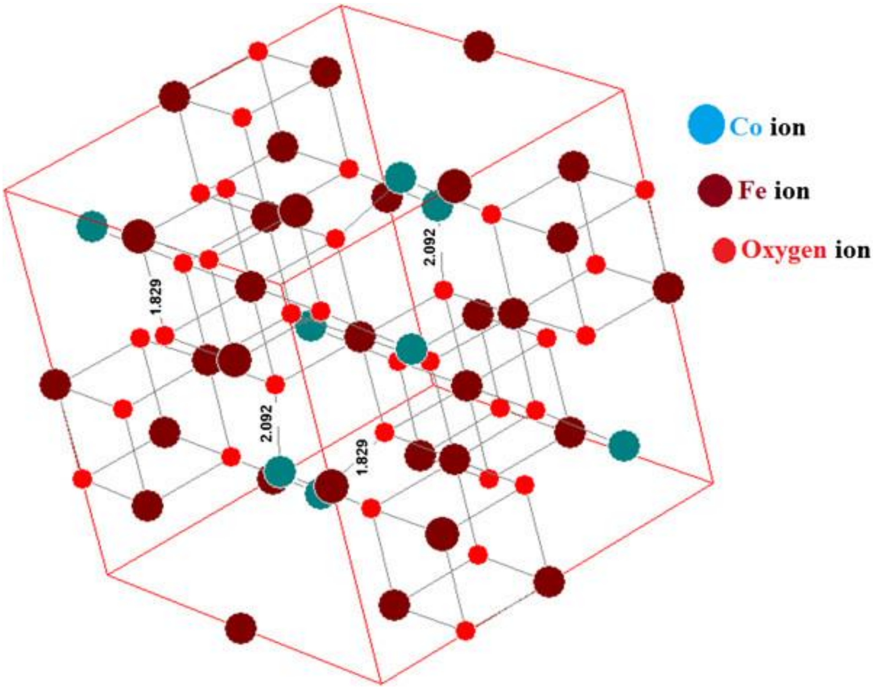

Fig 1.6. Unit cell of cobalt ferrite [28]

1.6.Magnetic and electric properties of cobalt ferrite

Cobalt ferrite is a ferrimagnetic material which exhibits room temperature M-H loop. Magnetic properties of the cobalt ferrite depend on the interactions among the cations (Co^{2+}, Fe^{2+}) occupied in the tetrahedral sites and octahedral sites. Three types of possible interactions in cobalt ferrite are A-A, A-B, B-B interactions, where A-tetragonal and B-octahedral sites. These interactions occur sometimes through anion (O^{2-}) and sometimes through direct interaction. Among these interactions, A-B interaction is the strongest and by nature it is antiferromagnetic. So the resultant magnetic moment is equal to the difference between A and B site ions. The magnetic moments of the cations in the tetrahedral site are parallel and in the same way spins of the cations in the octahedral sites are parallel. But the spin arrangement between tetrahedral and octahedral site is anti-parallel [29,30] shown in figure 1.8. In cobalt ferrite, spins of eight ferric ions in tetrahedral site cancel with the spins of the eight ferric ions in the octahedral site. So the resultant magnetic moment comes from the cobalt ion when it is in completely inverse spinel form. Resultant magnetic moment depends on irreversibility.

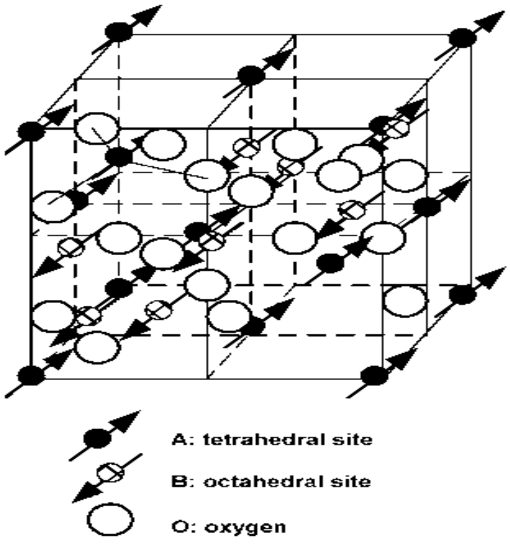

Fig 1.7. Spin structure of the cobalt ferrite in inverse spinel [10].

Spin alignment of cobalt ferrite is shown below when it is completely inverse spinel. The square bracket represents octahedral site. So the resultant spin comes from the cobalt ion which is equal to $3\mu_B$ per molecule when it is completely inverse structure [31,32].

$$Fe^{3+}[Co^{2+}\ Fe^{3+}]\ O_4$$

$$\downarrow \quad \uparrow \quad \uparrow$$

Cobalt ferrite is considered to be the semiconductor/insulator and it has high electrical resistance with low eddy current loss. This is the major advantage over the other ferromagnetic materials. The conduction in cobalt ferrite depends on the mobility and the density of charge carriers and is due to the electron exchange between Fe^{2+}-Fe^{3+} and hole transfer between Co^{3+}/Co^{2+} ions in octahedral sites. Frequency and temperature dependent study of electrical properties gives the better information about the localized charge carriers [33,34].

1.7. Brief discussion about literatures

Ramana et al. have studied structural, magnetic and dielectric properties of Mn substituted cobalt ferrites. The nonlinear variation of magnetic properties with Mn doping was explained by the cation distribution. The anisotropy constant and saturation magnetization decreased with temperature and dielectric dispersion with frequency was explained using modified Debye equation [35].

Razia et al. have investigated the effect of indium on electric and magnetic properties of cobalt ferrite nanoparticles. They observed that the decrease in saturation magnetization and increase in coercivity occurred due to decrease in particle size. In addition, high resistivity with low eddy current loss has observed in the In doped cobalt ferrite nanoparticles [36]. Pandit et al. studied same element effect on magnetic properties of the cobalt ferrite nanoparticles and observed nonlinear variation of saturation magnetization and increase in coercivity. In addition to that spin canting effect was observed in In substituted cobalt ferrite nanoparticles [37].

Dwivedi et al. have examined the effect of Mo^{6+} substitution on electric and magnetic properties of the cobalt ferrite and they observed the ferroelectricity in the Mo substituted cobalt ferrite. Ferroelectricity in the Mo substituted cobalt ferrite is due to the d^o in Mo^{6+} and giant dielectric behavior was observed due to the Maxwell Wagner polarization [38].

Sivakumar et al. have studied the effect of grain size, cation distribution, frequency and temperature variation on dielectric properties of the cobalt ferrite nanoparticles. Cobalt ferrite nanoparticles with 8 nm size exhibit good dielectric properties with low loss and non-Debye type dielectric relaxation [39]. Same authors explained the conduction mechanism in cobalt ferrite nanoparticles with different particle sizes in terms of hole and electron hoping. Cation distribution among the tetrahedral and octahedral sites greatly affected the resistance of the cobalt ferrite nanoparticles [40].

Gul et al. have studied the effect of Zn on structural, electrical and magnetic properties of cobalt ferrite nanoparticles. DC resistance was increased with Zn substitution while dielectric constant was decreased. Curie temperature decreased with increasing substitution of zinc [41]. Nlebedim et al. studied temperature dependent magnetic properties of the Zn substituted cobalt ferrite and observed increased magnetization with Zn substitution and decreased trend with temperature. They noticed that an inverse relation between magnetic susceptibility and coercive field and direct relationship between magnetic anisotropy constant and coercive filed [42].

Kamla bharati et al. have observed the enhancement in dielectric constant and electrical resistivity of cobalt ferrite with substitution of La. Conduction mechanism in the La substituted cobalt ferrite was explained using small polaron hoping and variable range hoping models [43]. Simona et al. had studied the magnetic properties of the La doped cobalt ferrite nanoparticles and observed drastic decrease in the particle size with La substitution. Surface effects plays important role in deciding the magnetic properties of the cobalt ferrite [44].

Kambale et al. [45] have synthesized the Dy^{3+} substituted cobalt ferrite nanoparticles at low temperature 600^0 C. They observed that the grain size and lattice constant were increased with the substitution, obeying vigards law. Room temperature magnetic measurements revealed that the saturation magnetization and coercivity were changed with Dy. Naik et al. [46] have studied the influence of distribution of metal cations in the crystal lattice and dimensions of the ferrite oxides on the resultant magnetic properties of Dy and Gd doped cobalt ferrite. They have co-related the particle dimension, spin orbit coupling and superparamegntic properties of substituted cobalt ferrite nanoparticles.

Kolekar et al. have studied the effect Mn on dielectric properties of the cobalt ferrite. Modified Debye law is applied to explain the dielectric constant dispersion with frequency at room temperature. Impedance spectroscopy was applied to analyze the dielectric relaxation, ac conductivity of the Mn substituted cobalt ferrite [47].

Pant et al. have studied the effect of Gd on finite size effects of the cobalt ferrite nanoparticles and noticed the decrease in crystalline size and superparamagnetism nature in Gd substituted cobalt ferrite [48]. Rana et al. prepared Gd substituted cobalt ferrite nanoparticles by chemical precipitation method and studied the electrical resistance and dielectric properties. Dielectric constant, dielectric loss and capacitance were increased with Gd substitution while electrical resistance was decreased [49]. Rahman et al. studied the structural and ac electrical properties of the Gd substituted cobalt ferrite and observed decreasing trend in ac conductivity with the addition of Gd [50].

Vasundhara et al. have studied the magnetic and dielectric properties of the cobalt ferrite nanoparticles. They observed the superparamagnetic nature for 6 nm sample and ferrimagnetic nature for 50 nm sample. They also observed the increasing trend of dielectric permittivity with the decrease in crystallite size [51].

Hsahim et al. have studied the effect of Ni^{2+} on electric and magnetic properties of the cobalt ferrite nano-ferrites. Dielectric constant was decreased with increase in Ni content and all exhibit semiconducting nature. Saturation magnetization and remnant magnetization were decreased with increase in percentage of Ni [52].

Ahmed et al. have studied the electrical properties of the Cu substituted cobalt ferrite nanoparticles synthesized by standard ceramic method. They observed the increment in dielectric constant, ac conductivity, dielectric loss and mobility with the substitution of Cu due to increase in vacancies in iron site [53]. Balavijayalakshmi et al. studied the effect of Cu on magnetic properties of the cobalt ferrite nanoparticles and observed decreasing trend in saturation magnetization, coercivity and remnant magnetization with Cu substitution [54].

Yadav et al. have studied the structural morphological, dielectric, magnetic and impedance properties of the Mn substituted cobalt ferrite. Mn substitution has significantly affected the magnetic properties and the conduction process due to the small polaron hoping [55]. Kambale et al. studied the effect of Mn on dielectric properties of cobalt ferrite nanoparticles and observed the nonlinear variation of saturation magnetization and decreasing trend in coercivity with Mn substitution. Dielectric properties exhibit increasing trend with Mn addition [56].

Effect of Ni substitution in the cobalt ferrite nanoparticles has been studied by Vanidha et al.[57]. They observed a semiconducting to metallic transition due to cation-cation interaction. And they observed from impedance spectroscopy that the grain boundary conduction is replaced by the grain conduction as transition takes from semiconductor to metal. Ghasemi et al. investigated the magnetic properties of the nickel and strontium simultaneously substituted cobalt ferrite nanoparticles using Mossbauer spectroscopy, synthesized by the sol-gel method. Coercivity, saturation magnetization are decreased and reflection loss in X band increased with the substitution [58].

Finite size effect has been studied by George et al. on the electrical properties of cobalt ferrite nanoparticles. They observed the enhancement of electrical properties with decreasing crystalline size and explained on the basis of correlated hoping model. In addition, the deviation from the Maxwell Wagner polarization has been observed due to twin contribution from the surface polarization and porosity [59].

Abbas et al. have studied the effect of Sn on structural and magnetic properties of the cobalt ferrite nanoparticles and observed the decrease in saturation magnetization, coercivity and remnant magnetization with substitution of Sn due to the nonmagnetic nature of Sn [60]. While Rahman et al. [61] have observed the enhancement of the electric and dielectric properties of the Sn substituted cobalt ferrite nanoparticles due to the exchange of electrons between the Sn^{2+} and Sn^{4+}.

Table 1.3. Literature

S. No	Dopant	Magnetic properties	Electric properties	Size	Reference
1.	Mn	Nonlinear variation with Mn	dielectric dispersion with frequency was explained using modified Debye equation	--------	C. V. Ramana, Y. D. Kolekar, K. Kamala Bharathi, B. Sinha, and K. Ghosh, Journal of Applied Physics 114 (2013) 183907.
2.	Mn	Nonlinear variation with Mn	The dielectric permittivity goes on increasing with the increase of Mn2+ concentration in the substituted Co-ferrites.	--------	S.P. Yadav, S.S. Shinde, A.A. Kadam and K.Y. Rajpure, Journal of Alloys and Compounds 555 (2013) 330–334.
3.	Mn	The nonlinear variation of saturation magnetization and decreasing trend in coercivity with Mn substitution	Dielectric properties exhibit increasing trend with Mn addition	--------	R C Kambale, P A Shaikh, C H Bhosale, K Y Rajpure and Y D Kolekar, Smart Mater. Struct. 18 (2009) 115028.
4.	Mn	Modified Debye law is applied to explain the dielectric constant dispersion with frequency at room temperature	Impedance spectroscopy was applied to analyze the dielectric relaxation, ac conductivity of the Mn substituted cobalt ferrite	---------	Y. D. Kolekar, L. J. Sanchez, and C. V. Ramana, Journal of Applied Physics 115 (2014) 144106
5.	In	the decrease in saturation magnetization and increase in coercivity	high resistivity with low eddy current loss has observed in the In doped cobalt ferrite nanoparticles	Decrease in particle size	Razia Nongjai, Shakeel Khan, K. Asokan, Hilal Ahmed, and Imran Khan, J. Appl. Phys. 112 (2012) 084321
6	In	nonlinear variation of saturation magnetization and increase in coercivity	All the samples possess comparatively low values of permeability and relative loss factor	-------	Rabia Pandit, K.K. Sharma , Pawanpreet Kaur , V.R. Reddy , Ravi Kumar, Jyoti Shah, Journal of Alloys and Compounds 596 (2014) 39–47

7	Mo^{6+}	Enhancement in magnetic behavior	ferroelectricity and giant dielectric behavior was observed	--------	G. D. Dwivedi, K. F. Tseng, C. L. Chan, P. Shahi, J. Lourembam, B. Chatterjee, A. K. Ghosh, H. D. Yang, and Sandip Chatterjee, physical review B 82 (2010) 134428.
8	Zn	Curie temperature decreased	dielectric constant was decreased		I.H. Gul, A.Z. Abbasi, F. Amin, M. Anis-ur-Rehman, A. Maqsood, Journal of Magnetism and Magnetic Materials 311 (2007) 494 – 499.
9	Zn	increased magnetization with Zn substitution and observation inverse relation between magnetic susceptibility and coercive field	----------------	--------	I. C. Nlebedim, M. Vinitha, P. J. Praveen, D. Das, and D. C. Jiles, Journal of Applied Physics 113 (2013) 193904.
10	La	-----------------------	observed the enhancement in dielectric constant and electrical resistivity of cobalt ferrite with substitution of La		K. Kamala Bharathi and C.V. Ramana, Journal of Materials Research 26 (2010) 584-591.
11	La	Surface effects plays important role in deciding the magnetic properties of the cobalt ferrite	----------------	decrease in the particle size	Simona Burianova, Jana Poltierova Vejpravova, Petr Holec, Jiri Plocek, and Daniel Niznansky, J. Appl. Phys. 110 (2011) 073902
12	Dy^{3+}	saturation magnetization and coercivity were changed with Dy	---------------------	grain size increased	R. C. Kambale, K. M. Song, Y. S. Koo, and N. Hur, Journal of Applied Physics 110 (2011) 053910.

13	Gd	superparamagnetism nature	Dielectric constant, dielectric loss and capacitance were increased with Gd substitution while electrical resistance was decreased	decrease in crystalline size	1) R.P. Pant, Manju Arora, Balwinder Kaur, Vinod Kumar, Ashok Kumar, Journal of Magnetism and Magnetic Materials 322 (2010) 3688–3691. 2)Anu Rana O.P. Thakur and Vinod Kumar, Materials Letters 65 (2011) 3191–3192
14	Ni	Saturation magnetization and remnant magnetization were decreased with increase in percentage of Ni	Dielectric constant was decreased, semiconducting to metallic transition due to cation-cation interaction	----------	1)Mohd. Hashim, Alimuddin , Shalendra Kumar , Sagar E. Shirsath, R.K. Kotnala Jyoti Shah and Ravi Kumar, Materials Chemistry and Physics 139 (2013) 364e374. 2)D. Vanidha, A. Arunkumar, S. Rajagopan, R. Kannan, J Supercond Nov Magn 26 (2013)173–182.
15	Cu	observed decreasing trend in saturation magnetization, coercivity and remnant magnetization with Cu substitution	increment in dielectric constant, ac conductivity, dielectric loss and mobility with the substitution of Cu		1) M A Ahmed, S F Mansour and M A Abdo, Phys. Scr. 86 (2012) 025705. 2)J.Balavijayalakshmi, N.Suriyanarayanan, R.Jayapraksah,Materials Letters 81 (2012) 52.
16	Sn	decrease in saturation magnetization, coercivity and remnant magnetization with substitution of Sn	the enhancement of the electric and dielectric properties of the Sn substituted cobalt ferrite nanoparticles		1)Y.M. Abbas, S.A. Mansour, M.H. Ibrahim, Shehab.E. Ali, Journal of Magnetism and Magnetic Materials 324 (2012) 2781–2787. 2)A. Rahman, M. A. Rafiq, M. Hasan, M. Khan, S. Karim and S.O. Cho, J. Nanopart Res 15 (2013) 1703.

1.8. Motivation

From the literature survey, it is concluded that magnetic and electric properties of cobalt ferrite system is largely dependent on the particle size. The particle size can be brought to nano scale by following chemical route of preparation. In some cases, substituted cations also contribute in reducing the particle size. This will help in reducing the calcination and sintering temperature so that particle growth can be suppressed to keep within the nano scale. The control growth of particle also controls the cation distribution and hence controls the related physical properties. Therefore, it is very interesting to study the effect of particle growth on magnetic and electric properties of $CoFe_2O_4$ system for fundamental research to broaden the idea of physical mechanism behind the cause. Again, the effect of dopants on controlling the particle size and cation distribution is another point of concern. From the wide scale application point of view of $CoFe_2O_4$, one of the highly used sectors is the core of transformer. The aim of replacing ceramic magnets in place of metallic magnets is to reduce the eddy current loss as the former hold high electric resistance compare to the latter.

1.9. Objective of the work

Accounting all these factors we have sum up the objectives of our thesis work which is described below.

1) To synthesize the bulk cobalt ferrite ($CoFe_2O_4$) system through solid state method.
2) To synthesize the nano cobalt ferrite system through auto combustion method.
3) To synthesize the modified nano cobalt ferrite systems with chosen dopants of Bi^{3+}, Cr^3 to replace the Fe-site and modified with K_2CrO_4.
4) To characterize with X-ray diffraction for structure analysis and average particle size calculation.
5) To characterize with field emission scanning electron microscope for surface morphology analysis and verifying nano scale of particles.
6) To characterize with X-ray photoelectron spectroscopy to identify the existing oxidation states of various cations.
7) To characterize with Mossbauer spectroscopy to locate the sites occupied by Fe cation.
8) To characterize with magnetic measurement instruments to obtain the required magnetic parameters.

9) To characterize with Impedance Analyzer and Electrometer to obtain the necessary electric parameters.
10) To correlate the obtained magnetic, electric properties with evolved particle size and justify with the physical mechanism.

References

[1] N. Sivakumar, A. Narayanasamy, and N. Ponpandian and G. Govindaraj, J. Appl. Phys. 101 , (2007) 084116.

[2] Yen-Pei Fu and Shao-Hua Hu, Ceramics International 36 (2010) 1311–1317.

[3] K.Kamala Bharathi, R.J.Tackett, C.E.Botez and C.V.Ramana, J. Appl. Phys. 109, (2011) 07A510.

[4] Ping Ren, JianGuo Guan and Xu Dong Cheng, Materials Chemistry and Physics 98 (2006) 90–94.

[5] N Sivakumar, A Narayanasamy, B Jeyadevan, R Justin Joseyphus and C Venkateswaran, J. Phys. D: Appl. Phys. 41 (2008) 245001.

[6] M Idrees, M Nadeem and M M Hassan, J. Phys. D: Appl. Phys. 43 (2010) 155401.

[7] W. Chen, W. Zhu, O. K. Tan, and X. F. Chen, J. Appl. Phys. 108, (2010) 034101.

[8] I.H. Gul, F. Amin, A.Z. Abbasi, M. Anis-ur-Rehman and A. Maqsood, Scripta Materialia 56 (2007) 497–500.

[9] S A.M. Pachpinde , M.M. Langade , K.S. Lohar , S.M. Patange , Sagar E. Shirsath, Chemical Physics 429 (2014) 20–26.

[10] Daliya S. Mathew and Ruey-Shin Juang, Chemical Engineering Journal 129 (2007) 51.

[11] Eva Céspedes, James M. Byrne, Neil Farrow, Sandhya Moise, Victoria S. Coker, Martin Bencsik,d Jonathan R. Lloydc and Neil D. Tellinga, Nanoscale 6 (2014) 12958.

[12] http://shodhganga.inflibnet.ac.in:8080/jspui/bitstream/10603/13720/7/07_chapter%201.pdf

[13] Raul Valenzuela, Magnetic ceramics, New York, Cambridge university press, 1994.

[14] E T Lacheisserie, D Gignoux and M Schlenker, New York, Springer, 2006.

[15] B.D.Cullity and C.D. Graham, Introduction to magnetic materials, New Jersey, Wiley, 2009.

[16] S. Soliman,1 A. Elfalaky,2 Gerhard H. Fecher,1 and Claudia Felser, Physical review B 83 (2011) 085205.

[17] C. N. Chinnasamy, A. Narayanasamy, N. Ponpandian, K. Chattopadhyay, K. Shinoda, B. Jeyadevan, K. Tohji, and K. Nakatsuka, T. Furubayashi and I. Nakatani, Physical review B 63 (2001) 184108.

[18] Dipali S. Nikam, Swati V. Jadhav, Vishwajeet M. Khot, R. A. Bohara, Chang K. Hong, Sawanta S. Malib and S. H. Pawa, RSC Adv.5 (2015) 2338.

[19] B. G. Toksha, Sagar E. Shirsath, M. L. Mane, S. M. Patange, S. S. Jadhav, and K. M. Jadhav, J. Phys. Chem. C 115 (2011) 20905–20912.

[20] Jeong Hyun Shim, Soonchil Lee, Jung Hye Park, Seung-Jin Han, Y. H. Jeong and Young Whan Cho, Physical review B 73 (2006) 064404.

[21] Sonal Singhal, J. Singh, S.K Barthwal and K. Chandra, Journal of Solid State Chemistry 178 (2005) 3183 – 3189.

[22] A. Franco, Jr.,F. L. A. Machado and V. S. Zapf, Journal of applied physics110 (2011) 053913.

[23] Ibrahim Sharifi, H.Shokrollahi, MohammadMahdiDoroodmand and R.Safi, Journal of Magnetism and Magnetic Materials 324 (2012) 1854–1861.

[24] Martin Kriegisch, Weijun Ren, Reiko Sato-Turtelli, Herbert Muller, Roland Grossinger,and Zhidong Zhang, Journal of Applied Physics 111 (2012) 07E308.

[25] Y. Melikhov, J. E. Snyder, D. C. Jiles, A. P. Ring, J. A. Paulsen, C. C. H. Lo and K. W. Dennis, Journal of applied physics99 (2006) 08R102.

[26] Adolfo Franco Jr. and Vivien Zapf, Journal of Magnetism and Magnetic Materials 320 (2008) 709–713.

[27] Chao Liu, Bingsuo Zou, Adam J. Rondinone, and Z. John Zhang, J. Am. Chem. Soc. 122 (2000) 6263-6267.

[28] Lawrence Kumar, Pawan Kumar, Amarendra Narayan and Manoranjan Kar International Nano Letters 3 (2013) 1.

[29] H. S. Mund, Shailja Tiwari, Jagrati Sahariya, M. Itou, Y. Sakurai and B. L. Ahuja, Journal of Applied Physics 110 (2011) 073914.

[30] C. E. Rodr´ıguez Torres, F. Golmar, M. Ziese, P. Esquinazi, and S. P. Heluani, Physical Review B 84 (2011) 064404.

[31] Daniel Fritsch and Claude Ederer, Physical Review B 82 (2010) 104117.

[32] Z. Szotek, W. M. Temmerman, D. Ködderitzsch, A. Svane, L. Petit, and H. Winter, Physical Review B 74 (2006) 174431.

[33] I.H. Gul, and A. Maqsood, Journal of Magnetism and Magnetic Materials 316 (2007)13.

[34] G. Dascalu , T. Popescu , M. Feder and O.F. Caltun, Journal of Magnetism and Magnetic Materials 333 (2013) 69–74.

[35] C. V. Ramana, Y. D. Kolekar, K. Kamala Bharathi, B. Sinha, and K. Ghosh, Journal of Applied Physics 114 (2013) 183907.

[36] Razia Nongjai, Shakeel Khan, K. Asokan, Hilal Ahmed, and Imran Khan, J. Appl. Phys. 112 (2012) 084321.

[37] Rabia Pandit, K.K. Sharma , Pawanpreet Kaur , V.R. Reddy , Ravi Kumar, Jyoti Shah, Journal of Alloys and Compounds 596 (2014) 39–47.

[38] G. D. Dwivedi, K. F. Tseng, C. L. Chan, P. Shahi, J. Lourembam, B. Chatterjee, A. K. Ghosh, H. D. Yang, and Sandip Chatterjee, physical review B 82 (2010) 134428.

[39] N Sivakumar, A Narayanasamy, C N Chinnasamy, and B Jeyadevan, J. Phys.: Condens. Matter 19 (2007) 386201.

[40] N. Sivakumar, A. Narayanasamy, K. Shinoda, C. N. Chinnasamy, B. Jeyadevan, J. Appl. Phys. 102 (2007) 013916.

[41] I.H. Gul, A.Z. Abbasi, F. Amin, M. Anis-ur-Rehman, A. Maqsood, Journal of Magnetism and Magnetic Materials 311 (2007) 494 – 499.

[42] I. C. Nlebedim, M. Vinitha, P. J. Praveen, D. Das, and D. C. Jiles, Journal of Applied Physics 113 (2013) 193904.

[43] K. Kamala Bharathi and C.V. Ramana, Journal of Materials Research 26 (2010) 584-591.

[44] Simona Burianova, Jana Poltierova Vejpravova, Petr Holec, Jiri Plocek, and Daniel Niznansky, J. Appl. Phys. 110 (2011) 073902.

[45] R. C. Kambale, K. M. Song, Y. S. Koo, and N. Hur, Journal of Applied Physics 110 (2011) 053910.

[46] S. R. Naik and A. V. Salker, J. Mater. Chem. 22 (2012) 2740.

[47] Y. D. Kolekar, L. J. Sanchez, and C. V. Ramana, Journal of Applied Physics 115 (2014) 144106.

[48] R.P. Pant, Manju Arora, Balwinder Kaur, Vinod Kumar, Ashok Kumar, Journal of Magnetism and Magnetic Materials 322 (2010) 3688–3691.

[49] Anu Rana O.P. Thakur and Vinod Kumar, Materials Letters 65 (2011) 3191–3192.

[50] Md.T. Rahman, C.V. Ramana, Ceramics International 40 (2014) 14533–14536.

[51] K. Vasundhara, S. N. Achary, S. K Deshpande, P. D. Babu, S. S. Meena, and A. K. Tyagi, Journal of Applied Physics 113 (2013) 194101.

[52] Mohd. Hashim, Alimuddin , Shalendra Kumar , Sagar E. Shirsath, R.K. Kotnala Jyoti Shah and Ravi Kumar, Materials Chemistry and Physics 139 (2013) 364e374.

[53] M A Ahmed, S F Mansour and M A Abdo, Phys. Scr. 86 (2012) 025705.

[54] J. Balavijayalakshmi, N.Suriyanarayanan, R.Jayapraksah, Materials Letters 81 (2012) 52.

[55] S.P. Yadav, S.S. Shinde, A.A. Kadam and K.Y. Rajpure, Journal of Alloys and Compounds 555 (2013) 330–334.

[56] R C Kambale, P A Shaikh, C H Bhosale, K Y Rajpure and Y D Kolekar, Smart Mater. Struct. 18 (2009) 115028.

[57] D. Vanidha, A. Arunkumar, S. Rajagopan, R. Kannan, J Supercond Nov Magn 26 (2013)173–182.

[58] Ali Ghasemi, Andrea Paesano Jr., Carla Fabiana Cerqueira Machado, Sagar E. Shirsath, Xiaoxi Liu, and Akimitsu Morisako, Journal of Applied Physics 115 (2014) 17A522.

[59] Mathew George, Swapna S Nair, K A Malini, P A Joy and M R Anantharaman, J. Phys. D: Appl. Phys. 40 (2007) 1593–1602.

[60] Y.M. Abbas, S.A. Mansour, M.H. Ibrahim, Shehab.E. Ali, Journal of Magnetism and Magnetic Materials 324 (2012) 2781–2787.

[61] A. Rahman, M. A. Rafiq, M. Hasan, M. Khan, S. Karim and S.O. Cho, J. Nanopart Res 15 (2013) 1703.

CHAPTER 2

Experimental methodology

This chapter describes the different experimental techniques which are used for the characterization of cobalt ferrite and its modified systems.

2.1. Introduction

This chapter describes the synthesis procedure, experimental methods and characterization techniques. The collected data and its analysis are presented in this thesis. All experimental works planned and executed in consultation with the supervisor to get more reliable data and analysis can be contributed to the physics knowledge through this work. The synthesis methods have been employed to prepare the bulk and nano cobalt ferrite with various sizes is discussed. Analytical techniques like X-ray Diffraction (XRD), Raman spectroscopy, X-ray Photoelectron Spectroscopy (XPS), Scanning Electron Microscopy (SEM), Field Emission Scanning Electron Microscopy (FESEM), DC and AC resistivity are used to characterize the samples. Electric and magnetic properties are studied by Impedance analyzer, Electrometer, Mossbauer spectroscopy and SQUID magnetometer.

2.2. Samples preparation

Cobalt ferrite is prepared by using two synthesize methods. Bulk cobalt ferrite is prepared by the solid state method and nano particles of cobalt ferrite are synthesized by the auto combustion method.

2.2.1. Solid state synthesis

Solid state method is one of the oldest synthesis techniques to prepare the polycrystalline materials. In this method the powder is usually prepared from the raw mineral oxides or carbonates by crushing, grinding and milling. The various steps involved in solid state method to prepare the cobalt ferrite are shown in the flow chart. Cobalt trioxide and iron trioxide are mixed in a stoichiometry proportions and grinded for 1 hour using agate mortar. The mixed powder was calcined at required temperature. Then the calcined powder was compacted or pelletized using uniaxial press using tungsten carbide die and finally sintered. A detail about calcination and sintering temperature is given in the respected chapters. The chemical reaction involved in this solid state reaction is given below. So the stoichiometry proportions of Co: Fe is 1:2.

$$4Fe_2O_3 + 2Co_2O_3 \longrightarrow 4CoFe_2O_4 + O_2$$

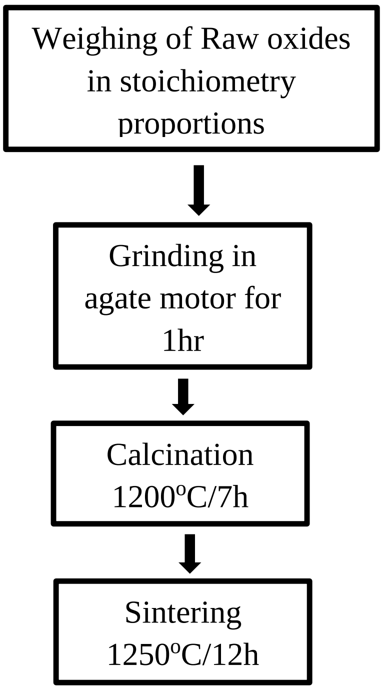

Fig 2.1. Flow chart for solid state reaction method for preparation of bulk Cobalt ferrite

2.2.2. Auto combustion method

Cobalt ferrite nanoparticles are prepared by the auto combustion method. This method is frequently used for synthesis of metal oxides. In this method metal salts are dissolved in water in stoichiometry ratios with addition of fuels like glycine, urea, citric acid etc. Resultant solution was heated with simultaneous mixing using magnetic stirrer. Then it involves thermally induced reaction of xerogel which is formed by the metal salts and fuel [1,2]. Generally nitrate salts are used to synthesize metal oxides due to solubility of nitrates in water at lower temperature [2] in addition, the fuel to metal nitrate ratio plays an important role to decide the reaction temperature and particle size etc.

Cobalt ferrite nanoparticles synthesized by taking cobalt nitrate and iron nitrate as precursor and glycine as fuel. In case of substitution, nitrate of substituted element was taken. Glycine to metal nitrates ratio has taken (G/N) 1.48 because the oxygen content of the oxidizer can be reacted to consume glycine entirely and no heat exchange required for the complete reaction [3]. First stoichiometry amounts metal nitrates were dissolved in water separately and glycine was dissolved in a separate beaker, finally three solutions are mixed in another beaker. The final solution was simultaneously heated and mixed using magnetic stirrer. Because of heating, water evaporates and viscous liquid form which automatically ignite to give black fluffy powder. This powder was grinded, calcined and sintered at required temperature for required time. Details about calcination and sintering temperature are given in the respected chapters.

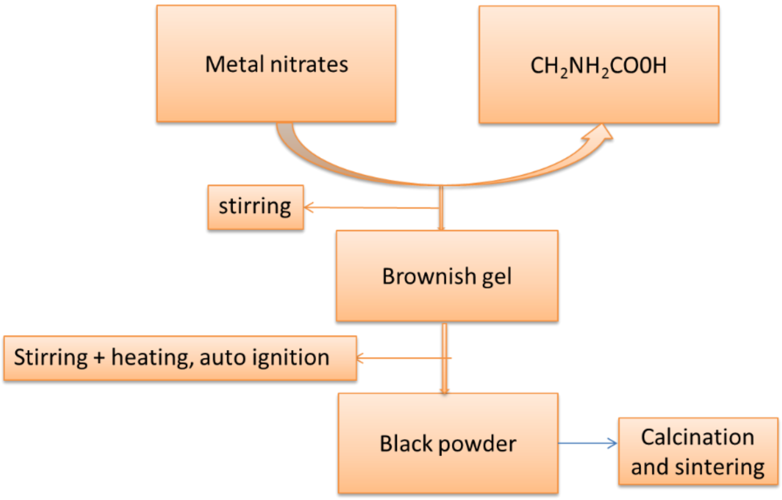

Fig 2.2. Flow chart of auto combustion synthesis method for cobalt ferrite nano particles

2.3. Characterization techniques

Materials are characterized by various techniques. These techniques to be used would depend on the type of material and information we required. Generally people are interested to know structure, composition, chemical state, electrical and magnetic properties etc. The characterization techniques are: X-ray diffraction, Raman spectroscopy, X-ray Photoelectron Spectroscopy, Scanning Electron Microscopy, Field Emission Scanning Electron Microscopy, Resistivity and SQUID. Summary of various techniques are discussed below.

2.3.1. Structural and microstructural characterization

2.3.1.1.X-ray diffraction

Physical properties of the materials strongly depend on the crystal structure which explains the atomic arrangement so knowledge about crystal chemistry is necessary to understand the properties like electric and magnetic properties. X-ray diffraction is one of the most significant and nondestructive technique for structure identification of the materials from which we can determine lattice constant, crystallite/particle/grain size and strain.

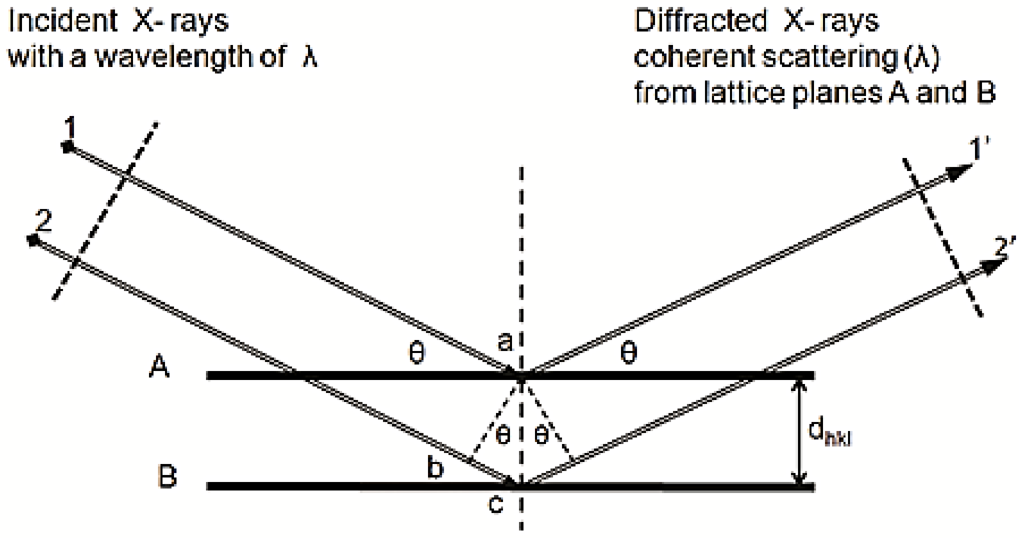

Fig. 2.3. Constructive interference from the parallel planes [4]

When the wave length of the x-ray is comparable to the distance between the atoms then they should diffracted by the atoms in solids and satisfying the Brag's law

$$2d \sin \theta = n\lambda \tag{2.1}$$

Where d is the inter-planar distance, θ is Bragg angle, n is order of the diffraction and λ is the wavelength of the incident wave. Figure 2.3 shows Bragg's diffraction from parallel planes. This law indicates that the constructive interference of diffracted waves takes place only when the inter-planar path difference is integral multiple of the incident wave length [5].

Fig 2.4. X-Ray Diffraction unit (**RIGAKU JAPAN/ULTIMA-IV)**

2.3.1.2.Raman spectroscopy

Raman spectroscopy is based on the phenomenon called Raman scattering, named after the Indian scientist Sir C.V. Raman who first discovered it in 1928. In Raman scattering measurement, a single frequency light, usually from a single mode laser source, shines on the sample and scattered light is measured off the angle with respect to the incident light to minimize Rayleigh’s scattering. The inelastically scattered light with lower {stokes scattering} or higher {anti-stokes scattering} frequencies can be measured with photo detector. The energy difference between the scattered and incident light so called Raman shift (usually given in a wave number $cm^{-1} = 1/\lambda$ with wavelength λ expressed in cm), equals to vibrational or phonon frequency of the sample, as long as selection rule is allowed. The spectrum is usually presented in terms of the intensity of the Raman scattered light as a function of Raman shift [6,7].

2.3.1.3.X-ray photoelectron spectroscopy (XPS)

XPS is based on the measurement of the kinetic energy of photoelectrons generated when the sample is illuminated with soft (1.5 kV) x-ray radiation in an ultra-high vaccum. If one x-ray photon with energy $h\nu$ is used to excite an atom in its initial state with energy E_i and to eject an electron with kinetic energy, KE, with the atom resulting in a final state with energy E_f, one would have the following equation based on total energy conservation

$$h\nu + E_i = KE + E_f \qquad 2.2$$

The difference between the photon energy and electron kinetic energy is called binding energy of the orbital from which the electron is ejected, which, based on the above equation, is equal to $E_f - E_i$. Since the photon energy is known from X-ray radiation source used and the electron KE can be measured, the binding energy can be determined, which gives the energy difference between final and initial state of the atom involved in transition. This binding energy is characteristics for different orbitals of specific elements and is roughly equal to the Hartree-Fock energy of the electron orbital. Therefore, peaks in the photoelectron spectrum can be identified with the specific atoms and surface composition can be analyzed. Because the photoelectrons are strongly attenuated by passage through the sample material itself, the information obtained comes from the sample surface, with a sampling depth on the order of 5 nm. Chemical bonding in molecules will cause binding energy shifts, which can thus be used to extract information of a chemical nature {such as atomic oxidation state} from the sample surface [6,7].

2.3.1.4.Scanning Electron Microscope (SEM) and Field Emission Scanning Electron Microscope (FESEM)

Optical microscopes have limited spatial resolution, usually on the order of a few hundred nm in the best case scenario, due to the diffraction limit of light. Higher resolution, a few nm or even sub nm, is needed for many applications, especially in the study of nano-materials. Scanning electron microscopy is a powerful and popular technique for imaging the surfaces of almost any materials with a resolution down to about few nm. The image resolution offered by SEM depends not only on the property of the electron probe, but also on the interaction of the electron probe with the specimen. The interaction of an incident electron beam with the specimen produces secondary electrons, with energy typically smaller than 50 eV, the emission efficiency of which sensitively depends on surface geometry, surface chemical characteristics and bulk chemical composition. SEM can thus provide information about the surface topology, morphology and chemical composition. FESEM gives clearer and less distorted pictures with spatial resolution to 1 ½ nm which is 3-6 times better than the conventional SEM. In addition to that it produces high quality and low voltages images with negligible electricalcharging of samples [6-8].

Fig 2.5. Scanning Electron Microscopy (JEOL JSM-6084LV)

Fig 2.6. Filed Emission Scanning Electron Microscopy (Nova NanoSEM/ FEI)

2.3.2. Electric characterization

2.3.2.1 DC resistance measurement

DC resistance of the samples measured by the Keithley Electrometer of model 6517B through two probe method. In this process current through samples measured by applying voltage across the sample considering as a resistance. Resistance (R) was calculated by using Ohms law. Resistivity can be obtained from the formula ρ= RA/l where A is area and l is thickness of the sample. The date acquisition was automated with the lab view software which is programing language for data acquisition.

Fig 2.7. DC resistance measurement unit

2.3.2.2.Impedance measurement (AC Resistance)

AC resistance measured by the HIOKI impedance analyzer model IM3570 using two probe method. The data was collected by using the software supplied by the HIOKI Company which connects computer the impedance analyzer. Impedance is a complex resistance experienced by the current when it passes through the circuit consists of resistors, capacitors and inductors. Similar to the resistance is the ratio of voltage to the current. Impedance has real and imaginary parts. Real part demonstrates the ability of circuit to resist the current and imaginary part relate to ability of circuit to store electrical energy. When AC voltage V of amplitude V_A and frequency f applied then it can be explained in terms of time t is

$$V(t) = V_A \sin(2\pi f t) = V_A \sin(\omega t) \qquad 2.3$$

where ω is radial frequency and is equal to 2πf. The current of the signal is, if it is a linear system [9],

$$I(t) = I_A \sin(\omega t + \varphi) \qquad 2.4$$

Then the impedance will be $Z^* = \frac{V(t)}{I(t)} = \frac{V_A \sin(\omega t)}{I_A \sin(\omega t + \varphi)} = Z_A \frac{\sin(\omega t)}{\sin(\omega t + \varphi)}$ 2.5

The voltage and current functions can also described as $V(t) = V_A e^{-i\omega t}$ and $I(t) = I_A e^{-i\omega t - i\varphi}$

$$Z^* = \frac{V(t)}{I(t)} = Z_A\, e^{-i\varphi} = Z_A\,(cos\varphi + isin\varphi) = Z_{real} + jZ_{im} \qquad 2.6$$

Real part of the impedance $Z_{real} = Z' = Z_A\ cos\varphi$ 2.7

Imaginary part of the impedance $Z_{im} = Z'' = Z_A\ sin\varphi$ 2.8

2.3.2.3. Cole-Cole plots

If any signal is applied to pure resistor then Z*= R (resistance) or applied to the pure capacitor then Z*= -j $(\omega c)^{-1}$ where C is capacitance. Real life systems cannot be represented by the neither pure resistor nor pure capacitor rather than the combination of resistor and capacitor. Let us consider an AC signal is applied to the parallel combination of the resistor and capacitor the impedance can be written as

$$Z^* = \frac{R}{1+(\omega RC)^2} - j\frac{\omega R^2 C}{1+(\omega RC)^2} \qquad 2.9$$

$$Z_{real} = \frac{R}{1+(\omega RC)^2} \qquad 2.10$$

$$Z_{im} = -\frac{\omega R^2 C}{1+(\omega RC)^2} \qquad 2.11$$

If real impedance plotted on the x axis and imaginary impedance plotted on the y axis then the plot is known as Cole-Cole plot [9].

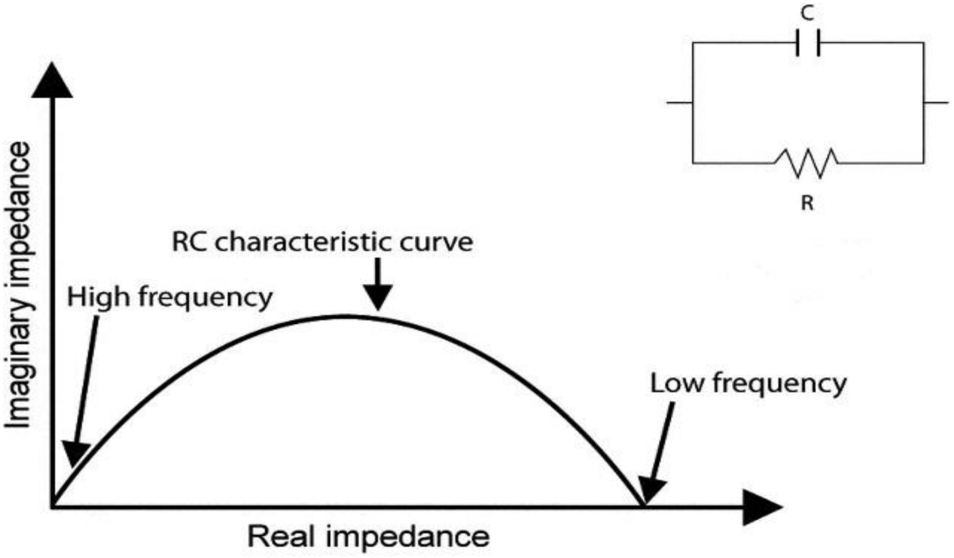

Fig 2.8. Cole-Cole plot [10]

Low frequency data is on the right side of the plot and higher frequencies are on the left as shown in figure 4. The impedance spectra often appear as single or multiple arcs in the complex plane. Cole Cole plots have great importance to study the electrical properties because the shape of the plot yields insight into possible conduction mechanisms [9].

2.3.2.4. Dielectric analysis

The dielectric analysis explains the permittivity and conductivity of material properties as a combined complex permittivity ϵ^* which is analogues to the complex impedance. Just like complex impedance it is also represented by its real and imaginary components

$$\epsilon^* = \epsilon' - j\epsilon'' \qquad 2.12$$

where ϵ' is real permittivity and often is called dielectric constant and ϵ'' is imaginary permittivity and referred as loss factor. The real permittivity can be calculated from the capacitance measured through the two probe method using impedance analyzer. Relation between capacitance and real permittivity is

$$\epsilon' = \frac{Cd}{A\epsilon_o} \qquad 2.13$$

Where d is the distance between the two electrodes and A is the area of the sample and ϵ_o is the permittivity of the free space [9].

2.3.2.5 Electric modulus

The modulus is the inverse of complex permittivity ϵ^* and can also be expressed as a derivative of complex impedance.

$$\mathrm{M}^* = \frac{1}{\epsilon^*} = M' - jM''$$

Where M' is Real part of the modulus and M" is imaginary part of the modulus. Fundamentally, complex electrochemical impedance (Z*), modulus *(M*)* and permittivity (ϵ^*) parameters are all determined by applying an AC potentialat a variable frequency and measuring output current through the sample. In a broader sense dielectric, modulus, and impedance analysis represent the same operational principles and can be referred to as subsets of a universal broadband electrochemical impedance spectroscopy.

2.3.3. Magnetic characterization

Room temperature field and temperature dependent magnetic properties are measured by the SQUID magnetometer. Room temperature Mossbauer spectrum is measured for all the samples using Fe^{57} as a source in the transmission configuration with constant acceleration mode.

2.3.3.1.SQUID magnetometer

This magnetometer is based on the tunneling of superconducting electrons across a very narrow insulating gap, called a Josephson junction between two superconductors. A superconducting measuring current flows through the ring, dividing so that equal currents pass through each of two Josephson junctions. A changing magnetic flux through the ring generates a voltage and a current in the ring, according to Faraday’s law. This induced current ads to the measuring current in one junction, and subtracts in the other. Because of the wave nature of the superconducting current, the result is a periodic appearance of resistance in the superconducting circuit, and the appearance of a voltage between two points, each voltage step corresponds to the passage of a single flux quantum across the boundary of the ring. The existence of the flux quantum was demonstrated in somewhat similar experiments on superconducting rings; its value is $\Phi_0 = h/(2e) \approx 2.067833758(46)\times10^{-15}$ weber. This sensitivity is rarely needed in a measurement of magnetic field, and in practice the device is most commonly linked to the coil to measure the flux from a small sample, and thus the small magnetization. In this form it is called a SQUID (superconducting quantum interference device) magnetometer. Since a superconducting Josephson device requires low temperature operation, it is usually used in conjunction with a superconducting solenoid [11].

2.3.3.2.Mossbauer spectroscopy

Mossbauer spectroscopy is useful technique to get the information about the structural, chemical and magnetic properties of the materials. Nucleus in atoms undergoes to the different transitions among energy levels associated with the absorption and emission. When a nucleus emits or absorbs gamma ray some energies can be lost as a recoil energy and it occurs in the form of phonons. Here the conservation of momentum is satisfied by the momentum of crystal as whole so practically no loss of energy. So Mossbauer found that the significant fraction of emission and absorption of the nucleus is recoil free and quantized with Lamb-Mossbauer factor. It means gamma ray emitted by one nucleus can be resonantly absorbed by the sample containing nucleus of same isotope [12].

References

[1] Andris Sutka and Gundars Mezinskis, Front. Mater. Sci. 6 (2012) 128–141.

[2] Raul Valenzuela, Magnetic ceramics, New York, Cambridge university press, 1994.

[3] A.B. Salunkhe, V.M. Khot, M.R. Phadatare, S.H. Pawar, Journal of Alloys and Compounds 514 (2012) 91–96.

[4] http://lipidlibrary.aocs.org/physics/xray/index.htm, 15/07/2015.

[5] B D Cullity, Elements of X-Ray Diffraction, Addison-Wesley Publishers, 1978.

[6] S K Kulakarni, Nanotechnology: principles and practice, Capital publishing company.

[7] Jin Zhong Zhang, Optical properties and spectroscopy of nanomaterials, world scientific publications

[8] http://www.photometrics.net/fesem.html, 15/07/2015.

[9] Vadim F. Lvovich, Impedance spectroscopy: Applications to Electrochemical and Dielectric Phenomena, a john wiley & sons, inc., publication, 2012.

[10] R. L. Jones, M. Thrall, and C. M. B. Henderson, Mineralogical Magazine 74 (2010) 507-519.

[11] B D Cullity and C D Graham, Introduction to magnetic materials, A John Willey& Sons, inc publication, 2012.

[12] Mossbauer spectroscopy, Wikipedia 15/07/2015.

CHAPTER 3

Electric and magnetic investigations on bulk cobalt ferrite

This chapter describes electric and magnetic transport properties of the bulk cobalt ferrite synthesized by solid state method. AC electrical properties studied in the temperature range 30^0 *C –* 250^0 *C as a function of frequencies varying from 100 Hz – 1 MHz. The low temperature (<* 75^0 *C) relaxation peak appears in imaginary impedance plot attributes to grain effect. Two sets of coexistence of peaks is observed at elevated temperature range. The coexistence is related to grains and grain boundaries found in temperature domain* 75^0 *C* $\leq T \leq$ 175^0 *C and again grain boundaries and electrode effect in domain* 200^0 *C* $\leq T \leq$ 250^0 *C. The Nyquist diagram shows three distinct semicircles at* 175^0 *C and* 200^0 *C. The impedance behavior has been modeled with equivalent circuit of RC-RC-RQ for* $T \leq 175^0$ *C and RC-RQ-RQ for* $T \geq 200^0$ *C. The stretching exponential factor* β *calculated from the well fitted double peaks of imaginary electric modulus spectra with KWW function of bulk cobalt ferrite. We found* $\beta_g = 0.62$ *and* $\beta_{gb} = 0.86$ *for grains and grain boundaries respectively. The Maxwell-Wagner polarization is responsible for the dielectric behavior. The high permittivity and conductivity has been explained by the help of exchange interaction of variable oxidation states of iron and cobalt ions. The room temperature M–H loop indicates its ferrimagnetic order and the temperature dependence of the field cooled loop exhibits maxima at 70 K temperature.*

3.1. Introduction

The material crystallized in spinel structure with transition cations of small ionic radii occupying octahedral and tetrahedral sites are exceptional in their behavior because of strong spin exchange interaction among the cations. Semiconductor cobalt ferrite (CFO) has inverse spinel structure with the ideal formula $(Fe)_A[CoFe]_B$ where A and B denotes tetragonal and octahedral sites respectively [1-5]. The magnetic and electrical properties of the CFO depend on the distribution of the cations in these sites [6,7]. It has drawn the attention of many researchers due to its uncompromising properties like high coercivity, resistivity, Curie temperature, chemical stability and mechanical hardness [8-12]. These properties make the material potential candidate for use in high density recording media, transformer cores, sensors, actuators, microwave devices (isolaters, circulaters), RF circuits, high quality filters and as electrode materials for Li batteries and solid oxide fuels [13-15]. The CFO system has been studied rigorously on the cause of its peculiar magnetic behavior as well as the enhanced properties by doping. However, sluggish advancement in studying electrical transport phenomenon and little study relative to dielectric properties of cobalt ferrite has been reported. Sivakumar et al. [16] has reported the grain size, cation distribution, frequency and temperature effect on dielectric behavior of the nano cobalt ferrite synthesized by precipitation technique. Gegore et al. [17] showed the role of surface polarization due to finite size effect on electrical properties prepared by sol-gel method. A major work of Chen et al. [18] has been reported on impedance spectroscopy of the cobalt ferrite thick films where they proposed the dominance of electrode polarization effect on conduction mechanism. Recent work of Rehman et al. [19] of nanostructured cobalt ferrite mentioned the semiconducting to metallic transition through an activation of polaron conduction. They have reported the grain and grain boundary effect as the major polarization effect on conduction mechanism.

In our work we tried to analyze the complete electric transport behavior of bulk cobalt ferrite. We got result much similar to that of Chen et al. [18] in thick film of electrode effect at high temperature but differed with the complete distinct feature of grains and grain boundaries. The coexistence of peaks relate to grains and grain boundaries at intermediate temperature and then grain boundaries and electrode effect at high temperature is observed which has never been reported in any ferrite system earlier. The surface polarization which was found responsible for dielectric behavior in nanostructured cobalt ferrite [17] is found substituted by the electrode interface effect in bulk CFO system. We take the help of electric modulus formalism to analyze the grains effect as it highlights the least capacitive region. The appearance of double peaks in imaginary modulus spectra is reported first time in CFO system. The peaks are well fitted with the KWW function from which we derive the stretching exponent factor β. The room temperature M-H loop was analyzed in terms of cation distribution among the tetragonal and octahedral sites.

3.2. Material and methods

Polycrystalline cobalt ferrite was prepared by the conventional ceramic method using Iron oxide (Fe_3O_4) and Cobalt oxide (Co_3O_4) powder as raw materials. The precursor powder was mixed and grinded for one hour and calcined at 1200^0 C for 7 hours. Calcined powder was mixed with binder and again grinded for one hour to make pellets. Finally the pellets were sintered at 1250^0 C for 12 hours. The crystal structure of the cobalt ferrite was determined by the X-ray diffractometer (Cu target) and surface morphology was studied by the SEM. Raman spectroscopy used to confirm the phase of the spinel ferrite. Impedance with respect to frequency was measured by the impedance analyzer up to 250^0 C. DC electrical resistance measured by the electrometer (Keithley 3517B) up 200^0 C. Room temperature field dependent magnetic measurement was done by the SQUID (Quantum Design MPMS SQUID VSM EVERCOOL, 5T) magnetometer.

3.3. Results and discussion

3.3.1. Structural analysis

Figure 3.1 shows the XRD pattern of the bulk cobalt ferrite which exhibits (311) peak as a major peak. All the peaks present in the XRD pattern correspond to spinel structure with no other impurity phases which indicate single phase cubic structured cobalt ferrite is formed. The lattice parameter of the cubic lattice was found to a = 8.39 Å. The SEM micrograph (Figure 3.2) of the cobalt ferrite indicates that the sample has dense microstructure and inhomogeneity in grain size. Two types of grain growth is observed. Size of the first type is around 10 μm and second type is 2 μm. Elemental mapping images of cobalt ferrite shown in figure 3.3. The images labeled the iron, cobalt, oxygen are obtained in cobalt ferrite compound.

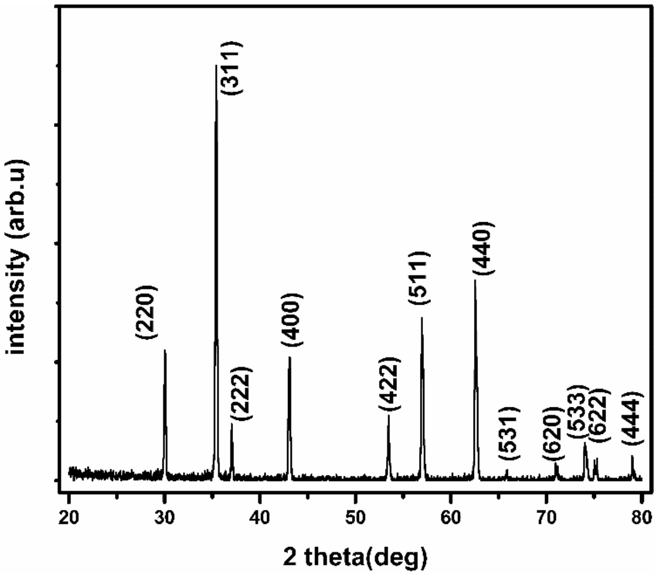

Fig 3.1. XRD pattern of cobalt ferrite

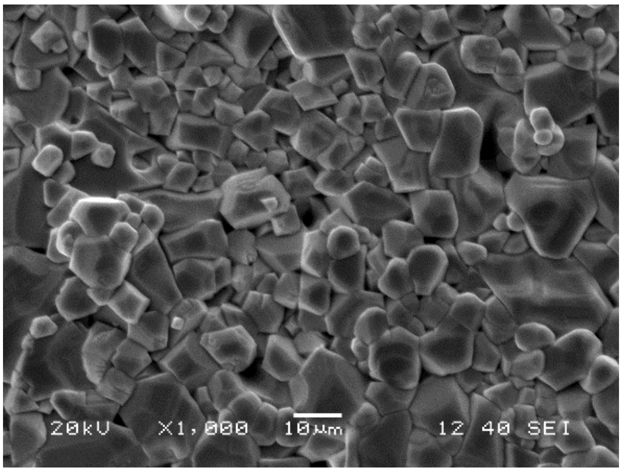

Fig 3.2. SEM image of the bulk cobalt ferrite.

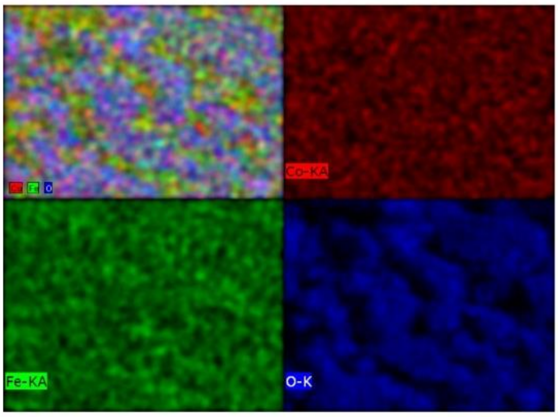

Fig 3.3. Mapping image of cobalt ferrite. The image labeled the O, Fe and Co

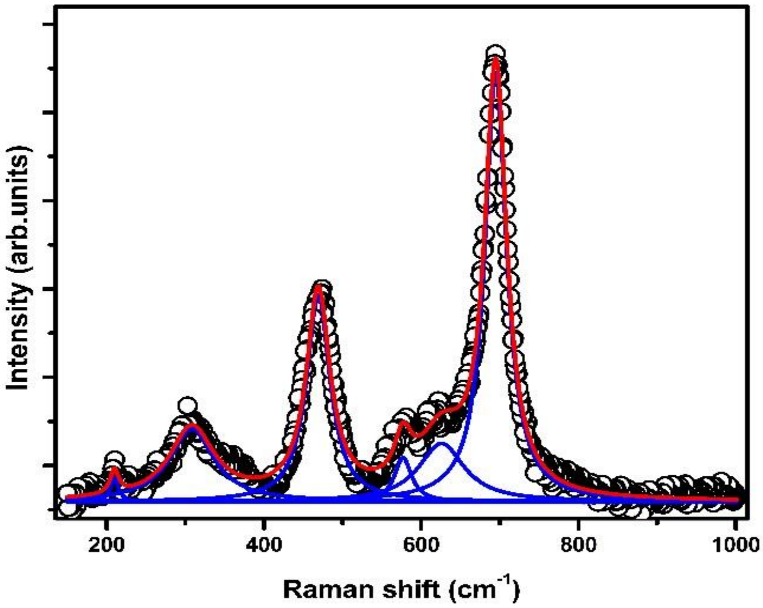

Fig 3.4. Raman spectra of the bulk cobalt ferrite

Raman spectroscopy of the cobalt ferrite is shown in figure 3.4. Raman spectroscopy is a nondestructive material characterization technique used for structural analysis. Cobalt ferrite crystallizes in spinel structure with Fd3m space group [19]. According to the group theory, Raman modes for the spinel structure [20] is given as

$$A_{1g}(R) + E_g(R) + T_{1g} + 3T_{2g}(R) + 2A_{2u} + 2E_u + 4T_{1u}(IR) + 2T_u$$

Among above modes six modes are active $2A_{1g}+E_g+3T_{2g}$ and four infrared modes ($4T_{1u}$) are active [21]. The modes above the 600 cm^{-1} corresponds to the symmetrical stretching of metal oxygen bonding at tetragonal sites and reflect the local lattice effects in the tetragonal sub lattice. The modes present at the below 600 cm^{-1} belongs to the symmetrical stretching of metal oxygen bonding at octahedral sites and reflect the local lattice effects in the octahedral site [22]. The most intense Raman peak in octahedral modes is 474 cm^{-1} and for tetrahedral site is 682 cm^{-1} in cobalt ferrite [23] but in our case we got the most intense peaks at 473 cm^{-1} and 694 cm^{-1}.

3.3.2. Data analysis

The real and imaginary impedance found from the formula $Z'=Z\cos\theta$ and $Z''=Z\sin\theta$ where Z ($Z' + i Z''$) is the complex impedance. The complex modulus ($M=M'+ i M''$) obtained from the "complex impedance using the relation $M'= \omega C_o Z''$ and $M''= \omega C_o Z'$ where $C_o= \varepsilon_0 A/t$ is the vacuum capacitance, $\varepsilon_0 = 8.85\,\mathrm{x}10^{-12}$ F/m is the permittivity of the free space, t is the thickness of the sample and A is the cross sectional area of the electrode deposited on the sample and ω is the angular frequency. The dielectric constant was calculated from the relation $\epsilon_r = Ct/\epsilon_o A$. The ac conductivity is calculated from the formula $\sigma = [Z'/(Z'^2+Z''^2)](A/t)$.

3.3.2.1. Impedance analysis

The real impedance (Z') variation with frequency is shown in Figure 3.5 in a range of frequency of 100 H_z to 1 MH_z within temperature domain 30^0 C to 250^0 C. The plot shows a decrease in impedance with increase in temperature. Above 75^0 C, a plateau of frequency independent nature of impedance is observed which relaxes to a fast frequency dependent region of negative slope. With elevated temperature, the Z' plateau strengthens itself as step response frequency shifts to high frequency side.

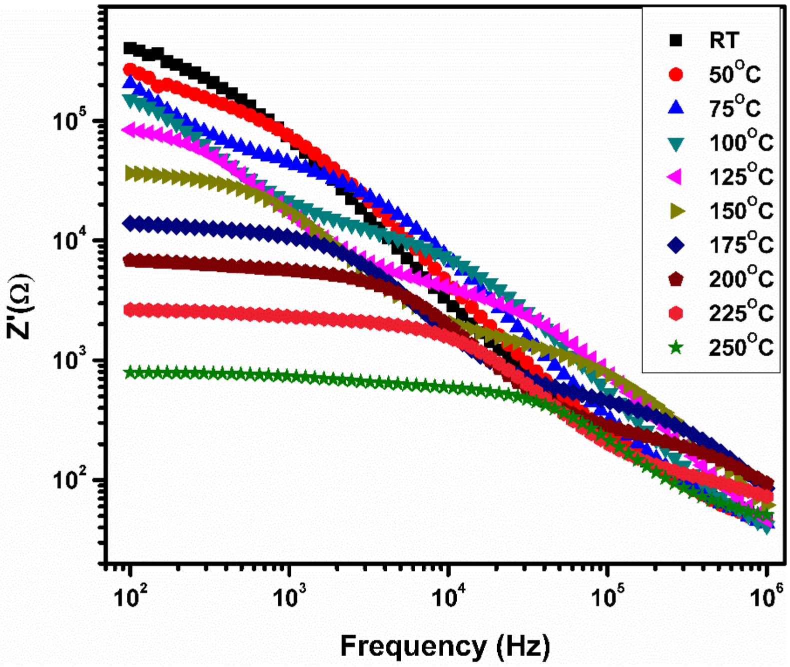

Fig 3.5. Frequency dependence of real part of impedance of bulk cobalt ferrite at selected temperatures

Figure 3.6 represents variation of imaginary impedance (Z'') as a function of frequency at different temperatures within experimental range of 100 H_z to 1 MH_z. The room temperature (RT) behavior shows single weak relaxation peak which ascribes to grain effect. With increase in temperature the peak shifts to higher frequency with decrease in intensity. At 75^0 C, an intense and broad peak enters through low frequency window. The coexistence of the intense and weak peak continues up to 150^0 C with peak shift towards high frequency end with reduced intensity and thereafter later one pushes out from frequency window. Another feeble peak appears at low frequency side at 175^0 C which gradually becomes prominent at elevated temperature and coexists with the intense one up to the last measured temperature 250^0 C. This unique feature of coexistence of two peaks has never been seen in any ferrite which was first time reported in Chen et al. [18]. While doing experiment with thick film of $CoFe_2O_4$, they found appearance of a weak peak at low frequency side at 100^0 C with already existing initially appeared broad peak which continues up to their measured end temperature. But unlike results on thick film of $CoFe_2O_4$, our work on bulk CFO system reports the appearance of successively three peaks with elevation of temperature with the coexistence of any two within frequency domain. While Chen et al. [18] proposed the co-contribution of grain and grain boundary showing a single relaxation behavior appeared as a broad peak followed by the appearance of relaxation process due to electrode interface effect, ours result reports the complete distinctive feature of all the intrinsic (grain) and extrinsic (grain boundary, electrode) effects. The peaks appear at elevated temperatures corresponds to the plateau relaxation frequency of Z' plot.

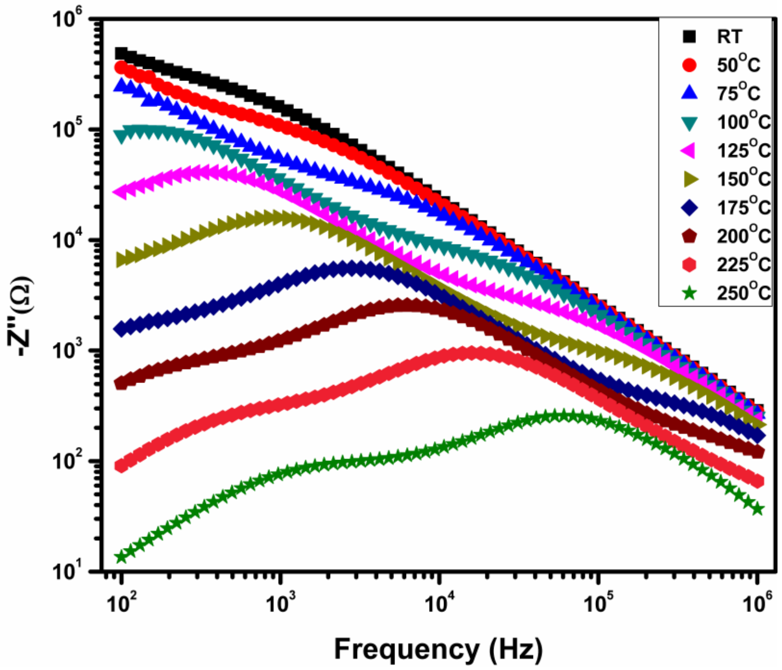

Fig 3.6. Frequency dependence of imaginary part of impedance of cobalt ferrite at selected temperatures

A polycrystalline system features with multi-grain arranged in different orientations has different effective regions which contribute to conductivity. Space charges trapped inside grain, grain boundaries and grain – electrode interfaces are the major charge carriers inside a ferrite system. The trapped charges inside grains activate at RT and follow short range hopping at low frequency side and localized hopping at high frequency domain. The relaxation behavior, therefore, observes at RT is completely liable to grains effect. The activation energy for charge carriers trapped near grain boundaries is comparatively higher which therefore; stagnate at their local sites with mere thermal oscillations. With elevation of temperature, the required thermal energy meets for the charge carriers and set their hopping mechanism. Therefore, the high temperature relaxation mechanism shown by the material at 75^0 C is attributed to grain boundaries. The charge carriers mostly follow long range order along the intergrain barriers. The electrode interface is characterized with a depletion region of ions and electrons. The thermal energy require for the liberation of depleted charges is little bit higher in these regions. Therefore, the charge carriers at this region activates at temperature higher than those of grain boundaries. The relaxation mechanism related to electrode interface effect comes later with elevated temperature.

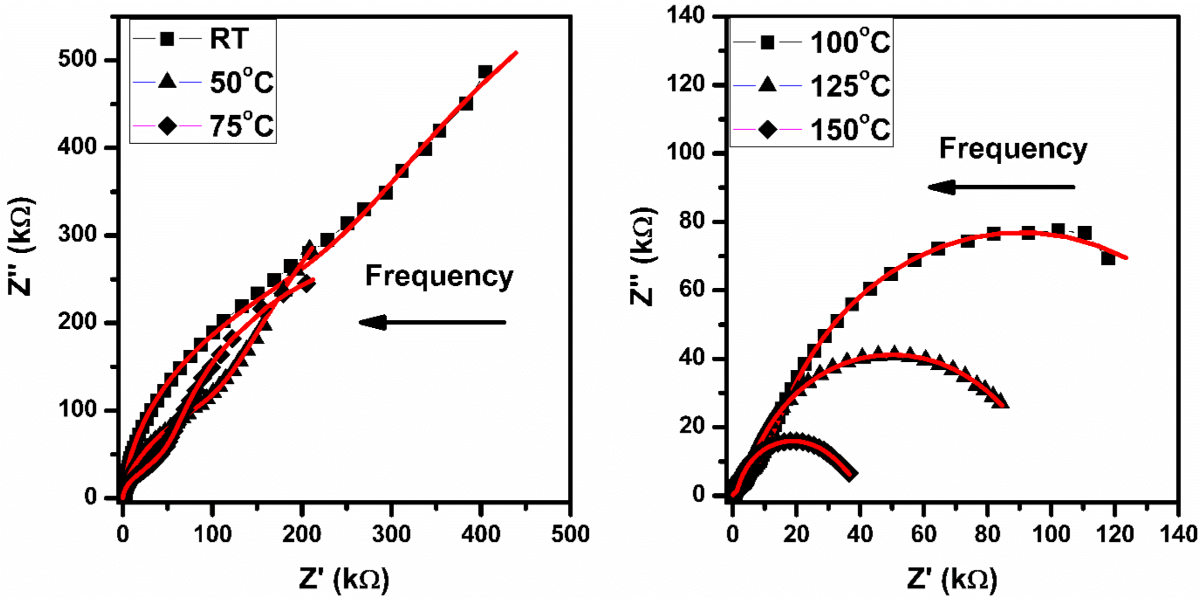

Fig 3.7 (a). Nyquist plots of cobalt ferrite at selected temperatures.

The Nyquist diagram of Z' vs Z'' (Figure 3.7) appears in the form of a semicircle or series of semicircles for an ideal dielectric showing Debye type relaxation. But most of the solids carrying various imperfections shows non-Debye type relaxation mechanism in which the semicircles appear asymmetry or little depressed having center below abscissa. Sometimes overlapped semicircles or arcs or spikes appear at different frequency regime within temperature domain which hints about

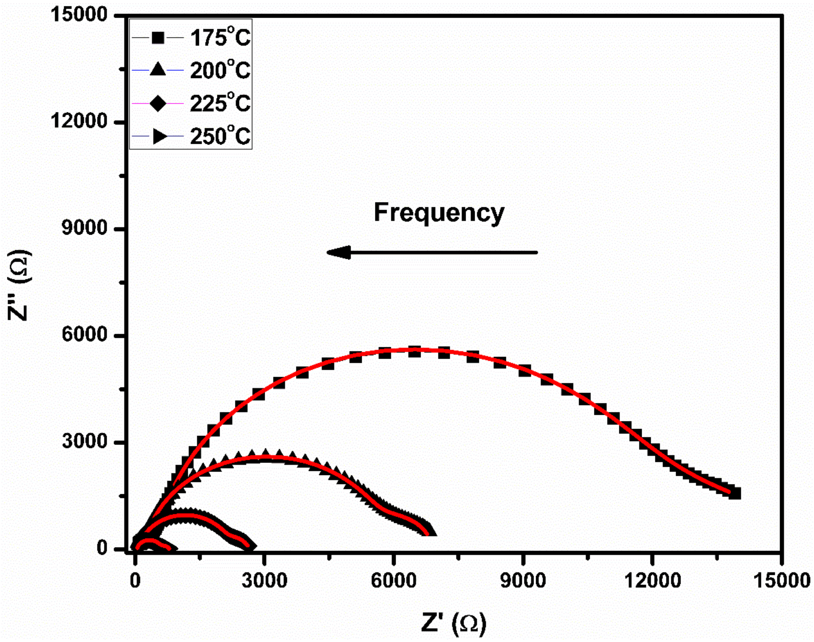

Fig 3.7 (b). Nyquist plots of cobalt ferrite at selected temperatures.

different relaxation and conduction mechanism. We observe three distinct semicircles of different radii at and around 175^0 C and 200^0 C in the Nyquist plot of CFO system. The semicircle appears at lowest frequency regime ascribes to electrode polarization effect, the middle one confers to grain boundary which appears at intermediary frequency range whereas the weak semicircle appears at high frequency side attributes to grain effect**.** Above 200^0 C and below 175^0 C**,** the three distinct semicircles turn up to two which suggests overlapping of either two effects. Contrast to the report of Chen et al. [18] on cobalt ferrite thick films, there is no such generation and degradation of semicircular arcs. In our work, rather reshaping of arcs takes place with elevation in temperature. At RT temperature, a semicircular arc of small radius appears at high frequency regime connected with a larger arc covering low frequency regime. The semicircular form at high frequency side suggests the conducting nature of grains whereas the arc with spike form at low frequency side indicates the resistive nature of grain boundaries and electrode interfaces. The evolution of arcs to semicircles with rise in temperature indicates increase in conductivity. This is due to the enhancement of hopping of space charges near grain boundaries and electrode interfaces at successive temperature range (75^0 C and 175^0 C respectively) whose response frequencies are different. Beyond 200^0 C, out of two Nyquist semicircles, one at lower frequency indicates increase in electrode interface conduction process whereas the one at high frequency side suggests the oneness in behavior of grains and grain boundaries. Unlike the co-contribution effect of grains and grain boundaries reported by Chen et al. [18], our result has shown the three distinct features of grain, grain boundaries and interface effects. Contrary to the report of Rahman et al. [24] of semiconductor to metallic transition in nanostructured $CoFe_2O_4$ within temperature range 27^0 C to 127^0 C, ours result shows no such transition, rather maintains its semiconducting nature up to 250^0 C.

In a comparative study of our work on bulk CFO with the nanostructured $CoFe_2O_4$ reported by Rahman et al. [24], electrode interface effect is absent in the later whereas it dominates after 175^0 C in our case. In comparision with cobalt ferrite thick film of Chen et al. [18] a single relaxation behavior reported for grains and grain boundaries whereas a distinct grain boundaries effect appears at 75^0 C is observed in our study which continues up to the end measured temperature. Therefore, we suggest the ratio of number of grain boundaries to electrode boundaries is a decisive factor of being dominant and prominent in high temperature impedance spectrum. The finite size of grains and number of grain boundaries make significant and distinctive contribution in bulk CFO system compared to the thick films where their contribution is indistinctive. These Nyquist semicircles are well fitted with the help of Z Simpwin software that gives equivalent circuits of RC-RC-RQ below 175^0 C and above with RC-RQ-RQ where Q is the constant phase element related to resistance and capacitance is $C= Q^{1/n} R^{(1-n)/n}$ and n =1 for pure capacitor and zero for resister [25].

3.3.2.2. Modulus analysis

The imaginary impedance loss spectra show a weak grain effect compare to grain boundaries and electrode effect which sometimes difficult to analyze. As electric modulus spectra highlight the smaller capacitance value [26], it will magnify the grain effects which will be easier to analyze. With this purpose, we have analyzed our results in the context of electric modulus formalism. Figure 3.8 shows M' vs M'' plot of bulk cobalt ferrite. The data indicates two well resolved semicircles: the first semicircle at low frequency regime represents the capacitive grain boundaries effect at elevated temperatures and the second one at high frequency regime represents the capacitive grain effect at low temperatures. Grain and grain boundary effect fall into two different temperature regions: (i) below 75^0 C as low temperature region and (ii) at and above 75^0 C as high temperature region. As per above classification, well resolved big semicircles appear at high frequency side which degenerate with increase in temperature. A new arc appears at 75^0 C at low frequency side which signals the evolution of grain boundaries effect. At about 125^0 C, the arc takes its full semicircle form and grows with elevation of temperature up to 250^0 C but the complete degeneration of grains effect never occurs. The most capacitive electrode effect is suppressed successfully.

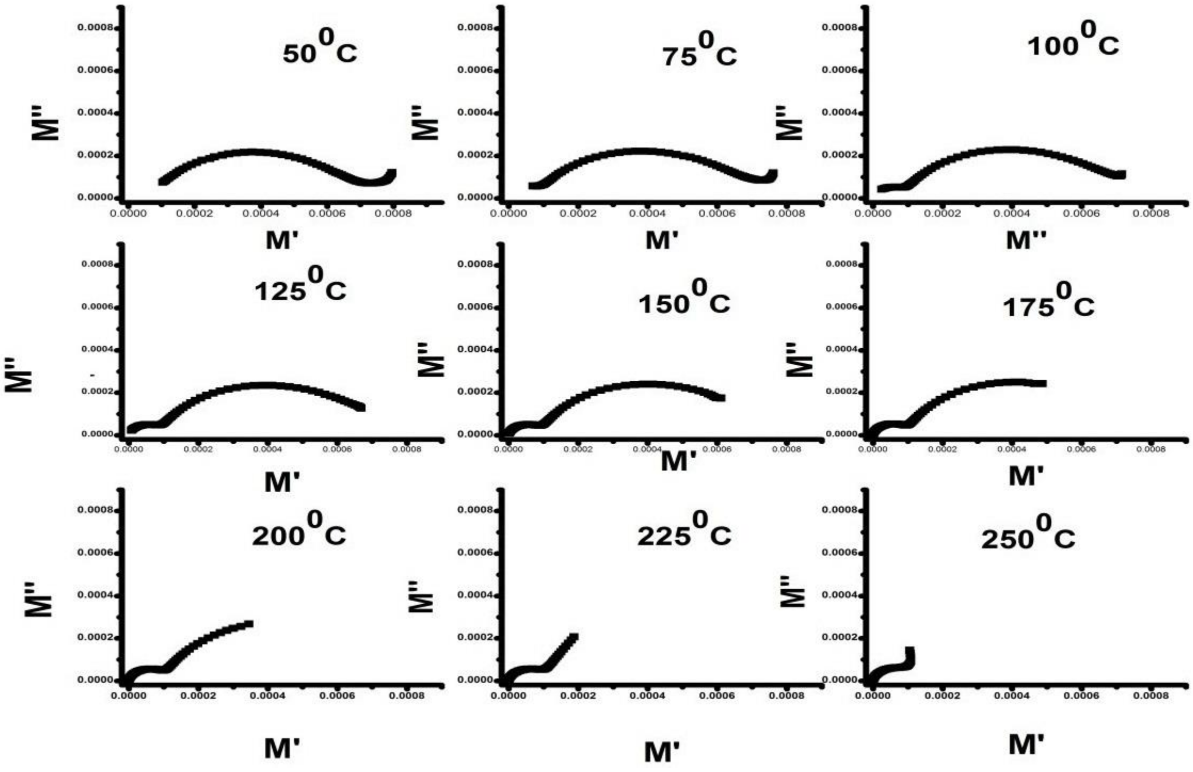

Fig 3.8. Cole-Cole plot of modulus of cobalt ferrite at selected temperatures.

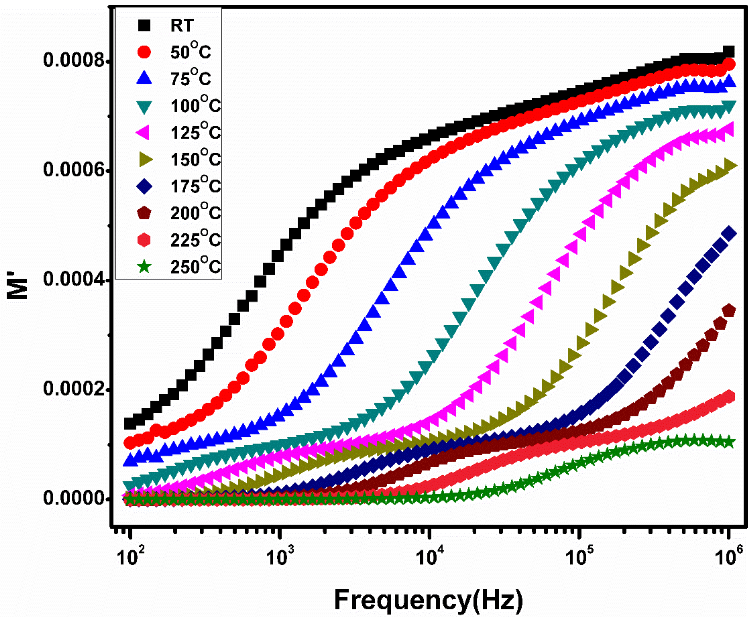

Fig 3.9. Frequency dependence of real electric modulus of cobalt ferrite at selected temperatures.

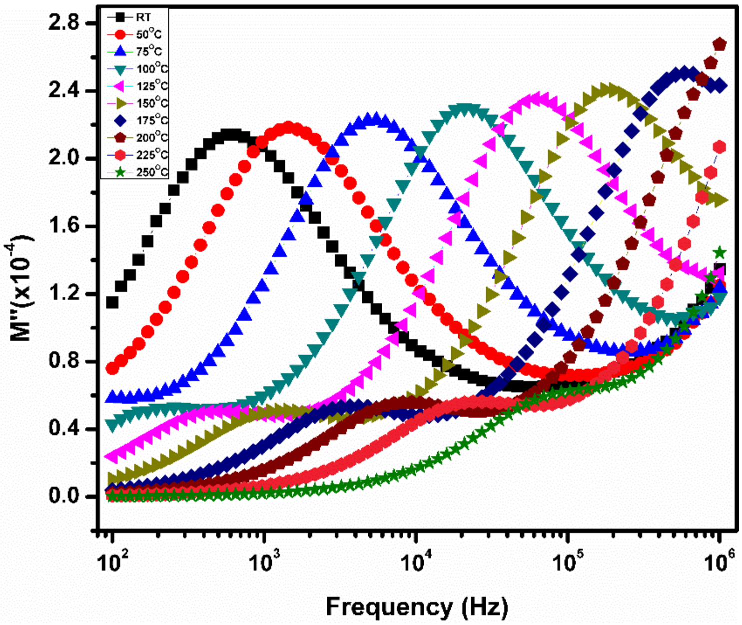

Fig 3.10. Frequency dependence of the imaginary part of the modulus of cobalt ferrite at selected temperatures

Figure 3.9 and 3.10 represent the real (M') and imaginary modulus (M'') variation against frequency of CFO system respectively. In M' plot, all the curves attain to asymptotic form at higher frequencies. The imaginary modulus spectra M'' against frequency of bulk CFO is shown in Fig.3.10 at all the studied temperatures. Similar to impedance spectra, at low temperature only one peak due to grains appear in the plot. The double peaks which appear within 75^0 C-175^0 C confirm the coexistence of grains and grain boundaries effects. The small height of grain boundaries peak is due to its higher capacitive value than grains. The response frequency of grains and grain boundaries correspond to two different frequency regimes. The peaks shift to higher frequency side with elevated temperature and the grains peak leave the frequency window at 200^0 C. The absence of any peak thereafter suggests the highest capacitive region of electrode effect has been suppressed.

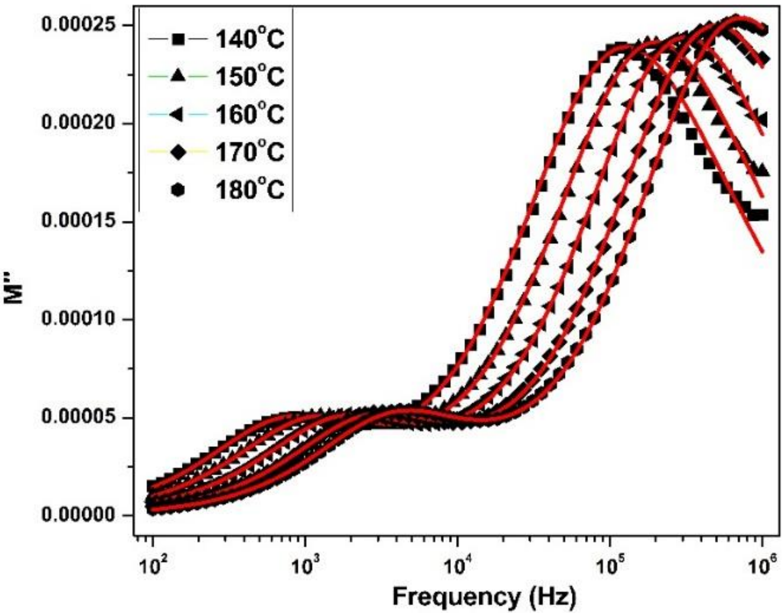

Fig 3.11. Fitted double curves of the imaginary modulus of cobalt ferrite

The double peak in imaginary modulus is well fitted (figure 3.11) with the Bergman proposed KWW function [27]

$$M'' = M''_{max}/[1 - \beta + \left(\frac{\beta}{1+\beta}\right)\left(\beta\left(\frac{\omega_{max}}{\omega}\right) + \left(\frac{\omega}{\omega_{max}}\right)^{\beta}\right] \qquad 3.1$$

Where M''$_{max}$ peak maxima and ω_{max} is corresponding frequency and β is the stretching factor ($0<\beta<1$) which decides whether the relaxation in dielectric is Debye or non-Debye in nature [28]. For an ideal dielectric $\beta = 1$. Relaxation time *t* can be found from the relaxation frequency w. The β_{gb} is found to be 0.86 and $\beta_g = 0.62$ from the fitted curve which is less than one which indicates the non-Debye type relaxation in the CFO system. Siva Kumar et al. [16] found increase in β value with grain size which we suppose due to increase in effective grain boundaries. This parameter also relates to the interaction among mobile charge carriers [28] which are stronger inside grain and comparably weak at grain boundaries. The grain interior experiences strong interaction among charge carriers which reduces their mobility as well as conductivity. In contrast, charge carriers experience weak interaction along grain boundaries which suggests increase in conductivity. The more flexibility in movement of carriers results more polarization which in turn raises the value of β near grain boundaries. The β parameter is also found to be independent of temperature and frequency.

3.3.2.3. Dielectric properties

The dielectric behavior of bulk $CoFe_2O_4$ is shown in the Figure 3.12. The low frequency regime observes high permittivity value whereas the high frequency regime observes comparatively low value. The relative permittivity value increases with elevation of temperature. Two relaxation processes appear, one at 75^0 C and another one at175^0 C at low frequency side shifts to higher frequency end with rise in temperature. Siva Kumar et al. [29] reported that space charge polarization plays a major role in inhomogeneous nature of dielectric properties in MnZn ferrites. The $PbZr_xTi_{1-x}O_3$/CFO layered thin films reported by Ortega et al. [30] have explained their unusual high dielectric constant due to contribution of grain boundaries effects. On the basis of above reports and our findings, the space charge polarizations near various interfaces (grain boundaries and electrode barrier) plays important role in contributing dielectric behavior of bulk CFO system. In ferrites, the exchange interaction of Fe^{2+}- Fe^{3+} is a dominating process of conduction mechanism in which electrons exchange displacement produce in the direction of applied field [31].

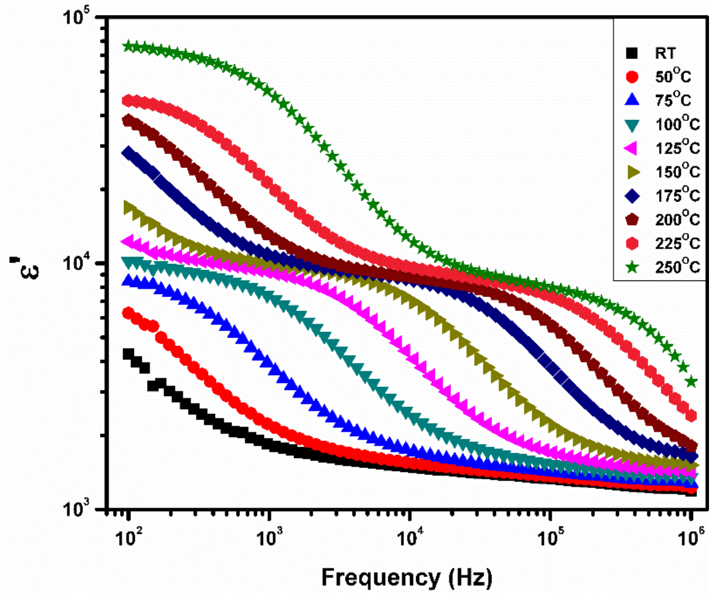

Fig 3.12. Frequency dependence of dielectric constant of cobalt ferrite at selected temperatures

Jonker [32] has studied the electrical conduction mechanism of ferrites $Co_{1-x}Fe_{2+x}O_4$ where he found two distinct regions of conductivity. He cited the low conductivity region contains Co^{2+} and Co^{3+} ions whereas high conductivity region contains Fe^{2+} and Fe^{3+} ions. But the presence of cobalt on the octahedral site of the inverse spinel favors a conduction mechanism $Co^{2+}+Fe^{3+} \leftrightarrow Co^{3+}+Fe^{2+}$, which explains the predominant conduction mechanism in cobalt ferrite. In bulk cobalt ferrite system, cations distributed as [Fe^{3+}](Co^{2+} Fe^{3+}) which suggests c-a-c interaction between Fe^{3+}-O^{2-}- $Fe^{3+}$and Co^{2+} - O^{2-}- Co^{2+} at octahedral sites is stronger as compared to c-c interaction [25] i.e. Fe^{3+}-Fe^{3+} or Co^{2+} - Co^{2+}.

The conduction and polarization behavior are interrelated as the former promotes the later. At high temperature, space charges near grain boundaries and electrode contacts are activated and have their displacement along the field direction. This causes space charge polarization which is highly temperature dependent. As temperature rises, thermal fluctuation helps them to follow the changing applied field which speeds up the polarization and also thermal energetic charge carriers travel through grains pile up near interfaces which enhances the polarization by a certain amount. This contributes to giant dielectric value of CFO system. At sufficient high frequency, space charge dipoles are unable to follow the fast changing ac cycles which reduces the polarization as well as permittivity value. But unlike any ferroelectric system, there is no such sharp decline of dielectric constant after transition temperature.

3.3.2.4. Dielectric loss

Dielectric loss represents the energy dissipation in a dielectric material [33]. It develops on account of lagging behavior of polarization from the applied ac filed due to the grain boundaries, impurities and imperfections in the crystal lattice of the materials [16,33]. It can be defined as [16]

$$Tan\delta \ = \frac{Z'}{Z''} = \frac{\epsilon'}{\epsilon''} = \frac{(\epsilon_0 - \epsilon_\infty)\omega\tau}{\epsilon_0 + \epsilon_\infty \omega^2 \tau^2} \qquad 3.2$$

where δ is the phase difference between the applied fields and induced current. Loss spectrum of the cobalt ferrite is shown in figure 3.13. Dielectric loss decreases with increasing frequency and increases with temperature. The decreasing nature of dielectric loss with frequency is due to the lagging of jumping rate of charge carriers behind applied field beyond a certain frequency. The loss is increasing with temperature because of the increase in mobility of charge carriers that increase the hoping rate which reduces the relaxation time. According to the above equation relaxation time is inversely proportional to the dielectric loss. Therefore, relaxation time decreases with increasing temperature that leads to increase in dielecric loss. There is a peak in the loss spectrum due to the jumping frequency of charge carriers between Fe^{3+}-Fe^{2+} nearly equal to that of the externally applied electric field, a maximum of loss may be observed and it appear as a peak [34]. The peak in loss spectrum shifts towards higher temperature with increasing frequency has been observed. This is because of the charge carriers unable to follow the field at higher frequencies hence, decrease in polarization [35].

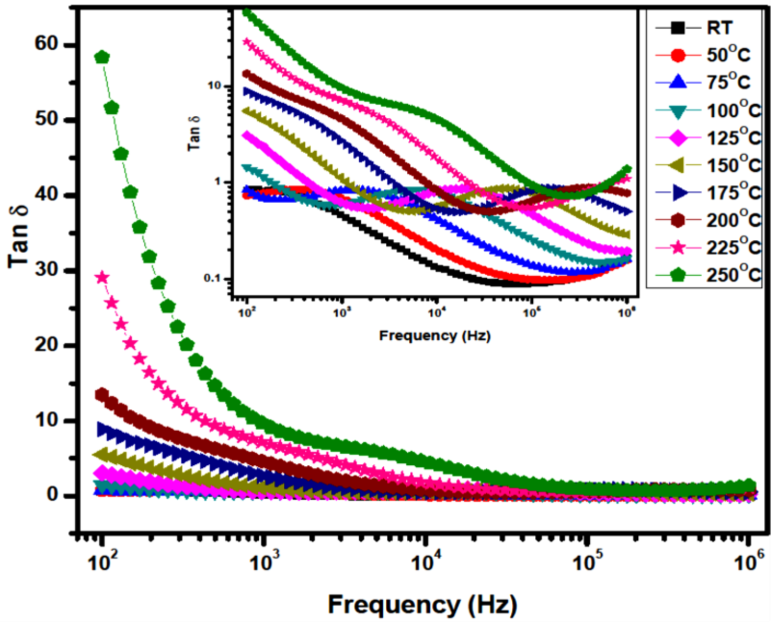

Fig 3.13. Loss spectrum of bulk cobalt ferrite

3.3.2.5. Conductivity analysis

Figure 3.14 represents the ac conductivity behavior of polycrystalline cobalt ferrite. In a comparative analysis with impedance spectra, the conductivity data gives two different results at low temperature belt (< 75^0 C) and high temperature belt (≥75 ^{0}C). The low temperature region shows a slow transition from a weak frequency dependent conductivity to strong frequency variant part. The high temperature belt shows a plateau region (almost frequency independent) represents dc conductivity which gradually varies to strong frequency variant region. The plateau region strengthens with elevated temperature. The high temperature belt ac conductivity plot can be categorized into three distinct regions, dc plateau followed by gradual frequency variant region and fast frequency dependent region. The dc conductivity arises due to movement of charge carriers of long range order which appears at <1 kHz at 75^0 C and extends up to <100 kHz at 250^0 C. The plateau followed by gradual frequency variant region which arises due to short range hopping of ions, electrons in conduction process [30]. The fast frequency dependent region appears at high frequency regime as the conduction process, is due to the localized relaxation hopping mechanism of ions or electrons.

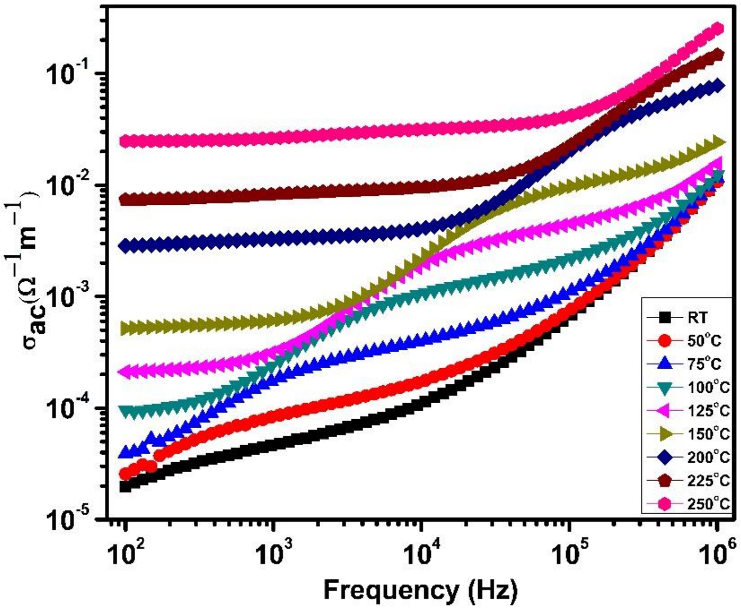

Fig 3.14. Frequency dependence of AC conductivity at selected temperatures for cobalt ferrite

According to jumping relaxation model the conductivity in ferrites is due to the hoping mechanism of charge carriers [30, 36]**.** There are two types of hopping mechanism, one is successful hopping and second is unsuccessful hopping. In successful hopping mechanism neighbor ion relaxes to a position when the concerned ion takes a new vacant site. This makes a possibility of long range movement of charge carriers and gives dc conductivity. In unsuccessful hopping, ions relax themselves by jumping forward and backward about their own site and are termed as localized relaxation hopping mechanism. This is highly frequency dependent and gives dispersive region. In comparative study with the impedance spectra, we notice that the dc plateau strengthens at high temperature when grain boundary and electrode interface become effective region for conduction mechanism i.e. successful hopping of ions find barrier layers as most preferable region. As frequency approaches relaxation point, charge carriers hop through short distance before the cycle changes. This results slow frequency variant region. Beyond relaxation frequency, thermal energy cannot drive the ions to a long range in order to follow the changing ac cycle rather a localized movement is possible which gives the fast frequency variant region.

3.3.2.6. DC electrical resistivity

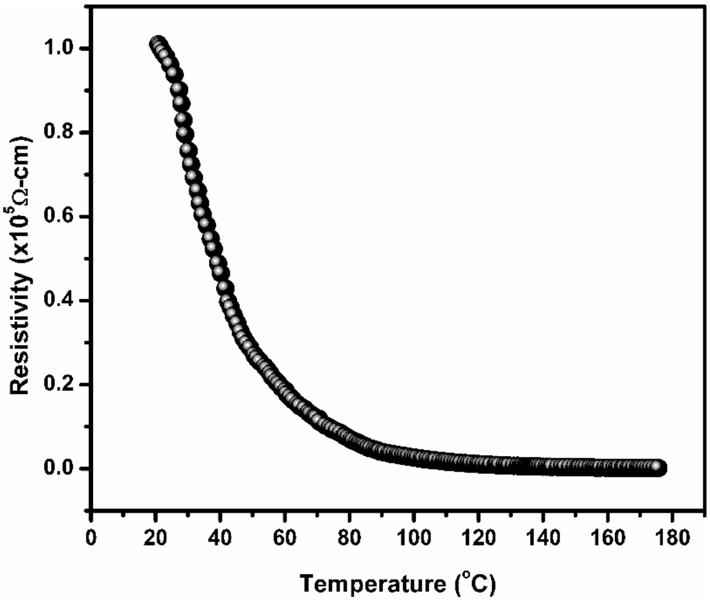

Fig 3.15. Temperature dependence of dc resistivity of cobalt ferrite

Temperature dependence of dc resistivity is shown in figure 3.15. Resistivity exponentially decreases with the temperature, which is typical semiconducting behavior of cobalt ferrite. The activation energy of the cobalt ferrite calculated by applying the Arrhenius law (shown in fig. 3.16) and is found to be 0.51 eV. The conduction in ferrites is due to the charge transfer between the multi oxidation states of same element present in the octahedral sites. (The detailed conduction mechanism is explained in the second chapter). Due to the increase in temperature, charge carriers gain thermal energy resulting in the increase in hopping rate and leads to decrease in resistance.

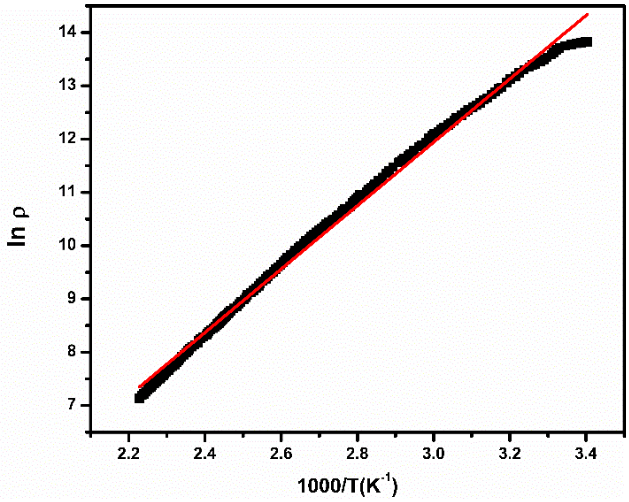

Fig 3.16. Arrhenius plot of the bulk cobalt ferrite

3.4. Magnetic properties

Room temperature field dependent magnetic properties of the cobalt ferrite is shown in the figure 3.17. It exhibits M-H loop at room temperature which represents the ordered state of sample at room temperature. Saturation magnetization and coercivity is found to be 80 emu/g and 273 Oe respectively for the sample. The magnetic properties of the cobalt ferrite strongly depends on the cation distribution between the tetrahedral and octahedral sites [37, 38] and grain/particle size of the ferrites [38,39]. In ferrimagnetic materials net magnetization is equal to difference between the individual magnetic moments of antiferromagnetically interacted octahedral (A) and tetrahedral (B) sites. i.e $M=M_A-M_B$ [40]. In bulk form cobalt ferrite exhibits inverse spinel structure where cobalt occupies only octahedral site and iron equally distributed in octahedral and tetrahedral sites [1-5]. So the magnetic moments of the iron cancel each other because of antiferromagnetic interaction and the magnetization contribution comes from cobalt only in ideal case.

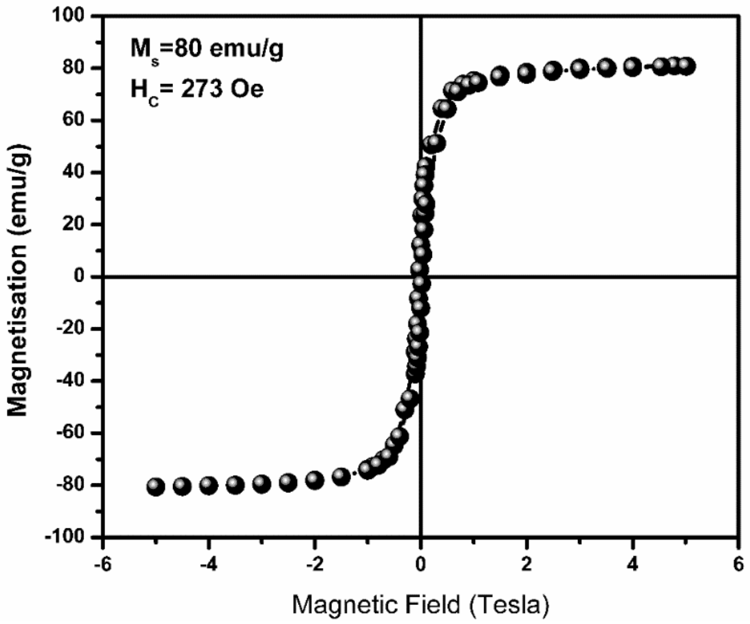

Fig 3.17. M-H loop of cobalt ferrite at room temperature

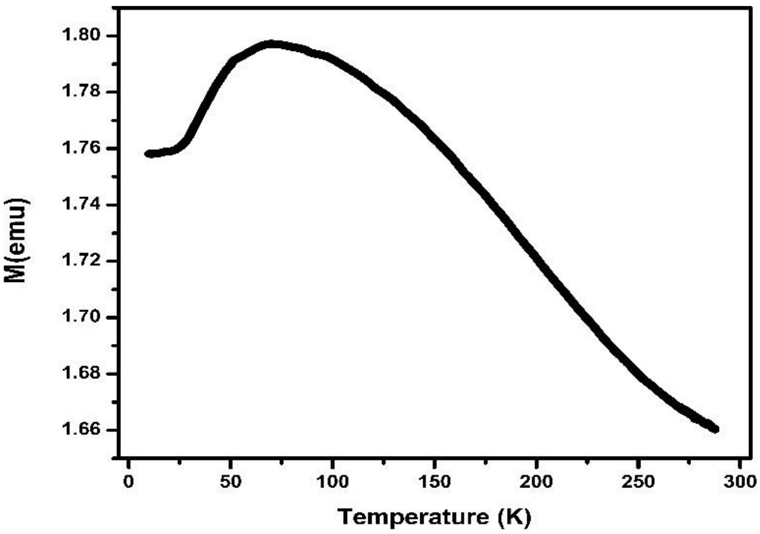

Fig 3.18. Temperature dependence of magnetization for cobalt ferrite at 100 Oe

The temperature dependence of the field cooled curve of the bulk cobalt ferrite is shown in figure 3.18. The magnetization increases with decreasing temperature and gets maximum value at 75 K. This nature is due to two oppositely interacted sub lattices A and B. If the magnetization of sub-lattice A decreases less rapidly with temperature than the sub-lattice B then the resultant magnetization increases with temperature before finally dropping to zero [41]. This kind of behavior also observed in the cobalt ferrite synthesized by the different methods [41- 43].

3.5. Conclusion

Single phase polycrystalline cobalt ferrite, synthesized by the conventional ceramic route was confirmed from the XRD analysis. The surface morphology was observed to be densely packed with irregular grains. By the help of complex impedance spectroscopy, the investigation successfully discovered Maxwell-Wagner polarization as responsible for the strong dielectric behavior of bulk $CoFe_2O_4$. Grain effects found to be dominated at low temperature whereas interfacial polarization played important role in conduction mechanism at high temperature which witnessed the inter-competition between grain boundary and electrode effect within frequency windows. The non-Debye type of relaxation behavior is confirmed from the stretched exponent parameter β value which is far away from unity, calculated from imaginary electric modulus spectra. The space charge polarization near interfaces is responsible for dielectric behavior of CFO system. Apart from electron exchange interaction in Fe^{2+} - Fe^{3+}, the inverse spinel favours a conduction mechanism $Co^{2+}+Fe^{3+} \leftrightarrow Co^{3+}+ Fe^{2+}$ in which long range order of charge movement happens at high temperature belt at intermediate frequency regime along with short range hopping and localized relaxation hopping mechanism at high frequency. Room temperature M-H loop indicates the orderedness of the ferrimagnetic cobalt ferrite. Temperature dependence of the magnetization exhibits maximum at 70^0 C due to its ferrimagnetic nature.

References

[1] A.K. Giri, E. M.Kirkpatrick, P. Moongkhamklang, and S.A. Majetich, Applied Physics Letters 80 (2002) 2341-2343.

[2] S.J.Lee, C.C.H Lo, P.N.Matlage, S.H.Song, Y.Melikhov, J.E.Snyder, and D.C.Jiles Journal Applied Physics 102 (2007) 073910.

[3] K.Kamal Bharati, R.J. Tackett, C.E.Botez and C.V. Ramana Journal Applied Physics 109 (2011) 07A510.

[4] Simona Burianova, Jana Poltierova Vejpravova, Petr Holec, Jiri Plocek and Daniel Niznansk, Journal Applied Physics 110 (2011) 073902.

[5] K.Vasundhara, S.N. Achary, S.K. Deshpande, P.D. Babu, S. S. Meena and A.K. Tyagi, Journal of Applied Physics 113 (2013) 194101.

[6] A.K. Nikumbh, A.V. Nagawade, V.B.Tadke and P.P. Bakare, Journal of Materials Science 36 (2001) 653.

[7] G.D. Dwivedi, K.F.Tseng, C.L. Chan, P. Shahi, J. Lourembam , B.Chatterjee, A.K. Ghosh, H.D.Yang and Sandip Chatterjee, Physical review B 82 (2010) 134428.

[8] A.Franco, Jr., and F.C.e Silva, Applied Physics Letters 96 (2010) 172505.

[9] S.J.Lee, S.H.Song, C.C. Lo, S.T. Aldini and D.C. Jiles, Journal Applied Physics 101 (2007) 09C502.

[10] A.Franco Jr., F.L.A Machado, V.S.Zapf and F.W. Fabris, Journal Applied Physics 109 (2011) 07A745.

[11] S.P.Yadav, S.S.Shinde, A.A. Kadam and K.Y.Rajpure, Journal of Alloys and Compounds 555 (2013) 330.

[12] Y. Cedeño Mattei, O. Perales-Perez, M.S.Tomar, F. Roman, P.M Voyles and W. G. Stratton, Journal Applied Physics 103 (2008) 07E512.

[13] A.V.R. Reddy, G. Ranga Mohan, D. Ravinder, B. S. Boyanov, Journal of materials science 34 (1999) 3169.

[14] K. Kamala Bharathi and C.V. Ramana, Journal of Materials Research 26 (2011)584.

[15] G. Dascalu, T.Popescu, M.Feder and O.F.Caltun, Journal of Magnetism and Magnetic Materials 333 (2013) 69.

[16] N. Sivakumar, A. Narayanasamy, C. N. Chinnasamy and B.Jeyadevan, J. Phys.: Condens. Matter 19 (2007) 386201.

[17] M.George, S.S. Nair, K.A. Malini, P.A. Joy and M.R. Anantharaman, J. Phys. D: Appl. Phys. 40 (2007) 1593.

[18] W. Chen, W. Zhu, O. K. Tan and X. F. Chen, Journal of Applied Physics 108 (2010) 034101.

[19] Cameliu Himcinschi, Ionela Vrejoiu, Georgeta Salvan, Michael Fronk, Andreas Talkenberger, Dietrich R. T. Zahn, David Rafaja, and Jens Kortus, Journal of Applied Physics 113 (2013) 084101.

[20] Razia Nongjai, Shakeel Khan, K. Asokan, Hilal Ahmed, and Imran Khan, Journal of Applied Physics 112 (2012) 084321.

[21] S. Urcia-Romero, O. Perales-Pérez, and G. Gutiérrez, Journal of Applied Physics 107 (2010) 09A508.

[22] Sateesh Prathapani, M. Vinitha, T. V. Jayaraman, and D. Das, Journal of Applied Physics 115 (2014) 17A502.

[23] Sateesh Prathapani, Tanjore V. Jayaraman, Eswara K. Varaprasadarao, and Dibakar Das, Journal of Applied Physics 116 (2014) 023908 .

[24] A. Rahman, M. A. Rafiq, S. Karim, K. Maaz, M. Siddique and M. M. Hasan, J. Phys. D: Appl. Phys. 44 (2011) 165404.

[25] A. Rahman, M. A. Rafiq, K. Maaz, S. Karim, S. O. Cho, and M. M. Hasan, Journal of Applied Physics 112 (2012) 063718.

[26] A. Rouahi, A. Kahouli, F. Challali, M. P. Besland, C. Vallée, B. Yangui, S. Salimy, A. Goullet and A. Sylvestre, J. Phys. D: Appl. Phys. 46 (2013) 065308.

[27] R.Bergman Journal of Applied Physics 88 (2000) 1356.

[28] K. S. Rao, P. M. Krishna, D. M. Prasad and D. Gangadharudu, J Mater Sci 42 (2007) 4801.

[29] N.Sivakumar, A.Narayanasamy, B. Jeyadevan, R.J.Joseyphus and Venkateswaran J. Phys. D: Appl. Phys. 41 (2008) 245001.

[30] N. Ortega, A. Kumar, P. Bhattacharya, S. B. Majumder and R. S. Katiyar, Physical Review B 77 (2008) 014111.

[31] S. M. Patange, S. E. Shirsath, B. G. Toksha, S. S. Jadhav and K. M. Jadhav, Journal of Applied Physics 106 (2009) 023914.

[32] G.H. Jonker, Journal of Physical Chemistry Solids 9 (1959) 165.

[33] Y. D. Kolekar, L. J. Sanchez, and C. V. Ramana, Journal of Applied Physics 115 (2014) 144106.

[34] N. Sivakumar, A. Narayanasamy, N. Ponpandian, and G. Govindaraj, Journal of Applied Physics 101 (2007) 084116.

[35] D. G. Chen, X. G. Tang, Q. X. Liu, Y. P. Jiang, C. B. Ma, and R. Li, Journal of Applied Physics, 113 (2013) 214110.

[36] R. Nongjai, S. Khan, K. Asokan, H. Ahmed, and I. Khan, Journal of Applied Physics 112 (2012) 084321.

[37] M. Atif, R. Sato Turtelli, R. Grossinger, and F. Kubel, Journal of Applied Physics, 113 (2013) 153902.

[38] Lawrence Kumar, Manoranjan Kar, Ceramics International 38 (2012) 4771.

[39] K. Vasundhara, S. N. Achary, S. K Deshpande, P. D. Babu, S. S. Meena, and A. K. Tyagi, 113 (2013) 194101.

[40] A. Bouhas, M. Amzal and B. Zouranen, Material chemistry and Physics 33 (1993) 80.

[41] A. Franco, Jr., F. L. A. Machado,V. S. Zapf, and F. Wolff-Fabris, Journal of Applied Physics, 109 (2011) 07A745.

[42] Y. Melikhov, J. E. Snyder, D. C. Jiles, A. P. Ring, J. A. Paulsen, C. C. H. Lo, and K. W. Dennis, J. Appl. Phys. 99 (2006) 08R102.

[43] N. Ranvah, I. C. Nlebedim, Y. Melikhov, J. E. Snyder, P. I. Williams, A.J. Moses, and D. C. Jiles, IEEE Trans. Magn. 45 (2009) 2861.

CHAPTER 4

Investigations on conduction mechanism and magnetic properties of cobalt ferrite nanoparticles

This chapter describes the electric transport and room temperature magnetic behavior of nano cobalt ferrite nanoparticles. Ac electrical properties were measured within frequency window of 100 Hz to 1 MHz in the range of temperature of 25^o C to 200^o C. No grain relaxation was observed whereas interfaces (grain boundary and electrode surface contact) became the dominant conduction regions. Both ac and dc conduction mechanism was investigated thoroughly. Overlapping of large polaron tunneling (OLPT) mechanism was found to be responsible for ac conduction process. The value obtained for mobility (10^{-10} cm^2/Vs) of charge carriers indicated the possible small polaron hopping for dc conduction process. The dc resistivity data was fitted with Mott and Davis model and the derived parameters confirmed the dc conduction of non- adiabatic nature which was due to small polaron hopping in nano cobalt ferrite. M-H loop at room temperature indicates the ferrimagnetic nature of the cobalt ferrite nanoparticles and exhibits lower saturation magnetization as compared to the bulk.

4.1. Introduction

Insulating magnetic materials are in growing demand for certain applications as they have the ability to suppress various losses, particularly the hysteresis loss. In this respect spinel ferrites have been a source of attraction for researchers for their strong magnetic behavior with insulating in nature [1- 4]. Nano ferrites have been observed with drastic change in magnetic properties counter to their bulk part [5]. Several Nano ferrites are rigorously studied and tuned their magnetic behavior with suitable dopants [6-9]. Cobalt ferrite (CFO) has been emerged as the highly studied material in this case [10-12].

CFO has spinel structure in which larger oxygen ions forms FCC lattice and the octahedral and tetrahedral interstitial sites formed by the oxygen ions occupied by the metal cations (Co^{2+}, Fe^{2+}) [13,14]. The general formula of CFO can be represented by $(Co_{1-X}\ Fe_X)_A$ $(Co_XFe_{2-X})_B\ O_4$ where A, B and x represents tetrahedral, octahedral and degree of inversion respectively [15,16]. The degree of inversion mostly depends on the synthesis procedure and calcination temperature [17,18]. If x =1 then it is a completely inversion structure with chemical formula $(Fe)_A(Co\ Fe)_BO_4$, if x = 0 then it is normal spinel otherwise it is mixed spinel. The CFO generally exhibits mixed spinel structure in which both sites occupied by the fraction of metal cations [19-21]. The nano ferrites will be more versatile material if it will be open for both magnetic and electric application. Investigation of electric transport behavior through impedance spectroscopy has taken a new shape in this direction to analyze the electric properties of nano ferrites, which we observed; a little attention has been paid yet to nano cobalt ferrite. Arun kumar et al. [22] has reported that the behaviour of nano CFO depends upon the particle size. For particle size ranging around 6 nm, the material shows metallic trend of nature whereas semiconducting nature reflects for bigger size of 52 nm. Kannan et al. [23] also observed the same metallic behaviour of nano CFO for particle ranges 2-16 nm with superparamagnetic properties. Rehman et al. [24] has also reported the semiconducting to metallic transition of nano CFO of range 10 nm which they prepared by co precipitation method. All the above studies have focused that the electrical behaviour of nano CFO is particle size dependent and below or around 50 nm the metallic behaviour substitutes the general semiconducting nature of CFO.

In our present work we have investigated the electrical properties of nano CFO of range far bigger than 50 nm and less than 100 nm, which we have prepared by auto combustion technique. We have correlated the obtained result with our previous work [25] on bulk CFO.

In contrast to bulk behavior where both grain and interfacial effect exist; we found that in nano CFO, only the interfacial effect such as grain boundary and surface polarization were the major region of conduction and the responsible source for their dielectric behavior. Nano particle which also behave as nano grain has insufficient room for any type of intra-grain relaxation properties. Room temperature M-H loop study reveals that saturation magnetization is lower than the bulk cobalt ferrite but enhanced coercivity observed in cobalt ferrite nanoparticles.

4.2. Materials and methods

CFO nanoparticles were prepared by the auto combustion method. Analytical grades cobalt nitrate $Co(NO_3)2.6H_2O$, ferric nitrate $Fe(NO_3)_3.9H_2O$ were taken as oxidants while glycine $C_2H_5NO_2$ was employed as fuel to drive the combustion reaction. The stoichiometric amounts of these nitrates dissolved in the deionized water to make precursor solution which was stirred and preheated up to 100^0 C to get the voluminous fluffy product. Finally this powder was calcined at 750^0 C for three hours. The crystal structure, phase identification and particle size of the CFO was determined by the Rigaku Ultima-IV X-ray diffractometer (Cu target) and the morphology of the CFO nanoparticle was estimated by the Nova NanoSEM-450 Field emission scanning electron microscopy (FESEM). Impedance with respect to frequency was measured by using HIOKI impedance analyzer (model IM3570) from 100 Hz to 1 MHz up to 200^0 C. DC resistance was measured by the Keithley electrometer (model 6517B) up to 200^0 C.

4.3. Results and discussion

4.3.1. Structural analysis

X-ray diffraction pattern of the CFO nanoparticles is shown in figure 4.1. There are no secondary peaks and all the peaks belong to spinel CFO. The particle size of the CFO nanoparticles estimated using Scherer formula

$$d = \frac{0.94\lambda}{\beta cos\theta} \qquad 4.1$$

where λ is wavelength of the x-ray, β the is full width half maximum and θ is the Bragg angel. By considering the most intense plane (311), the particle size was found to be 70 nm. The lattice parameter was estimated by using formula $a = d(h^2 + k^2 + l^2)^{1/2}$ where d is the spacing and (h,k,l) are the miller indices, is found be 8.372 Å. A typical FESEM image of the CFO nanoparticles

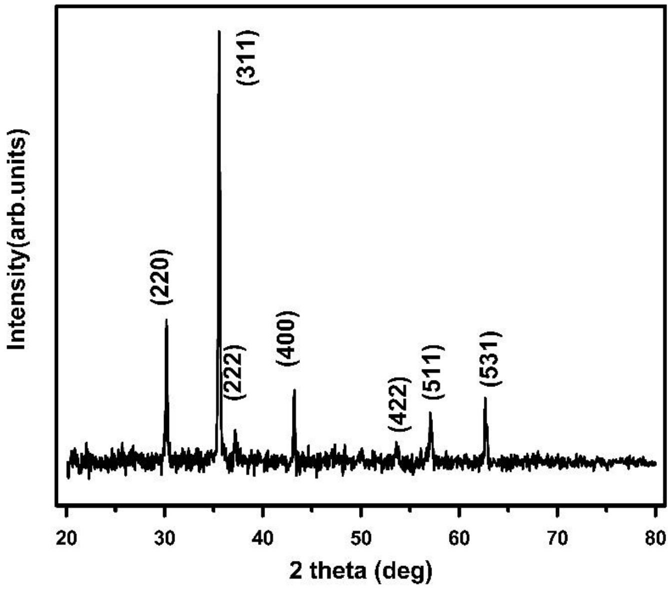

Fig 4.1. XRD pattern of the cobalt ferrite nanoparticles.

is shown in the figure 4.2. It has clearly seen that the particles are agglomerated and the average particle size found from the size distribution is 67 nm which is comparable to the particle size obtained from the XRD data. The particle size distribution of cobalt ferrite nanoparticles is shown in figure 4.3.

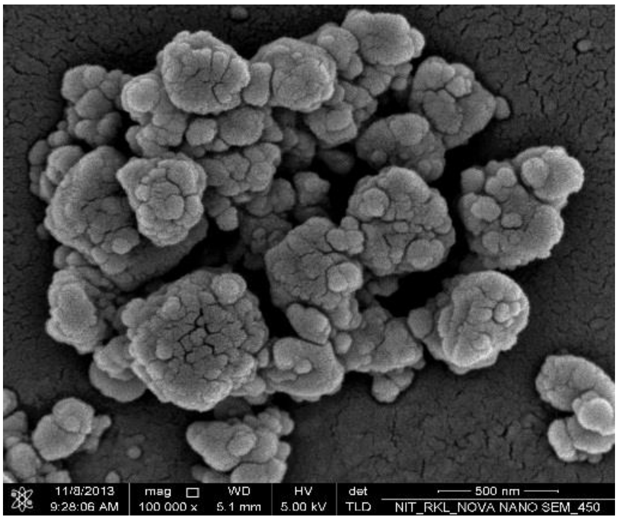

Fig 4.2. FESEM image of the cobalt ferrite nanoparticles.

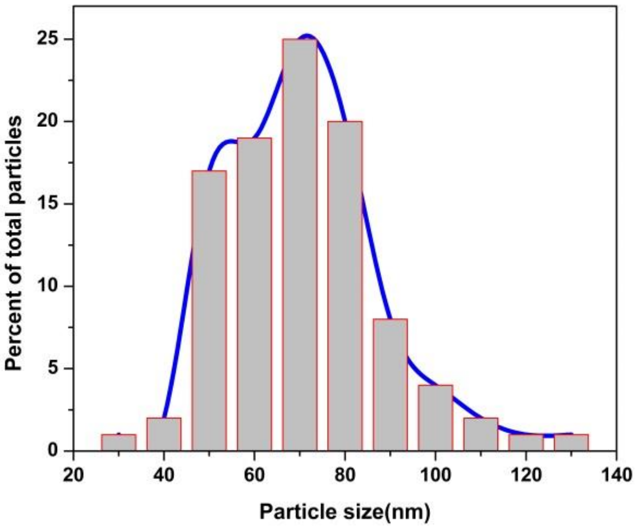

Fig 4.3. Particle size distribution of cobalt ferrite nanoparticles

Raman spectroscopy

Raman spectra of the cobalt ferrite nanoparticles are as shown in figure 4.4. The vibrational modes above 600 cm^{-1} are related to tetrahedral sites and the modes below belong to octahedral. The most intense peak observed at 467 and 690 cm^{-1} are for octahedral and tetrahedral sites respectively but in bulk cobalt these peaks appeared at 469 and 694 cm^{-1} may be due to the variation in cation distribution among these sites.

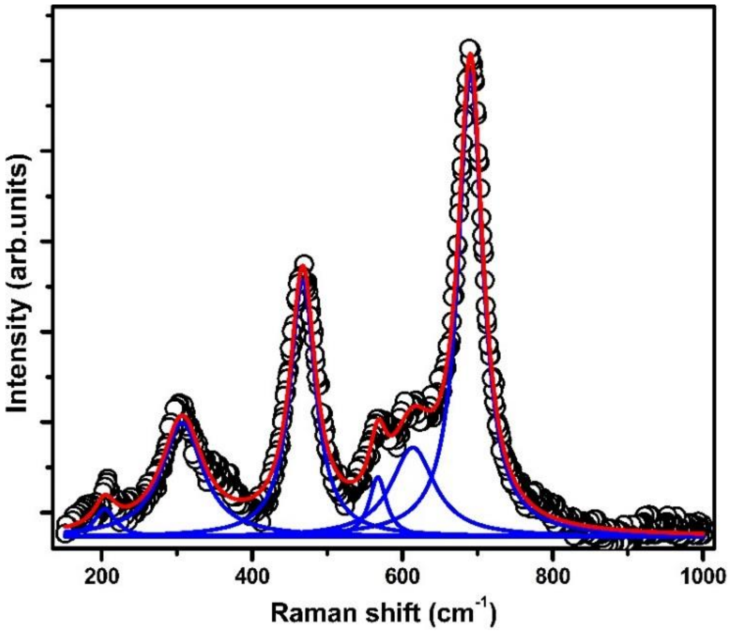

Fig 4.4. Raman shifts of the cobalt ferrite nanoparticles

4.3.2. Impedance analysis

The complex impedance spectroscopy was used to examine the electrical properties of a polycrystalline samples and their interfaces with conducting electrodes in a wide range of frequencies and different temperatures. The real (Z') and imaginary (Z") parts of complex modulus (Z = Z' + i Z") can be obtained using the formula Z'=Z cosθ and Z"=Z sinθ [26]. Cole-Cole plots of the impedance were fitted with the RCQ-RQ up to 50^0 C and after fitted with RQ-RQ using Z simpwin software, where Q is the constant phase element related to the resistance and capacitor is $C= Q^{1/n} R^{(1-n)/n}$ [19].

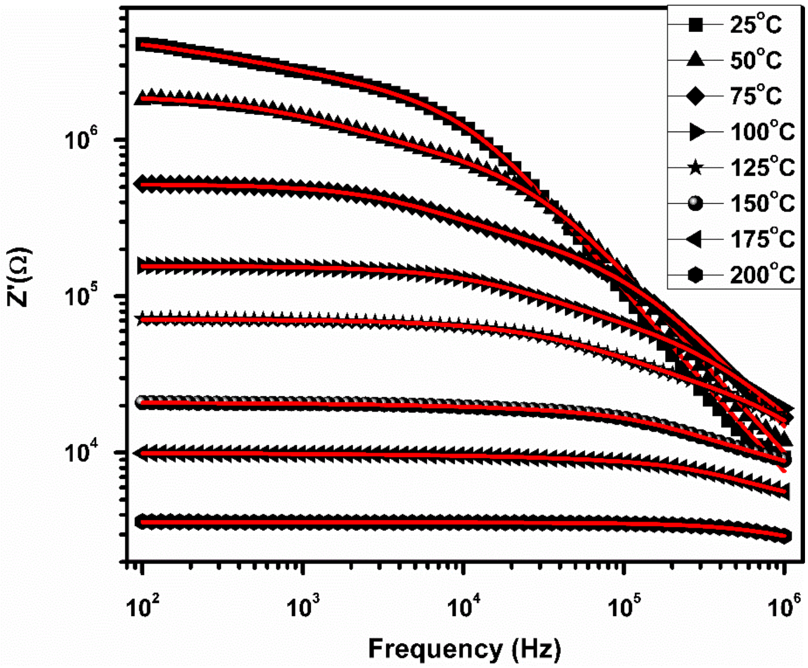

Fig 4.5. Dependence of real impedance of cobalt ferrite nanoparticles on frequency at selected temperatures

Figure 4.5 shows the variation of Z' with frequency at different measured temperatures. The spectra contain two regions; (i) a frequency independent plateau gives the dc resistance and (ii) a dispersive region. The long range or localized movement of the charge carriers are the cause of the shape of the real impedance curve. The long range movement of charge carriers is possible due to their successful hopping in which their neighbor charge particles relaxe to their position. This results in dc conductivity and in turn dc resistivity in impedance plots. The localized movement of charge carriers occurs due to their unsuccessful hopping in which they relax to their own site [27,28]. This results in ac conductivity and in turn gives the dispersive nature to the impedance plot these regions are linked to the conducting behavior of charge carries inside the material and have a very similar shape to that of ac conductivity [29].

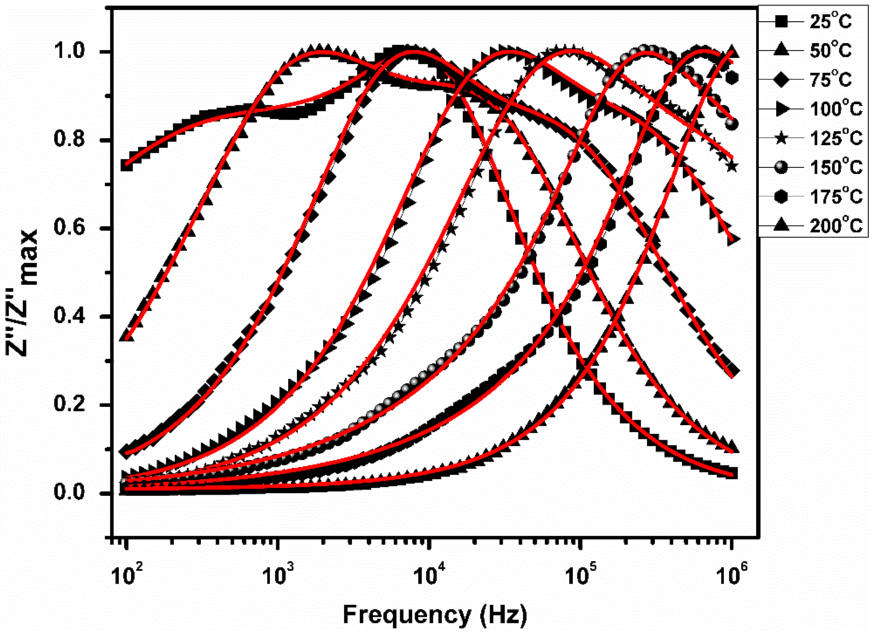

Fig 4.6. Dependence of imaginary impedance of cobalt ferrite nanoparticles on frequency at selected temperatures

The relaxation peaks in Z" spectra give information regarding contribution of different constituent parameters like grain, grain boundary or electrode interface to the electrical behaviour of the source material. Figure 4.6 shows the frequency dependence of imaginary impedance at different temperatures for nano CFO within the measured frequency window 100 Hz -1 MHz. Two relaxation peaks appear near low and intermediate frequency belt respectively at room temperature (RT). With elevation of temperature, the relaxation peaks shift towards higher frequency side. The co-appearance of two peaks in the same spectrum continues up to 125^0 C and after which only one peak exists throughout the studied higher temperature. This result is in contrast to our study on bulk CFO [25] in which two peaks co-appeared at RT which followed by the coexistence of three peaks at subsequent higher temperature and then again two peaks dominated the spectra at the highest studied temperature. The sequential appearance of peaks at different frequency zones aided to easily distinguish the contribution from grain, grain boundary and surface interface effect. In this context, to distinguish the role of different factors in nano CFO is a little bit challenging.

Assuming that nano grains have no sufficient room for charge carriers to follow any applied frequency for relaxation effect we are suggesting only the interfacial effects such as grain boundary and surface polarization are responsible for relaxation mechanisms. On the basis of this suggestion, we ascribe relaxation peak at higher frequency belt to grain boundary effect at RT and that at lower frequency zone ascribes to surface polarization effect.

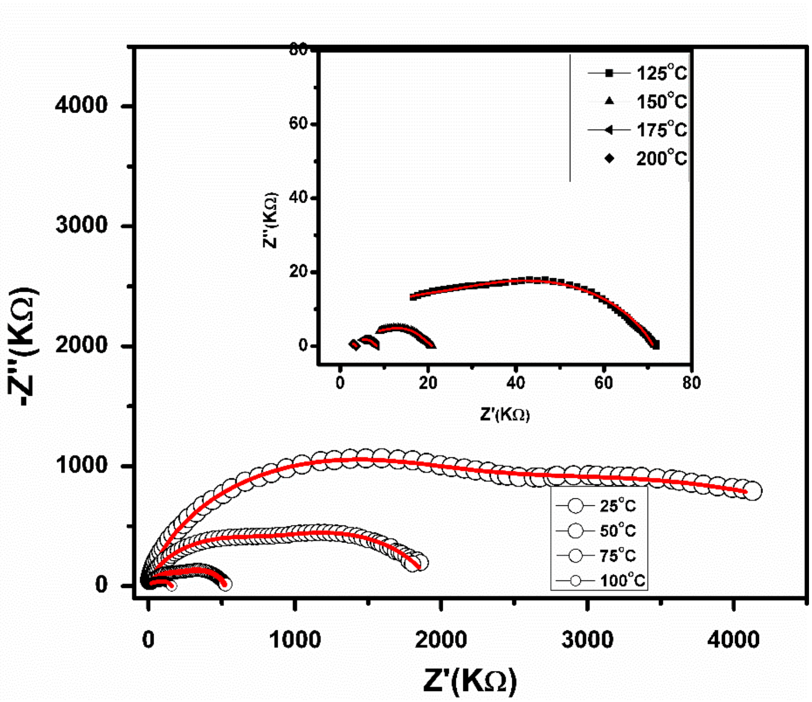

Fig 4.7. Cole-Cole plots of impedance of cobalt ferrite nanoparticles at selected temperature

The existence of these two relaxation processes also being identified in the cole-cole plot shown in Figure 4.7 but the exact conduction mechanism cannot be confirmed. The cole-cole plot which takes the variation of Z' against Z" shows two distinct semicircles. The nature of semicircular arc or arcs, which are either distinct or overlapped, are very much useful in analyzing various electrical relaxation processes [25]. The asymmetry and depressed semicircle arcs indicate the non-Debye type of relaxation [26,30]. The radius of semicircular arcs is equivalent to the resistance of the material [25]. The decreasing value of radius of arcs with increasing temperature suggests the insulating or semiconducting nature of the prepared nano CFO. The growth or diminish of semicircles gives ideas about the dominant role of different conduction mechanism. As per our assumption, grain boundary effect dominates at RT with larger size of semicircle arc than the surface polarization effect. As temperature elevates, surface effects grows and at about 50^0 C almost equal contributions takes place and thereafter surface effect dominates over the grain boundary contribution. This indicates with elevation of temperature, thermally generated charge carriers accumulate and activate at different interfacial discontinuities [25]. As reported in bulk CFO [25], the grain effect dominated at RT and with rise in temperature grain boundary effect grew in the cost of grain effect. Later surface polarization effect arose at sufficiently high temperature (175^0 C) and grain effect vanishes thereafter. But in nano CFO, throughout studied temperature, only the presence of these two semicircles is observed with the continuous growth of arc appeared at lower frequency at RT. This strengthened the assumption of presence of surface polarization effect at RT but the absence of grain effect is not solidified. There may be any co-contribution effect of grain and grain boundary as reported by Chen et al. [28]. To remove this ambiguity, we have carried out the electric modulus formalism which has the ability to highlight the effect of least capacitive region [30].

4.3.3. Modulus analysis

The complex electrical modulus is related to the permittivity is $M^* = \frac{1}{\varepsilon^*} = M' + iM''$ where M' and M'' are found by the relation $M'' = \omega C_o Z'$ and $M' = \omega C_o Z''$ where $C_o = \varepsilon_o A/t$, $\varepsilon_o = 8.854 \times 10^{-12}$ F/m and A is area and t is thickness of the sample.

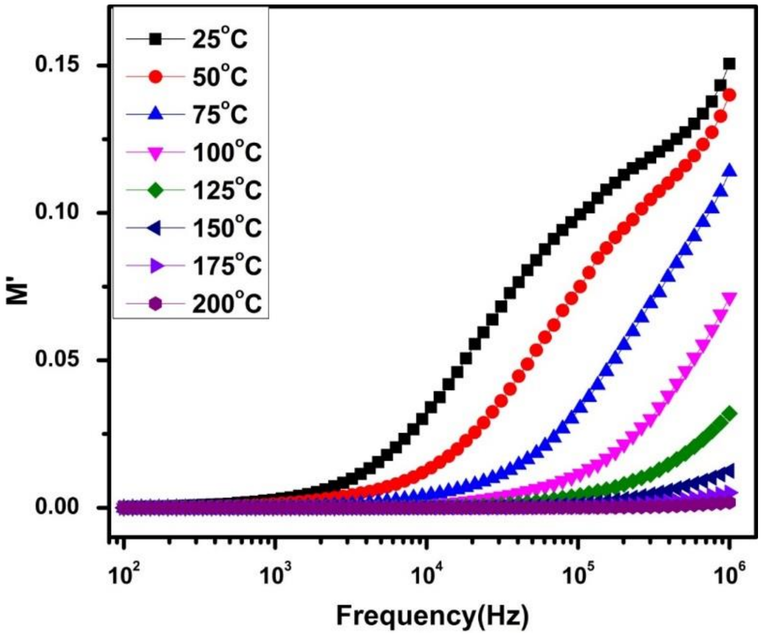

Fig 4.8. Dependence of real modulus of cobalt ferrite nanoparticles on frequency at selected temperatures

Figure 4.8 shows the frequency dependence of the real modulus over wide range temperatures (25^0 C-200^0 C). It is characterized by the very low value at lower frequency and continuously dispersing as frequency increases. Figure 4.9 shows the M" plot against the frequency at different set of temperatures. Unlike Z" spectra where two relaxation peaks appear at RT and thereafter continues up to 125^0 C, only one peak is visible throughout the spectrum at all studied temperature. This shows one of the relaxation peak has been suppressed. To support this data we have also plotted the variation of M' against M" which is shown in Figure 4.10.

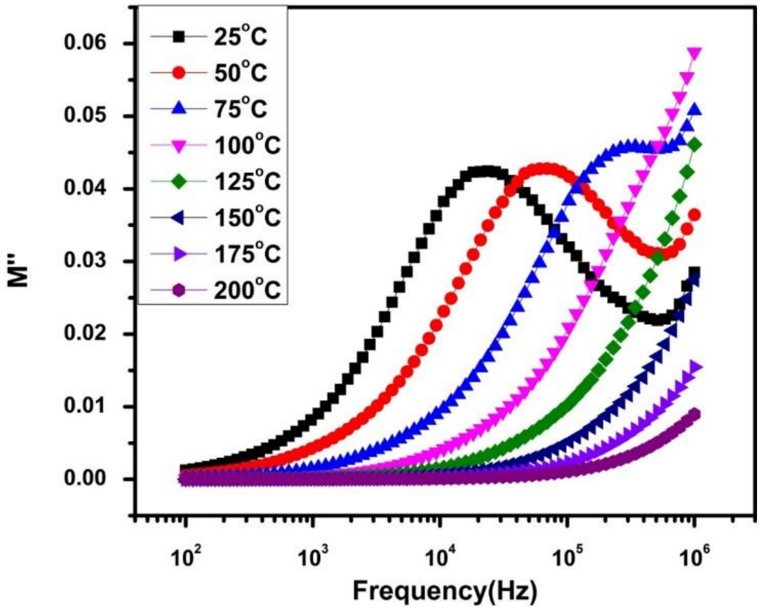

Fig 4.9. Dependence of imaginary modulus of cobalt ferrite nanoparticles on frequency at selected temperatures

Comparing with Cole Cole of impedance, plots between M' vs. M" can well resolve the individual relaxation process. Sometimes the co-contribution of different relaxation processes appears as a single semicircle in cole-cole of impedance, which resolves into distinct arcs in modulus formalism [28]. Contrary to cole-cole of impedance where two semicircles appear, Fig.4.7 shows only one semicircle. This indicates one of the relaxation processes has been suppressed which we attribute to surface polarization effect. The appearance of single semicircle indicates the absence of co-contribution from grain effect and the corresponding relaxation mechanism occurs in grain boundary. The diminishing semicircular arcs with rising temperature suggests the gradually reduction of grain boundary contribution to the conduction mechanism. For further confirmation we have plotted combined Z" and M" against frequency which is shown in Figure 4.11. This shows the relaxation peak at higher frequency end of Z" matches to the sole peak that appears in M". This indicates the peak corresponds to lower frequency belt of former is suppressed in the latter case. This confirms our assumption that the interfaces are the dominant conduction regions in nano CFO and the relaxation mechanisms are due to grain boundary and surface effect in their corresponding frequency zones at RT.

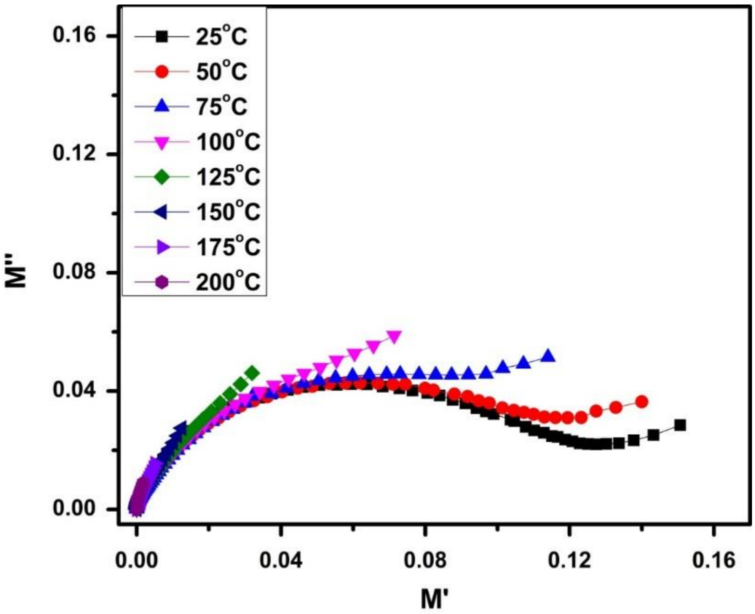

Fig 4.10. Cole-Cole plots of modulus of cobalt ferrite nanoparticles at selected temperatures.

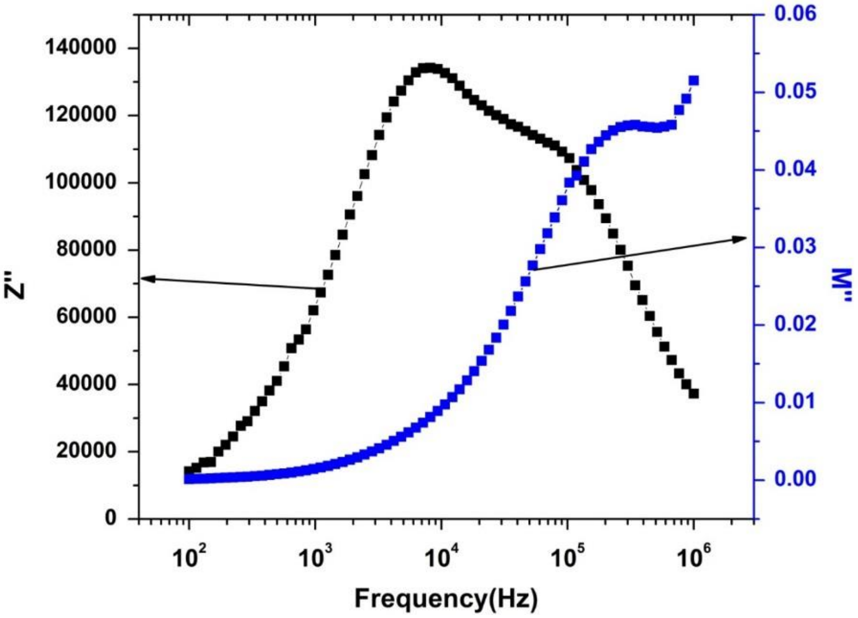

Fig 4.11. Comparison of M'' and Z'' for cobalt ferrite nanoparticles at 75^0 C

4.3.4. AC Conductivity analysis

Conductivity of the CFO nanoparticles derived from the impedance data using the formula $\sigma = [Z'/(Z'^2+Z''^2)](t/A)$ [32]. The conductivity spectrum of the CFO nanoparticles is shown in the figure 4.12. The spectrum contains two different regions: (i) a frequency independent region of plateau shape mostly considered as dc conductivity part and (ii) a highly dispersive region. The detailed mechanism of such behavior is already discussed in real impedance case.

The conduction mechanisms which are responsible for such type of behaviour can be explained by the Jonscher power law [27]

$$\sigma_t(\omega) = \sigma_{dc} + \sigma(\omega)$$

$$\sigma_t(\omega) = \sigma_{dc} + B\omega^n \qquad 4.2$$

Where $\sigma_t(\omega)$ is the total conductivity, σ_{dc} is the dc conductivity, $\sigma(\omega)$ is frequency dependent conductivity also known as ac conductivity and ω is the frequency, n (frequency exponent) and B are the temperature and material intrinsic property dependent constants. It is supposed that the ac and dc conductivities arise due to completely different mechanism. If similar mechanism is responsible for both the ac and dc conductivities then σ_{dc} is expressed as simply $\sigma(\omega)$ in the limit $\omega \rightarrow 0$ and the eqn.(2) is no longer valid [33].

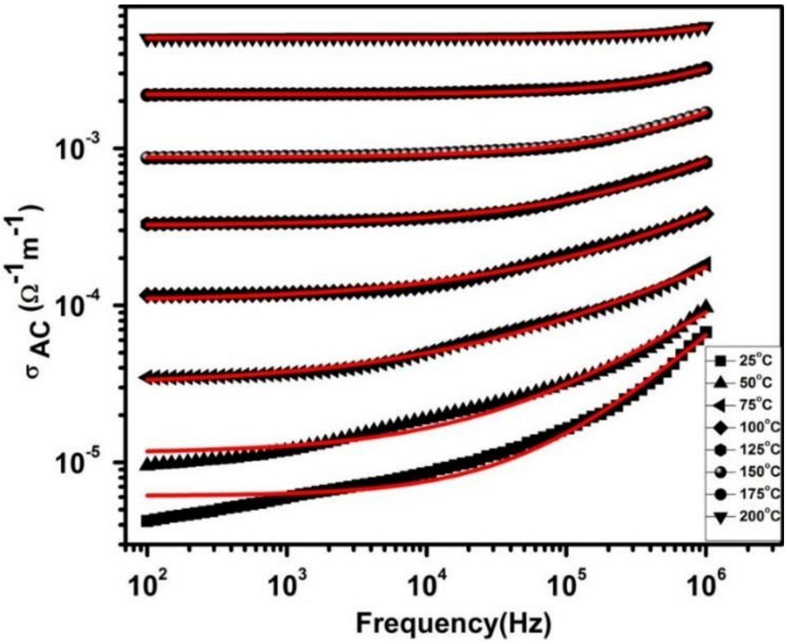

Fig 4.12. Dependence of AC conductivity on frequency at selected temperatures and its fitting curves from single power law.

The variation of frequency exponent ‘n’ with the temperature also suggests some possible model of conduction mechanisms. Temperature independent ‘n’ behaviour suggests quantum mechanical tunneling conduction mechanism. If value of ‘n’ decreases with temperature, then correlated barrier hoping type of mechanism dominates the conduction process and if ‘n’ increases with temperature then small polaron conduction is predominant. If with increase in temperature, ‘n’ decreases, attains a minimum and increases thereafter, then overlapping large polaron tunneling (OLPT) is the most probable conduction process. Figure 4.13 shows the variation of frequency exponent ‘n’ with temperature from which we conclude in nano CFO, the OLPT type of conduction mechanism prevails. Our result agrees with the earlier report of Rahman et.al [24] where they suggested the OLPT conduction mechanism in CFO nano particles. Gopalan et al. [34] also reported large polaron tunneling taking place in manganese ferrite nanoparticles. The ac conductivity in overlapping large polaron tunneling conduction mechanism is [35, 36]

$$\sigma_{ac} = [\pi^4 e^2 k_B T \frac{\{N(E_f)\}^2}{12}] x [\frac{\omega R_\omega^4}{2\alpha k_B T + \frac{\omega_{HO} r_P}{R_\omega^2}}] \qquad 4.3$$

Then the total conductivity is

$$\sigma_t(\omega) = \sigma_{dc} + [\pi^4 e^2 k_B T \frac{\{N(E_f)\}^2}{12}] x [\frac{\omega R_\omega^4}{2\alpha k_B T + \frac{\omega_{HO} r_P}{R_\omega^2}}] \qquad 4.4$$

The frequency exponent $n = 1 - [(8\alpha R_\omega + \frac{6\omega_{HO} r_P}{R_\omega k_B T})/(2\alpha R_\omega + \frac{\omega_{HO} r_P}{R_\omega^2})^2]$ 4.5

The polaron hoping energy is $\omega_H = \omega_{HO}(1 - r_p/R)$

$$\omega_{HO} = e^2/4\epsilon_p r_p \qquad 4.6$$

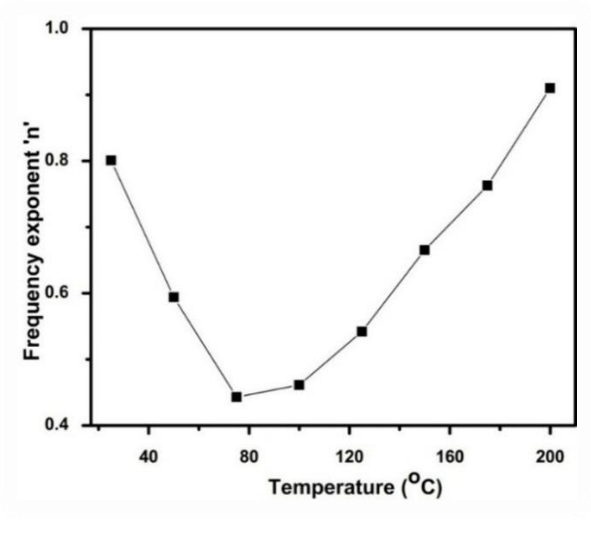

Fig 4.13. Temperature dependence of the frequency exponent ‘n’.

The hoping length can be calculated by the quadratic equation

$$R_{\omega}'^{2} + [\beta\omega_{HO} + \ln(\omega\tau_0)]R_{\omega}' + \beta\omega_{HO} r_p = 0 \qquad 4.7$$

Where α is inverse localization length, r_p is polaron radius, ω_{HO} is activation energy associated with the charge transfer between the overlapped sites, $N(E_f)$ density of energy levels at Fermi level, R_ω is tunneling distance, k_B is Boltzmann constant, T is temperature in K, $\beta = 1/k_BT$, $R'_\omega = 2\alpha R_\omega$, $r'_p = 2\alpha r_p$.

4.3.5. DC resistivity analysis

The temperature dependent dc resistivity study of prepared nano CFO is carried out to distinguish its basic behaviour in Figure 4.14. An exponential decreasing value of resistivity with temperature is observed, which is a typical nature of the insulators. DC resistivity of the ferrites primarily determined by the resistivity of the grain boundaries since ferrites considered to be composed of conductive grains separated by the resistive grain boundaries [37,38].

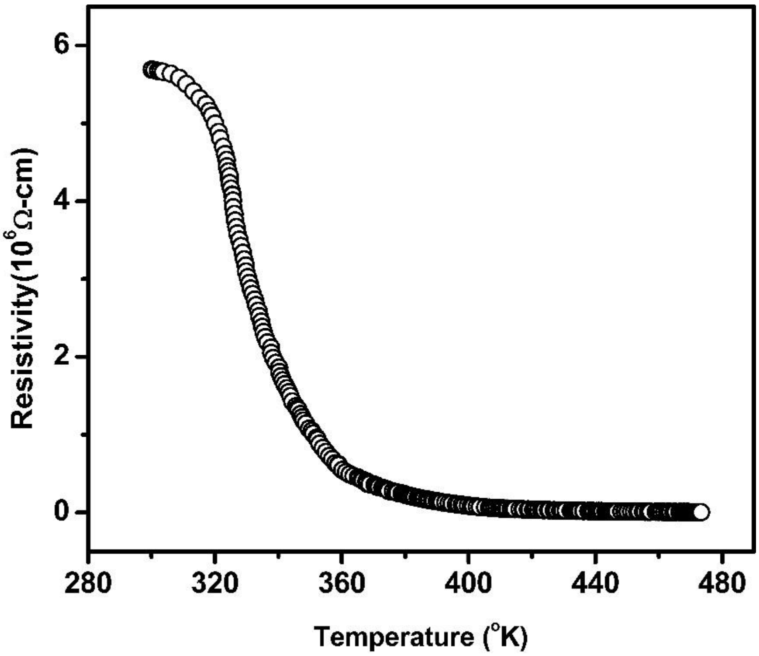

Fig 4.14. The variation of resistivity with temperature of cobalt ferrite nanoparticles

The charge conduction in ferrites can be explained by Verwey hoping mechanism. According to this mechanism conduction in ferrites is due to the electron or hole exchange between ions of the same element present in more than one valence state distributed randomly in the crystallographic sites. The hopping probability depends on the separation of the ions, activation energy and as well as temperature. In CFO there is an electron exchange between Fe^{2+}-Fe^{3+} and hole hopping between Co^{3+}- Co^{2+} cations [22,39].

We have also calculated the mobility of nano CFO from the measured dc resistivity data by applying Eqn. (6).

$$\left.\begin{aligned} \mu &= 1/ne\rho \\ n &= N_A \rho_m n_{Fe}/M \end{aligned}\right\} \qquad 4.8$$

where 'e' is charge of the carrier, ρ is resistivity, n is the concentration of charge carrier, N_A is Avogadro number, n_{Fe} is number of iron atoms present in the chemical formula, ρ_m is the density and M is molecular weight [40].

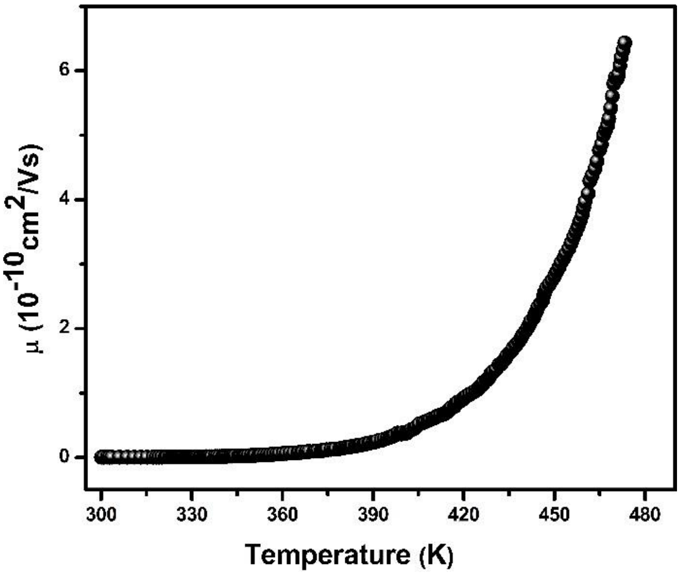

Fig 4.15. Temperature dependence of mobility of cobalt ferrite nanoparticles

Figure 4.15 shows the variation of mobility with temperature. After a slow variation up to 100^0 C, the mobility steeply rises thereafter to a maximum range of $6x10^{-10}$ cm^2/Vs. This obtained value is quite smaller compared to the mobility of electrons and holes [41]. Therefore, the dc conduction process does not involve movement of holes or electrons in nano CFO, rather the range of mobility suggests the small polaron conduction mechanism is the most probable one in this case. A small polaron arises as a result of an electron trapped by a site due to the displacement of adjacent atoms or ions. Small polaran conduction mechanism takes place inside the material whose conducting electrons belong to incomplete filled orbitals (d, f) [42]. Low value of mobility, temperature independent Seebeck coefficient and thermally activated hoping are important features of the small polaran conduction mechanism. In a similar study on lanthanum doped CFO, Bharti et al. reported the activation of small polaron conduction process in the temperature range of 220-300 K [43].

In order to confirm the small polaron conduction process in our sample, we have fitted the dc resistance versus temperature plot with the model proposed by Mott and Davis [44]. The model explains electron-phonon interaction basically small polaron as a dominant conduction process and is suitable to the high temperature electronic transport properties of the transition metal oxide systems. According to this model resistivity is given by [44-49]

$$\rho/T = \rho_\alpha \exp(E_p/k_B T) \qquad 4.9$$

Where E_P is the activation energy of the polaron such that

$$E_P = E_H + \frac{E_D}{2} \qquad T > \frac{\theta_D}{2} \qquad 4.10$$

$$E_P = E_D \qquad T < \frac{\theta_D}{4} \qquad 4.11$$

where, E_H – polaron hopping energy, E_D – disorder energy, and θ_D- Debye temperature.

$$\rho_\alpha = \left[\frac{K_B}{\upsilon_{ph} N e^2 R^2 C(1-C)}\right] \exp(2\alpha R) \qquad 4.12$$

where, T - absolute temperature, k_B - Boltzmann constant, R $\{=(1/N)^{1/3}\}$is the average interstice spacing, υ_{ph} - optical phonon frequency, C - fraction of sites occupied by the polaron, α - electron wave function decay constant. For nano CFO system, we have found the value of E_P (= 601 meV) from the slope of the linear portion of ln (ρ/T) vs 1/T plot. The deviation of fitted line from linearity gives Debye temperature θ_D (=642.84 K) as shown in figure 4.16.

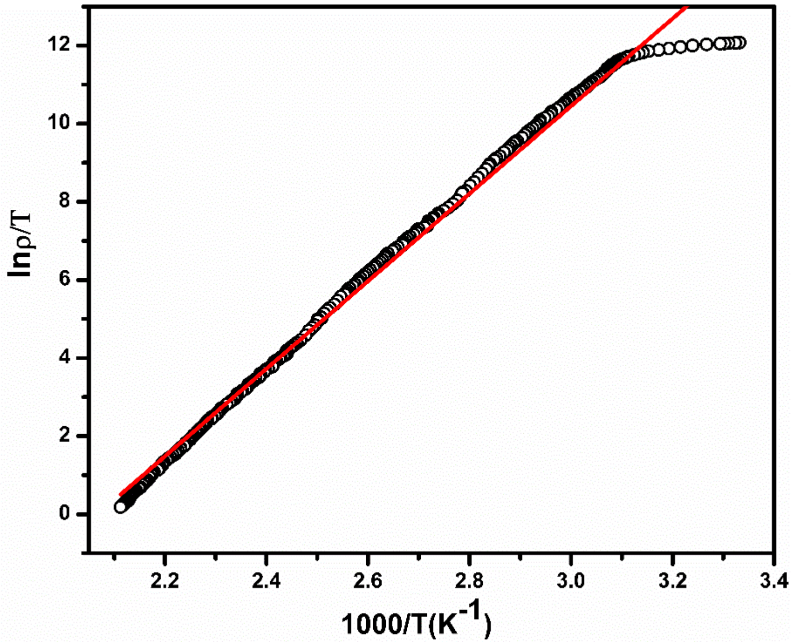

Fig 4.16. Variation of ln(ρ/T) as a function of inverse temperature for cobalt ferrite nanoparticles

If we define J – polaron bandwidth which has its expression

$$J(T) = 0.67h\upsilon_{ph}\left(\frac{T}{\theta_D}\right)^{\frac{1}{4}} \qquad 4.13$$

where, υ_{ph}(= $K_B\theta_D$/h) - optical phonon frequency which is 1.3396x10^{13} in the present case, then for small polaron conduction, below equation must satisfy.

$$J < \frac{E_H}{3}, \qquad 4.1$$

Putting the required values, J(T) comes out to be 30.67 meV. The value of E_H can be determined by applying following formula

$$E_H = \frac{e^2(r_p^{-1} - R^{-1})}{4\varepsilon_p} \qquad 4.15$$

where, r_p – polaron radius, R - average interstice spacing, ε_p - the effective dielectric constant given by,

$$\frac{1}{\varepsilon_p} = \frac{1}{\varepsilon_\infty} - \frac{1}{\varepsilon_o} \qquad 4.16$$

The polaron radius can be calculated using the formula

$$r_p = \frac{1}{2}[{}^{\pi}/_{6}]^{1/3}R \qquad 4.17$$

The value of the r_p is calculated to be nearly 0.74 A°, ε_p is calculated to be (= 6.40668) and R = 1.828 A°. Substituting the above values, E_H found to be 506 meV. Comparing the two values of J(T) and E_H, eqn. 9 is satisfied. This confirms the small polaron conduction mechanism as per the proposition in nano CFO. For further information of its thermodynamic nature, Holstein's condition is studied which says

$$\left.\begin{array}{lll} \text{Such that,} & J > \phi & \text{for adiabatic condition} \\ & J < \phi & \text{for non-adiabatic condition, where} \\ & \multicolumn{2}{l}{\phi = \left(\frac{2k_B T E_H}{\pi}\right)^{\frac{1}{4}} \left(\frac{h\upsilon_{ph}}{\pi}\right)^{\frac{1}{2}}} \end{array}\right\} \qquad 4.18$$

We put the required values to get, ϕ (= 42.56 meV) which is greater than the value of J (= 30.67 meV). This shows the conduction process is non-adiabatic in nature. We have also calculated the electron-phonon coupling constant γ which is very crucial parameter in controlling various properties of material and defined by

$$\gamma = \frac{2E_H}{h\upsilon_{ph}} \qquad 4.19$$

If γ is greater than 4 then, there exists a strong electron-phonon interaction. For nano CFO system, it is found to be 18.26 which suggest a strong interactive system among electrons and phonons.

4.3.6. Dielectric constant

The frequency dependence of dielectric constant of CFO nanoparticles in the frequency domain of 100 Hz to 1 MHz and temperature range of 25^0 C-200^0 C is shown in Figure 4.17. The dielectric constant is obtained by using the formula $\varepsilon_r = Ct/\varepsilon_o A$, where C is the capacitance of the sample. The typical nature of decreasing dielectric constant value with increasing frequency is observed from the plot. The dielectric constant which is related to the different types of polarization processes or in clear sense how dipoles generate, can be ascertained by studying the frequency or temperature dependent relative permittivity plot. Two relaxations appear at RT which shifts to higher frequency side with elevation in temperature. This indicates two different regions of dominating polarization effect. In ferrites, space charge polarization is the major contributing factor towards relative permittivity

[50,51]. As conduction and polarization are supplementary to each other, therefore, same mechanism is responsible for the dielectric nature of nano CFO system. The electron or hole exchange in multi-oxidation states of elements present in CFO system contributes a lot towards polarization. The dielectric constant depends on the concentration of Fe^{2+} ions present in the ferrite system [52].

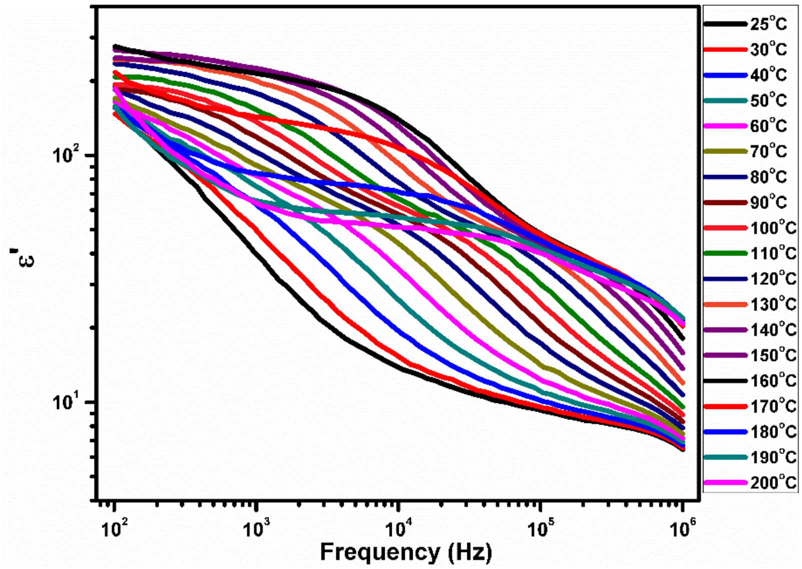

Fig 4.17. Frequency dependence of dielectric constant of cobalt ferrite nanoparticles at different temperature

The more concentration of Fe^{2+}, the more will be the dielectric constant as per expectation due to the charge transfer between the Fe^{2+}- Fe^{3+}. Up to the relaxation frequency, the hopping charge carriers are able to follow the changing ac field i.e. complete polarization, results high dielectric constant value. Beyond the relaxation frequency, incomplete polarization occurs as charge carriers are not able to follow fast changing applied ac field. This reduces the dielectric constant value [53]. The presence of Co^{3+}- Co^{2+} in the CFO nanoparticles system supply the p type charge carriers also. The localized displacements of the p type charge carriers in the direction of applied field contribute to the polarization in addition to the n type charge carriers. The contribution due to the p type charge carriers is less compared to the n type charge carriers and opposite sign. This is because the mobility of p type charge carriers is less compared to the n type charge carriers and their contributions to the polarization decrease more rapidly even at lower frequencies also. The dielectric constant of the CFO nanoparticle increases with increase in temperature which is natural behavior of the ferrites. This is due to enhanced value of mobility of the charge carriers which in turn stimulates hoping rate. The larger values of dielectric constant at lower frequencies are due to the all contributions like electronic, ionic, electrode and grain boundary effects whereas in high frequencies it is only due to the electronic and ionic polarization only which is temperature independent. So the temperature effect is not significant at high frequencies, rather significant in low frequencies [54, 55].

4.4. Magnetic properties

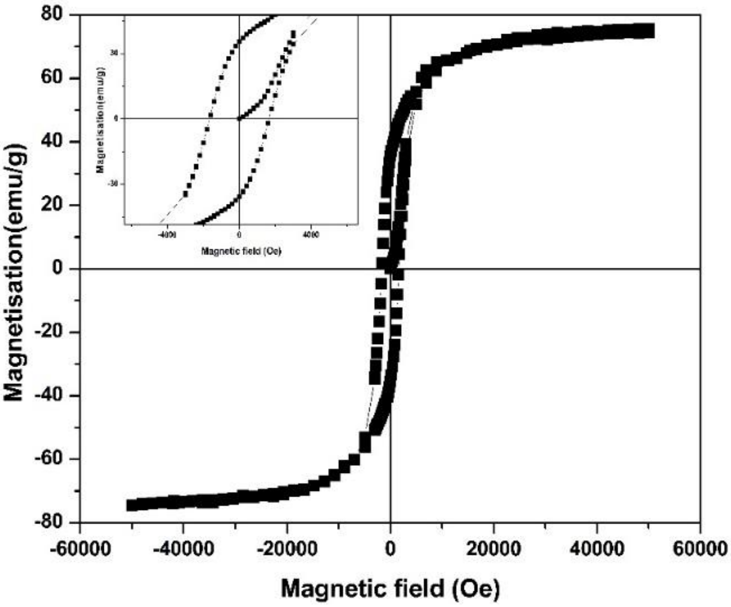

Fig 4.18. Room temperature M-H loop of cobalt ferrite nano-particles.

Figure 4.18 shows the room temperature (RT) field dependent magnetic properties of the cobalt ferrite. It exhibits loop at RT indicates the ordered or ferrimagnetic nature of the cobalt ferrite. Saturation magnetization and coercivity found to be 80 emu/g and 1650 Oe respectively. Comparative to the bulk cobalt ferrite, cobalt ferrite nanoparticle exhibits lower saturation magnetization and higher coercivity. Magnetic properties of the cobalt ferrite nanoparticles greatly affected by the particle size, synthesis procedure and cation distribution [56,57].This can be explained on the basis of surface disorder due to random distribution of cations and canted spin structure. The surface disorder arises due to the broken exchange bonds, high anisotropy on the surface [58, 59]. Cobalt ferrite is inverse spinel in bulk but in nano level Co^{2+} is arbitrarily occupied both the tetrahedral and octahedral sites so some of smaller Fe^{3+} (0.645 Å) are migrated to octahedral site to replace the heavier Co^{2+} (0.72 Å) cations [19-21]. Shifting of Fe^{3+} cations induce compressive strains due to the smaller distance between the B site ions compared to the A site ions in nanoparticles. These compressive strains may break the surface exchange bonds which results in the canted spin structure. This kind of structure not only weakens the AA or BB interaction but also AB interaction leads to lower magnetization values at RT compared with the bulk cobalt ferrite [58].

4.5. Conclusions

The electric transport properties of nano CFO of size ~70 nm were discussed in this chapter. Grain boundary conduction and surface polarization were the major contributors to its conductivity and dielectric properties. OLPT type of conduction was responsible for ac conduction process as was confirmed from variation of frequency exponent n with temperature. But the mobility value obtained in the experiment agreed with the small polaron responsible for dc conduction. Small polaron conduction mechanism in dc resistivity was explained by the Mott and Davis model. Electron and hole exchange among Fe^{2+}- Fe^{3+} and Co^{3+}- Co^{2+} were found to be major contributor to dielectric constant value. Room temperature M-H loop of cobalt ferrite nanoparticles indicates its ordered state and showed lower saturation magnetization value and higher coercivity as compared to the bulk cobalt ferrite.

References

[1] Z. Szotek, W. M. Temmerman, D. Ködderitzsch, A. Svane, L. Petit and H. Winter, Physical review B 74 (2006) 174431.

[2] K. Brachwitz, T. Bontgen, M. Lorenz, and M. Grundmann, Applied physics letters 102 (2013) 172104.

[3] Vincent G.Harris, AntonGeiler, YajieChen, SoackDaeYoon, MingzhongWu , AriaYang, Zhaohui Chen, PengHe, PatanjaliV.Parimi, XuZuo, CarlE.Patton, ManasoriAbe, OlivierAcher and CarmineVittoria, Journal of Magnetism and Magnetic Materials 321 (2009) 2035–2047.

[4] Diego Guti´errez, Michael Foerster, Ignasi Fina, and Josep Fontcuberta, Physical Review B 86 (2012) 125309.

[5] Xavier Batlle, N. Perez, P. Guardia, O. Iglesias, A. Labarta, F. Bartolome, L. M. Garcla, J. Bartolome, A. G. Roca, M. P. Morales, and C. J. Serna, Journal of applied physics 109 (2011) 07B524.

[6] Simona Burianova, Jana Poltierova Vejpravova, Petr Holec, Jiri Plocek, and Daniel Niznansky, Journal of applied physics 110 (2011) 073902.

[7] R. H. Kadam, A. R. Biradar, M. L. Mane, and Sagar E. Shirsath, Journal of applied physics 112 (2012) 043902.

[8] Muhammad Javed Iqba, Zahoor Ahmad, Turgut Meydan, and Yevgen Melikhov, Journal of applied physics 111 (2012) 033906.

[9] Biao Zhou, Ya-Wen Zhang, Yue-Jun Yu, Chun-Sheng Liao, and Chun-Hua Yan, Physical Review B 68 (2003) 024426.

[10] Y. Cedeño-Mattei, O. Perales-Perez, M. S. Tomar, F. Roman, P. M. Voyles,and W. G. Stratton, Journal of applied physics 103 (2008) 07E512.

[11] K. Khaja Mohaideen and P. A. Joy, Applied physics letters 101 (2012) 072405.

[12] A. Franco, Jr. and F. C. e Silva, Applied physics letters 96 (2010) 172505.

[13] S. J. Leea and C. C. H. Lo, Journal of applied physics 102 (2007) 073910.

[14] T. Dhakal, D. Mukherjee, R. Hyde, P. Mukherjee, M. H. Phan, H. Srikanth, and S. Witanachchia, Journal of applied physics 107 (2010) 053914.

[15] A. K. Giri, E. M. Kirkpatrick, P. Moongkhamklang, and S. A. Majetichc, applied physics letters 80 (2002) 2341.

[16] H. S. Mund, Shailja Tiwari, Jagrati Sahariya, M. Itou, Y. Sakurai, and B. L. Ahuja, Journal of applied physics 110 (2011) 073914.

[17] E. Manovaa, T. Tsonchevab, D. Panevaa, I. Mitova, K. Tencheva, L. Petrov, Applied Catalysis A: General 277 (2004) 119–127.

[18] Muhammad Javed Iqbal, Mah Rukh Siddiquah, Journal of Alloys and Compounds 453 (2008) 513–518.

[19] Atta ur Rahman, M. A. Rafiq, K. Maaz, S. Karim, Sung Oh Cho and M. M. Hasan, journal of applied physics 112 (2012) 063718.

[20] A. Franco, Jr. and F. C. e Silva, Journal of applied physics 113 (2013) 17b513.

[21] I. C. Nlebedim, R. L. Hadimani, R. Prozorov, and D. C. Jiles, Journal of applied physics 113 (2013) 17A928.

[22] A. Arunkumar, D. Vanidha, K. Oudayakumar, S. Rajagopan, and R. Kannan, Journal of applied physics 114 (2013) 183905.

[23] R. Kannan, S. Rajagopan, A. Arunkumar, D. Vanidha, and R. Murugaraj, Journal of applied physics 112, 063926 (2012).

[24] Atta ur Rahman, M A Rafiq, S Karim, K Maaz, M Siddique and M M Hasan, J. Phys. D: Appl. Phys. 44 (2011) 165404.

[25] R.K. Panda, D. Behera, Journal of Alloys and Compounds 587 (2014) 481-486.

[26] M. M. Costa, G. F. M. Pires, Jr., J. Terezo, M. P. F. Grac¸ and A. S. B. Sombra, Journal of applied physics 110 (2011) 034107.

[27] N. Ortega, Ashok Kumar, P. Bhattacharya, S. B. Majumder, and R. S. Katiyar, Physical Review B 77 (2008) 014111.

[28] W. Chen, W. Zhu, O. K. Tan, and X. F. Chen, Journal of applied physics 108 (2012) 034101.

[29] Ashok Kumara, B.P. Singh a, R.N.P. Choudhary and Awalendra K. Thakur, Materials Chemistry and Physics 99 (2006) 150–159.

[30] Robert H. Cole, Journal of applied physics 23 (1955) 493-499.

[31] R. K. Dwivedi, D. Kumar and O. Parkash, Journal of materials science 36 (2001) 3657 – 3665.

[32] Wei Li and Robert W. Schwartza, Applied physics letters 89 (2006) 242906.

[33] A. Ghosh, Physical review B 47 (1993) 1537.

[34] E Veena Gopalan, K A Malini, S Saravanan, D Sakthi Kumar, Yasuhiko Yoshida and M R Anantharaman, J. Phys. D: Appl. Phys. 41 (2008) 185005.

[35] R. Punia, R. S. Kundu, Meenakshi Dult,S. Murugave and N. Kishore, Journal of applied physics 112 (2012) 083701.

[36] Makram Megdiche , Carine Perrin-pellegrino and Mohamed Gargouri, Journal of Alloys and Compounds 584 (2014) 209–215.

[37] M.L.S. Teo , L.B. Kong , Z.W. Li , G.Q. Lin and Y.B. Gan, Journal of Alloys and Compounds 459 (2008) 567–575.

[38] S. M. Patange, Sagar E. Shirsath, B. G. Toksha, S. S. Jadhav, and K. M. Jadhav, Journal of applied physics 106 (2009) 023914.

[39] K.H. Rao, S.B. Raju, R.G. Gupta, and R.G. Mendiratta, Solid State Communications 36 (1980) 777-780.

[40] Uzma Ghazanfar , S.A. Siddiqi , G. Abbas, Materials Science and Engineering B 118 (2005) 132–134.

[41] Veena Gopalan E, On the Synthesis and Multifunctional Properties of some Nanocrystalline Spinel Ferrites and Magnetic Nano composites, Ph.D Thesis (2009).

[42] V L Mathe, K K Patankar, S D Lotke, P B Joshi and S A Patil, Bull. Mater. Sci.25 (2002) 347-350.

[43] K. Kamala Bharathi and C.V. Ramana, Journalof Materials Research 26 (2010) 584-591.

[44] Wasi Khan, Alim H. Naqvi, Maneesha Gupta, Shahid Husain, and Ravi Kumar, The Journal of chemical physics 135 (2011) 054501.

[45] Sudipta Pal, Aritra Banerjee, E. Rozenberg and B. K. Chaudhuri, Journal of applied physics 89 (2001) 4955.

[46] Aritra Banerjee, S. Pal, and B. K. Chaudhuri, Journal of chemical physics 115 (2001) 1550.

[47] P. Brahma, S. Banerjee, S. Chakraborty and D. Chakravorty, Journal of applied physics 88 (2000) 6526.

[48] I. Ahmad, M. J. Akhtar, M. Younas, M. Siddique, and M. M. Hasan, Journal of applied physics 112 (2012) 074105.

[49] A. Memon and D.B. Tanner , Journal of materials science 34 (1999) 3853-3858.

[50] R.C. Kambale, P. A Shaikh, C. H Bhosale, K.Y Rajpure and Y. D Kolekar, Smart Mater. Struct. 18 (2009) 115028.

[51] R.C. Kambale, P.A. Shaikh, C.H. Bhosale, K.Y. Rajpure and Y.D. Kolekar, Smart Mater. Struct. 18 (2009) 085014.

[52] Razia Nongjai, Shakeel Khan, K. Asokan, Hilal Ahmed, and Imran Khan, Journal of applied physics 112 (2012) 084321.

[53] N. Sivakumar, A. Narayanasamy, B. Jeyadevan, R. Justin Joseyphus and C. Venkateswaran, J. Phys. D: Appl. Phys. 41 (2008) 245001.

[54] C. V. Ramana, Y. D. Kolekar, K. Kamala Bharathi, B. Sinha, and K. Ghosh, Journal of applied physics 114 (2013) 183907.

[55] N. Sivakumar, A. Narayanasamy, C. N. Chinnasamy, and B. Jeyadevan, J. Phys.: Condens. Matter 19 (2007) 386201.

[56] K. Vasundhara, S. N. Achary, S. K Deshpande, P. D. Babu, S. S. Meena, and A. K. Tyagi, 113, (2013) 194101 .

[57] A. Bouhas, M. Amzal and B. Zouranen, Material chemistry and Physics, 33 (1993) 80-84.

[58] M. Younas, M. Nadeem, M. Atif, and R. Grossinger, J. Appl. Phys. 109 (2011) 093704.

[59] J. Jacob and M. A. Khadar, J. Appl. Phys. 107 (2010) 114310.

CHAPTER 5

Effect of Bi on electric and magnetic properties of cobalt ferrite nanoparticles

---

In this chapter we have prepared Bismuth substituted nano-cobalt ferrite ($CoFe_{2-x}Bi_xO_4$, x= 0, 0.05, 0.1, 0.15) by auto combustion technique. The single phase XRD pattern confirmed the successful substitution of the larger cation. Surface morphology from FESEM image indicated the control particle growth (50 nm – 160 nm) as a result of bismuth substitution. The increased particle size has effectively modified the electrical properties of the system in three major ways: (a) increase in resistivity, (b) evolution of grain relaxation and (c) reduction in dielectric loss and surface conduction. Additionally, magnetic behavior is also affected due to control particle growth. Magnetic hysteresis study at room temperature confirmed the rise in saturation magnetization (M_S = 74.5 to 86.5 emu/g.) and reduction in coercivity (H_C = 1633 to 1524 Oe).

5.1. Introduction

Ferrite ceramics has dragged the attention of researchers as an alternative for metallic ferromagnetic materials. The high eddy current losses of metallic ferromagnets have made it unpopular for the application of cores in transformers, electronic inductors and electromagnets. High resistive nature of ceramic ferrites generates very low eddy current which is very suitable for the above applications. Ferrites also provide opportunity for its memory application in computers for which high saturation magnetization is the desired parameter. Moderate saturation magnetization, high coercivity, high Curie temperature, magneto-striction, spin filtering efficiency, high magneto-crystalline anisotropy of Cobalt ferrite [1-3] has made it very interesting to investigate and modify for application purposes. This nano dimension controls the magnetic and electric behavior of $CoFe_2O_4$ system [7, 8]. A lot of modifications have been carried out to improve both magnetic and electric properties for its wide applicability. But high dielectric loss at low frequencies has made it unpopular for electrical application [9, 10]. Our work has intended to minimize the dielectric loss without compromising magnetic properties. The high dielectric loss in CFO system results due to early arrival of surface conduction both in nano and in bulk form which is a matter of concern. Our previous report on nano cobalt ferrite had shown the absence of grain effect at room temperature and appearance of surface conduction even at room temperature [11]. Similar works on nano CFO system with various particle sizes and thin film also report early presence of surface conduction and high dielectric loss [10, 12]. Our electric transport study of bulk cobalt ferrite system also evidenced the early arrival of surface conduction about 175^0 C [8]. It is observed that material resistance is high when the charge conduction confine within the grains and material resistance is low when the charge carriers escape to various interfaces. The resistance of a material dips its low when surface conduction dominates over grain boundaries. Low temperature sintering results in less densification and presence of porosity will promote space charge conduction. But the high temperature sintering process results fully densification and large grain size still it attends early surface conduction and high dielectric loss [8,13]. This requires modification of nano CFO system with suitable dopants which will enhance the control particle growth at low temperature sintering.

In this work, our main objective is to increase resistance in order to lower the eddy current effect, reduce dielectric loss and enhance remnant saturation for the noble aforesaid application purpose by modifying the CFO system. For this purpose, we aimed at inducing the grain effect in CFO system by substituting the (Fe^{3+}/Fe^{2+}) site by Bi^{3+}ion. Since percentage of Fe ion presence is the key factor for low resistance and huge dielectric loss [12,14], we preferred its substitution by bismuth ion. Again, most of the literatures have also reported the grain growth effect of Bi substitution due to its lone pair effect [15]. Franco et al. [16] have earlier modified the nano CFO system with bismuth substituting in cobalt site. They have reported enhancement in saturation magnetization, decrease in magnetic anisotropy constant and increase in coercivity. All these factors motivated us to substitute bismuth at iron site to observe its effect on electric and magnetic properties. In this work, we have reported the evolution of particle growth in a control manner in nano CFO system due to Bi substitution. We have discussed how the bismuth modification has induced attractive electrical and magnetic properties in CFO system for technological applications.

5.2. Materials and Methods

Bi substituted cobalt ferrite nanoparticles ($CoFe_{1-x}Bi_xO_4$ where x= 0, 0.05, 0.1, 0.15) were prepared by the auto combustion method. The detailed procedure was explained in previous chapter. The combustion powder was calcined at 600^0 C for 3 hours with 5°/min heating rate. Rigaku Ultima-IV, X-ray diffractometer (Cu target) used for the phase and structural identification and Nova NanoSEM-450 Field emission scanning electron microscopy (FESEM) is used for morphology study. The ac electrical properties of the nanoparticles is measured by the HIOKI impedance analyzer (model IM3570) from 100 Hz to 1MHz and dc electrical resistance is measured by the Keithley electrometer (model 6517B) in the temperature range of 25° to 200° C. Room temperature filed dependent magnetic properties is studied by the SQUID magnetometer with maximum applied field of 6 T.

5.3. Results and discussion

5.3.1. Structural analysis

Figure 5.1 shows the room temperature XRD pattern of parent and Bi substituted cobalt ferrite samples. It is noticed that the position of peaks are assigned to cobalt ferrite is in accordance with the JCPDS card no 22-1086 and 74-2403. All the samples show the characteristic reflections of spinel structure with most intense reflection (311) and without any detectable secondary phases. So it revealed that ferrite particles are synthesized in spinel structure with Fd3m space group. The shifting of highest intense peak (311) towards lower diffraction angle is shown as inset in figure 5.1. The lattice constant was determined using the relation $a = d(h^2 + k^2 + l^2)^{1/2}$ and plotted against composition figure 5.2. It is observed that lattice constant increases from 8.37 to 8.40 Å with Bi substitution. This indicates the successful substitution of larger Bi3+ ion (0.96 Å) [15] in place of Fe3+ ion (0.64 Å) [17,18].

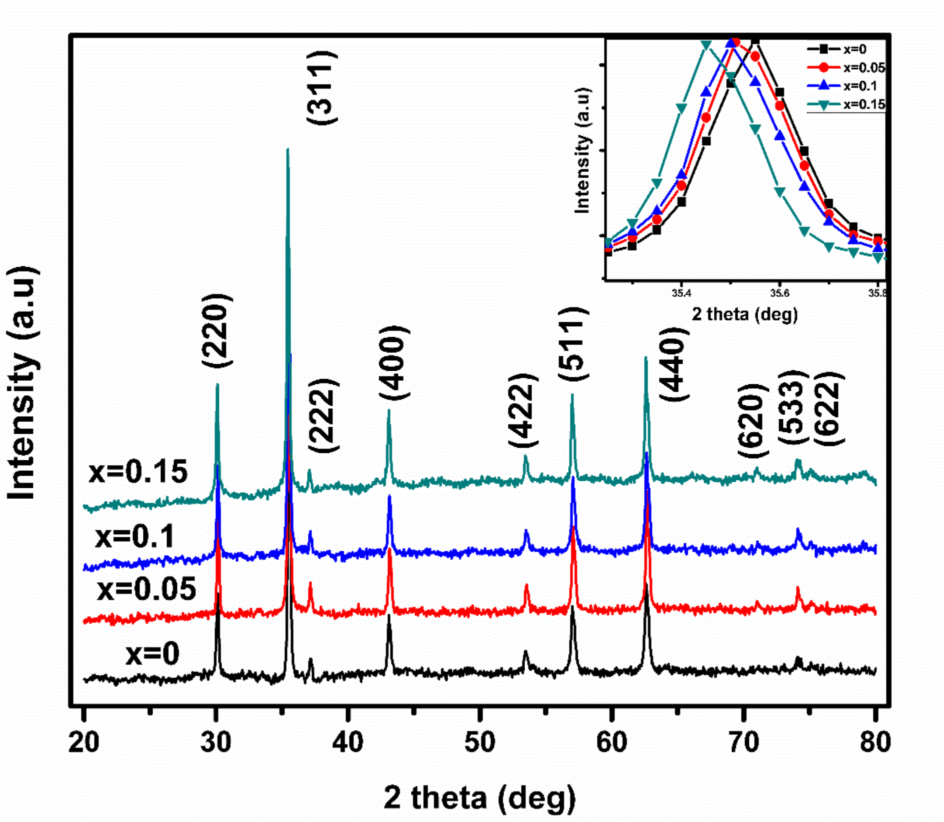

Fig 5.1. XRD pattern for Bi substituted cobalt ferrite nano particles.

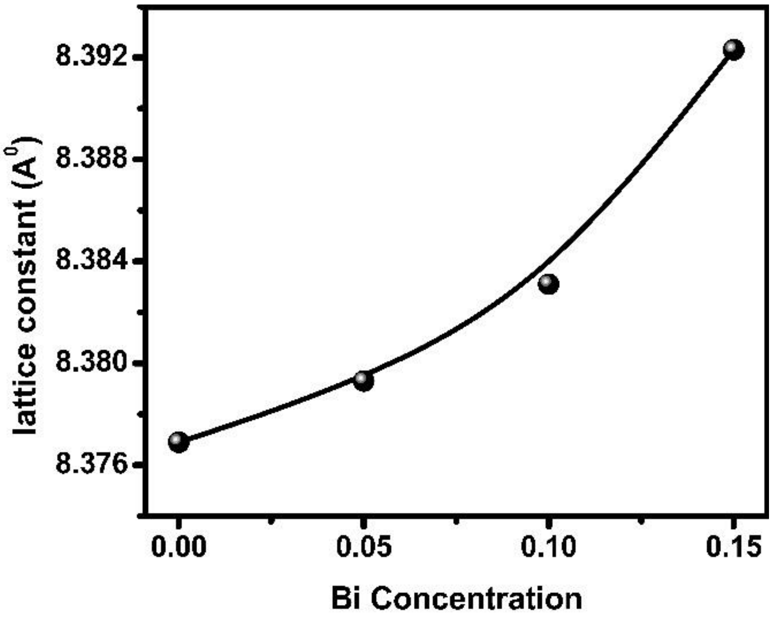

Fig 5.2. Variation of lattice constant with varying Bi concentration in cobalt ferrite

Hoping lengths of octahedral sites and tetrahedral sites are calculated using relations [19].

$$L_A = 0.25a\sqrt{3} \qquad 5.1$$

$$L_B = 0.25a\sqrt{2} \qquad 5.2$$

It is observed that both octahedral and tetrahedral hoping length increases with increasing Bi substitution as is shown in figure 5.3. The distance between the magnetic ions increases as Bi substitution increases. This behavior can be explained on the basis of ionic radius difference between constituted ions. The ionic radius of the bismuth is 0.96 Å larger than the iron 0.64 Å. Hence the distance between magnetic ions increases as Bi increases.

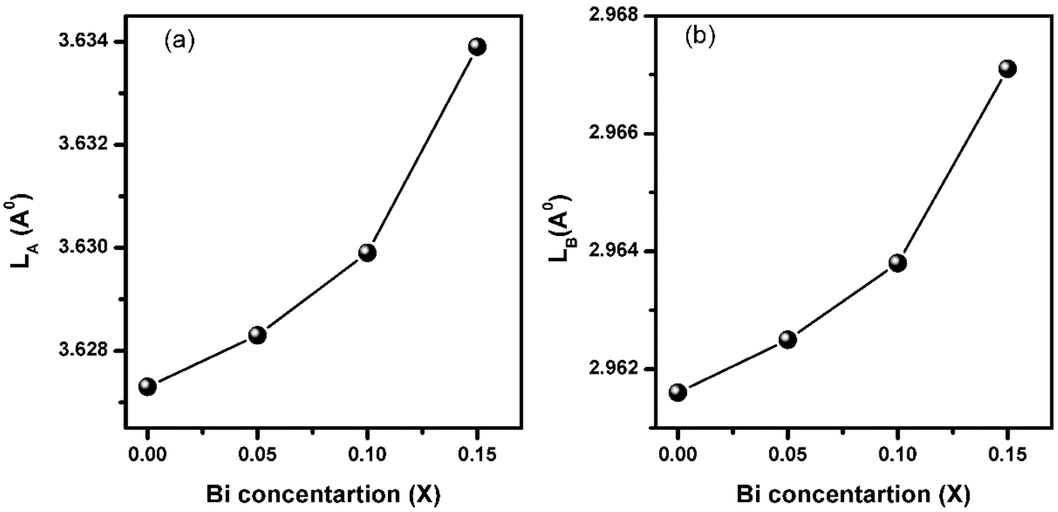

Fig 5.3. Variation of hoping length (a) tetrahedral (L_A) and (b) octahedral (L_B) sites as a function of Bi concentration

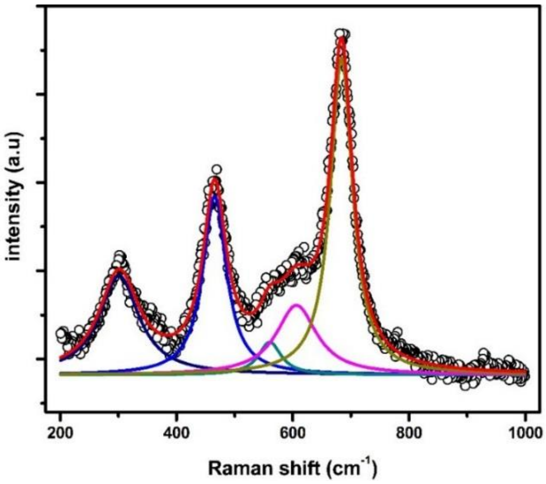

Fig 5.4. Raman spectra of 0.1 Bi substituted cobalt ferrite nanoparticles.

For further confirmation of Bi substitution, we have measured the Raman spectra of the 0.1 Bi substituted cobalt ferrite nanoparticles shown in figure 5.4. The active Raman modes of spinel structure which are characteristic to the spinel ferrites are observed in the Raman spectra of Bi substituted cobalt ferrite nanoparticles. All the observed Raman modes fitted with Lorentzean function and it is best fitted by the five distinct peaks. The modes below 600 cm^{-1} related to octahedral sites and above belong to tetrahedral sites [20]. The most intense peak in octahedral regions is observed at 465 $cm^{-1}$and for tetrahedral site at 683 cm^{-1}.

Figure 5.5 shows the FESEM image of the parent and modified cobalt ferrite ($CoFe_{1-x}Bi_xO_4$, x = 0, 0.15). The apparent particle growth is visible as an effect of Bi substitution. Lijun et al. has reported a similar particle growth due to Bi substitution in NiCuZn ferrite [16]. The particle size grows controllably from ~ 50 nm for parent to ~160 nm in Bi modified system. The increase in lattice constant which creates internal strain may be a possible reason for promoting particle growth [21].

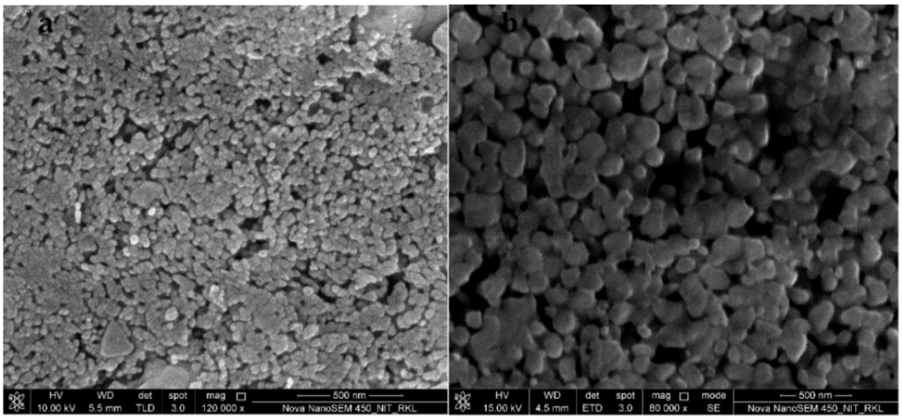

Fig 5.5. FESEM image of the (a) cobalt ferrite and (b) 0.15 Bi modified cobalt ferrite

5.3.2. Impedance Analysis

The real and imaginary impedance found from the formula $Z' = Zcos\theta$ and $Z'' = Zsin\theta$ where Z (=Z'+iZ") is the complex impedance. The complex modulus (M=M'+M") obtained from the complex impedance using the relation M'= wC_oZ'' and M"= wC_oZ' where $C_o = \frac{\varepsilon_o A}{t}$ is the capacitance in vacuum, $\varepsilon_o = 8.85\mathrm{x}10^{-12}$ F/m is the permittivity of the free space, t is the thickness of the sample and A is the cross sectional area of the electrode deposited on the sample and ω is the angular frequency. The dielectric constant was calculated from the relation $\varepsilon_r = \frac{Ct}{\varepsilon_o A}$ and resistivity ρ = RA/l where R is resistance, A is area and l is the length.

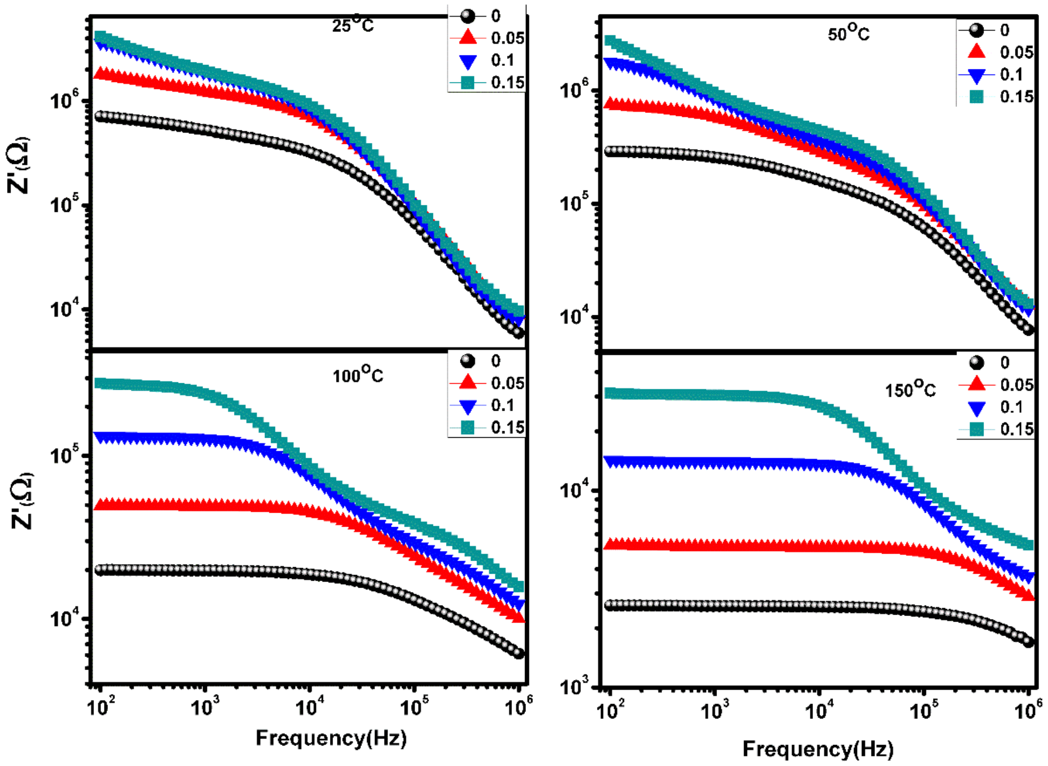

Fig 5.6. Frequency dependence of the real impedance of cobalt ferrite and Bi modified cobalt ferrite with selected temperatures.

Figure 5.6 shows the real impedance spectrum of pure and Bi modified nano CFO system within the frequency window of 100 Hz to 1 MHz in the temperature domain 25^0 C-200^0 C. The plateau region in the Z' refers a relaxation process and indicates dc resistance which arises due to the conduction of space charges [12]. With the elevation of temperatures, the enhanced thermal energy enables the space charges to follow higher frequencies which results in the widening of dc plateau. But the arrival of dc conduction implies the degradation of insulating behavior in a material. Bismuth substitution in CFO system has successfully suppressed the space charge conduction which can be construed from Figure 5.6. The late arrival of dc plateau increases with increase in bismuth content. The dc resistance in CFO system also increases in a significant value in the modified CFO system. From the spectrum, it is clear that there is a significant rise of resistance in Bi modified nano CFO. The decaying of resistance in pure CFO is observed to be faster than that of Bi-modified system.

For the confirmation of above results we have carried out the dc resistance measurement of parent as well as the bismuth modified systems. Figure7 shows temperature dependence of the dc resistance of all the samples, plotted in the temperature range of 25^0 C -200^0 C. The variation of resistance with temperature indicates the semiconducting nature of all the studied samples. Several investigations on cobalt ferrite have reported earlier which evidenced that the particle size has a strong influence on its electrical properties [12, 22]. Metallic to semiconducting transition occurs for particle size 2 – 16 nm as reported by Kannan *et al.* which also concluded that the transition temperature also changes with the size of the particle [23]. In contrary to above report, Rahman et al. [24] found the semiconducting to metallic transition for cobalt ferrite when particle size ranges to 10 nm. But Arun et al. [25] reported the metallic to semiconducting transition for particle size 6 nm and detailed that there exists no such transition when the particle size is greater than 50 nm. This concludes that the resistance of cobalt ferrite depends upon the size of the particle and therefore we propose that the increasing behavior of resistance with bismuth content must have some relation with the controlled grain growth of modified CFO systems.

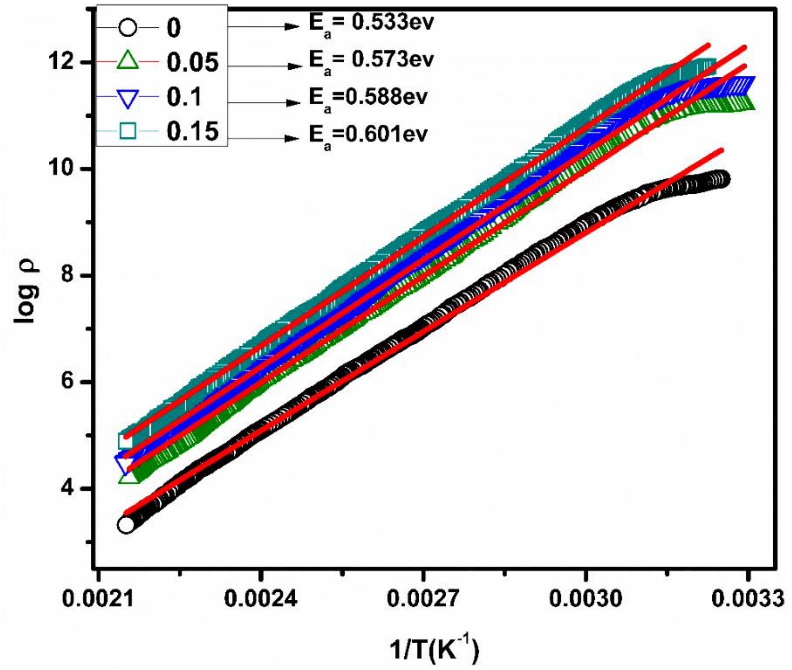

Fig 5.7. Temperature dependence DC resistance of Bi modified cobalt ferrite nanoparticles.

It was observed that the dc resistance increases with the substitution of bismuth. The activation energy is calculated by fitting dc resistivity data with Arrhenius relation (eq 5.3) and is given in the figure 5.7.

$$\rho = \rho_o \exp(\frac{E_a}{k_B T}) \qquad 5.3$$

In an earlier work reported by Nongjai et al. [26] have shown the increase in resistance with increase in indium content in cobalt ferrite. This resulted in insulating grain boundaries and hence increased in resistance. It also reported the reduced particle size with the substitution.

Contrary to the above report, Bismuth modification resulted in both the increase in resistance as well as particle size and therefore no possibility of relating with grain boundary concentration. In a very interesting investigation carried out by Sivakumar et al. [27], it is reported that the resistance of cobalt ferrite increases with increase in grain size though it is unexpected. It is a general feature in spinel ferrites that the conductivity is due to electron hopping between Fe^{2+} - Fe^{3+} which occurs in octahedral site. Taking Mossbauer study, they confirmed that the increase in grain size prompted Co ion to migrate towards octahedral site and Fe ion followed reverse migration towards tetrahedral site to maintain stability of spinel structure. This reduced the Fe ion concentration in octahedral site and hence the decrease in conductivity of the system. This mechanism is quite supportive to our result. The increase in particle size due to bismuth substitution in CFO system must have experienced the above explained cation migration. Though in octahedral site, hopping of hole takes place between Co^{2+} - Co^{3+} but its contribution towards conductivity is very less comparably to electron conduction [13,27] and as a whole the conductivity of the system reduces. As a result resistance of the system increases.

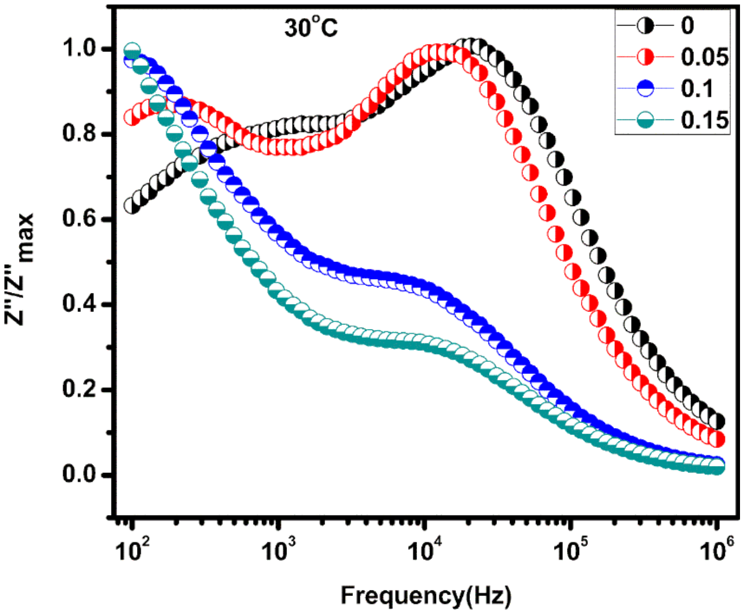

Fig 5.8. Frequency dependence of normalized imaginary impedance of parent and Bi modified cobalt ferrite nanoparticles.

To gather more information and distinguish intrinsic (grain) and extrinsic (grain boundary and electrode contact face effect) we have investigated the imaginary impedance (Z") spectra, imaginary electric modulus (M") and their combined behavior. Figure 5.8 shows the imaginary impedance vs. frequency plot of the parent and the modified system. The two prominent peaks in parent system (represented in black spheres) is seen to have corresponding peaks in modified systems which are depressed and shifted towards lower frequency zone.

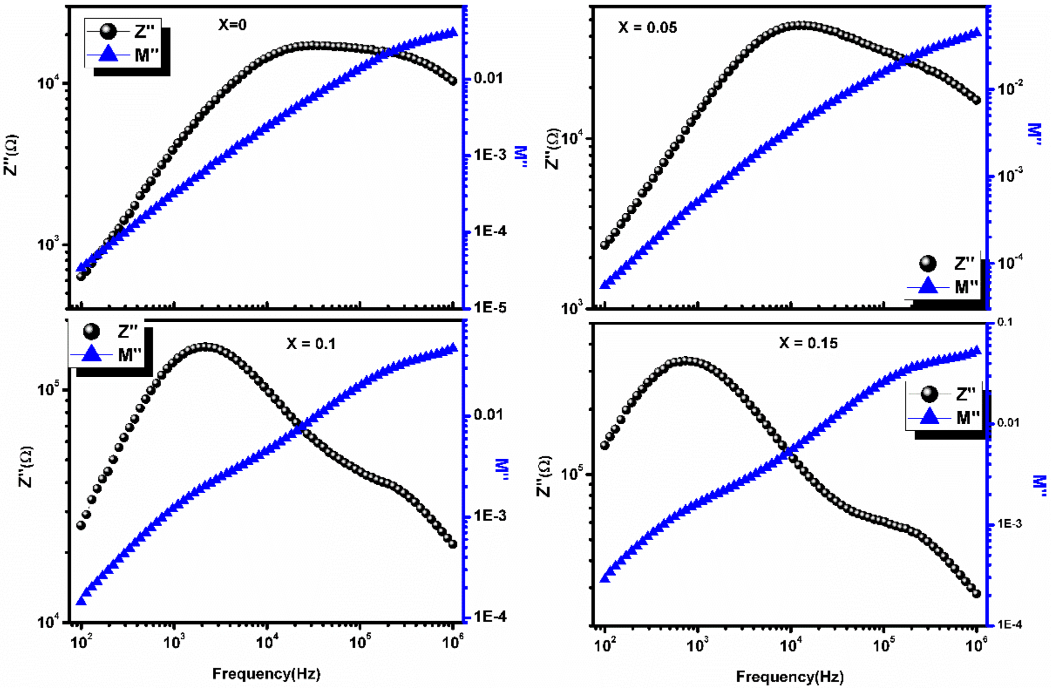

Fig 5.9. Combined plot of frequency dependence of imaginary impedance and modulus of parent and modified cobalt ferrite with varying composition.

The depression in peak at higher frequency side is maximal for higher concentration of bismuth. In our earlier work on dielectric relaxation and conductivity study of CFO system [11], we have reported the absence of grain effect in nano form (70 nm). The interfacial effects like grain boundary and surface polarization dominate the conduction mechanism from room temperature (25^0 C). The prominent grain growth in Bi modified CFO system, observed in FESEM image, can be hardly digested for absence of grain effect. Therefore, we have drawn the combine plot (Figure 5.9) of both the imaginary impedance (Z") and electric modulus (M") to identify the intrinsic and extrinsic effect as the latter has the ability to suppress the electrode surface polarization effect [28]. The relaxation peaks due to surface polarization effect in Z" spectra at lower frequency belt are successfully suppressed in M" plot for parent CFO system. But, this suppression does not occur in Bi-modified CFO system. This indicates that there is no presence of surface effect till maximum studied temperature (200^0 C). Rather, the less prominent peak which was assumed as the depressed one of corresponding parent system has its unique identity which we assume as the presence of grain effect.

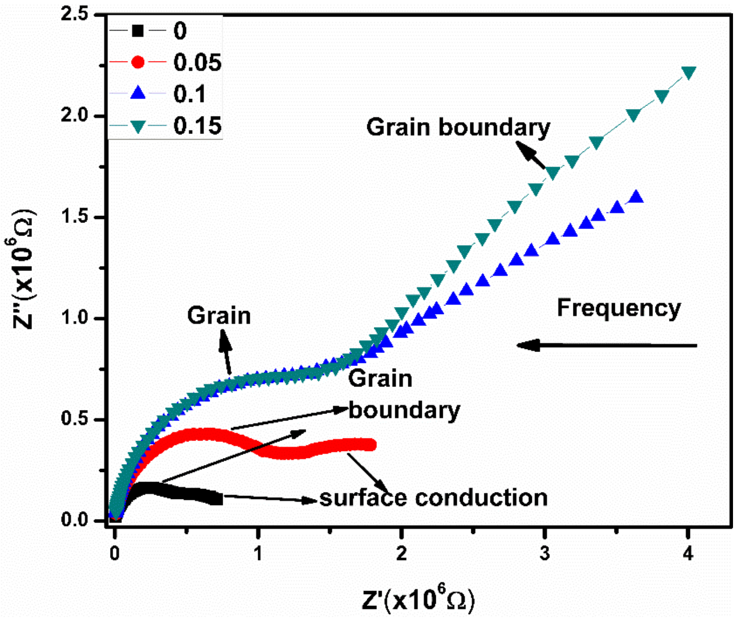

Fig 5.10 (a). Room temperature Cole-Cole plots of Bi substituted cobalt ferrite nanoparticles

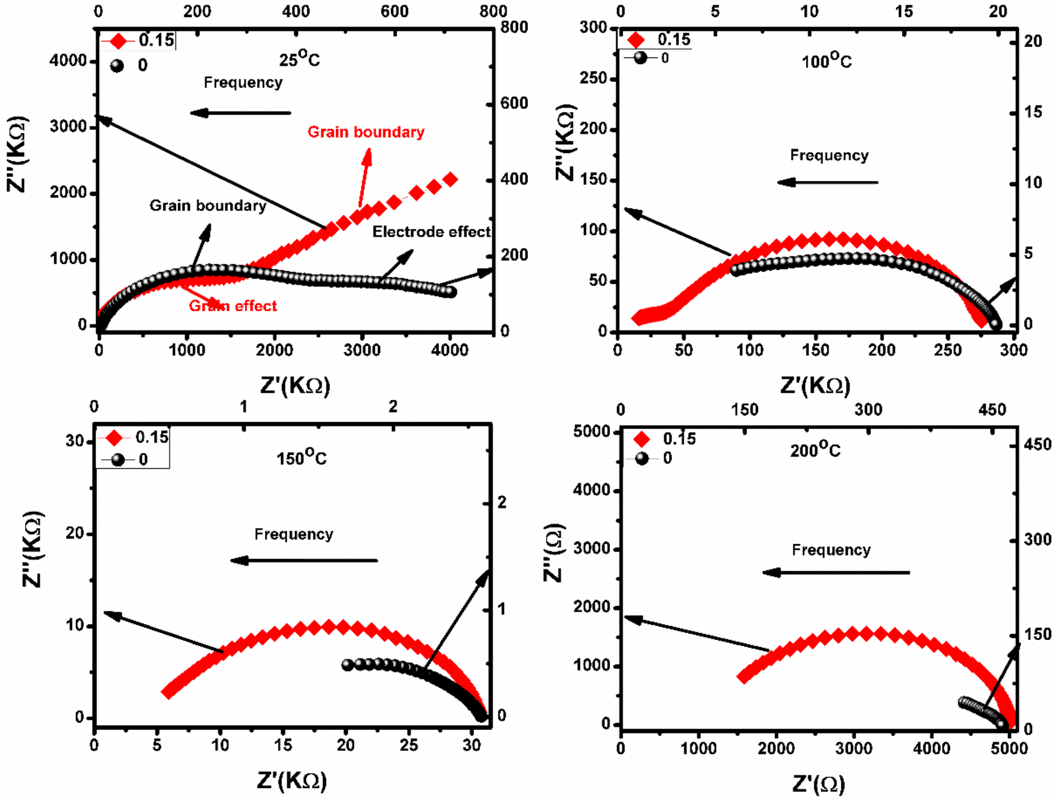

Fig 5.10 (b). Cole-Cole plots of cobalt ferrite and 0.15 Bi substituted cobalt ferrite with varying temperature.

Figure 5.10 (a) shows the evolution of Nyquist semicircles at room temperature in which two semicircles appear in parent system attribute to grain boundary and electrode surface effect But in the modified system, the appeared peaks are identified as grain and grain boundary effect. The evolution is shown up to 200^0 C in figure 5.10 (b) in which the black spheres represents for the parent system and the red one for the modified system. The grain boundary effect vanishes around 100^0 C and thereafter, an electrode surface effect dominates in parent system. But in the modified system, the grain boundary resistance is found to be increased about an order which continues up to the maximum studied temperature. Unlike parent system, no surface conduction appears in modified one up to the 200^0 C temperature. This confirms the bismuth modification has successfully suppressed the surface conduction which is unwanted for application purpose.

The effect of grain growth is quite interesting and discernible in dielectric loss behavior which is shown in figure 5.11. In its frequency dependent graph, a large reduction is observed at low frequency ($< 10^5$ Hz) belt in modified CFO system whereas; at higher frequency there is no significant difference. The dielectric value depends upon the polarizability which arises due to intragrain conduction due to electron or hole exchange interaction between Fe^{2+}/ Fe^{3+} and Co^{2+}/ Co^{3+} and the intergrain conduction is inhibited by the potential barriers at grain boundaries due to space charges [13,14,29]. The strength of potential barrier depends upon the deposited amount of space charges in polarized state. The increase of surface area of the grain will result in more space charge polarization and hence strong potential barrier to prevent intergrain charge transportation [29]. As the grain in bismuth modified CFO system has larger surface area than parent one therefore, the potential barrier at grain boundaries is stronger in former case. This results in a large increase in resistance of the material as we have already found in earlier results. Here we consider when space charge polarization decays i.e. grain boundary conduction takes place then the intergrain conduction dominates due to weakening of barrier potential. This reduces the grain as well as grain boundary polarizability which appear as dielectric loss. In parent system, grain boundary conduction takes place very early due to comparably weak barrier potential. As space charge polarization is a low frequency response therefore, the dielectric loss is more in low frequency regime. However, the evolution of grain in bismuth modified CFO has ability to sustain sufficient grain polarization due to strong space charge polarization near grain boundaries and this is confirmed from the relaxation behaviour appears in both frequency and temperature dependent dielectric loss features.

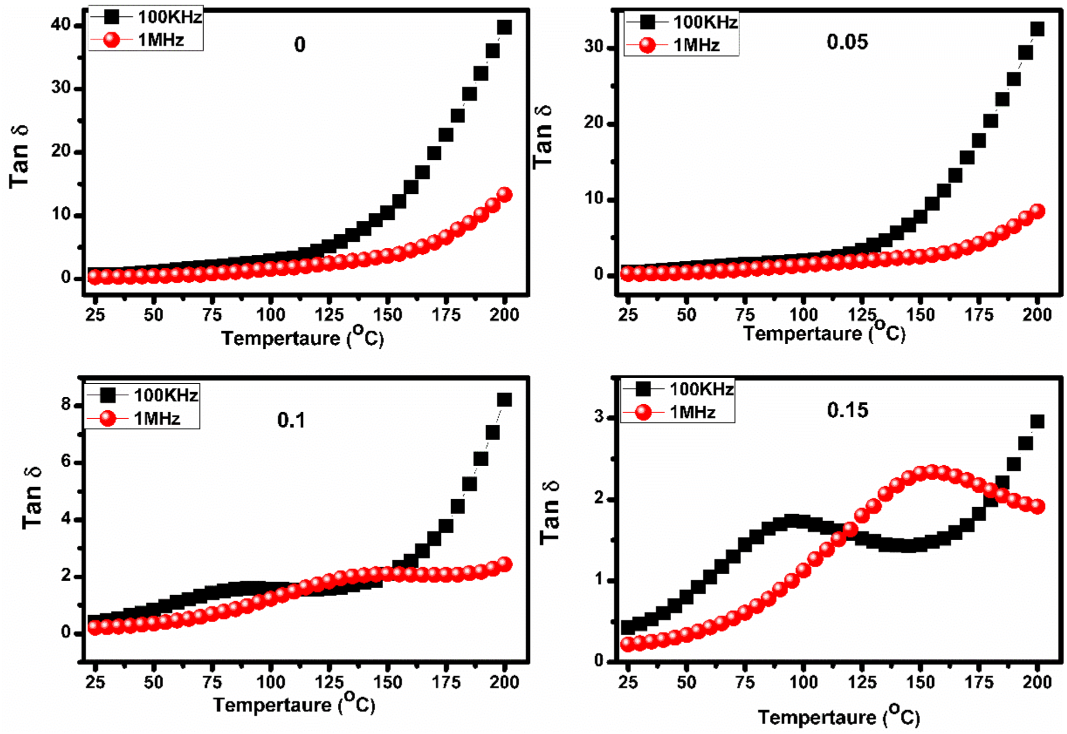

Fig 5.11 (a). The temperature dependence of dielectric loss of parent and Bi modified cobalt ferrite nanoparticles.

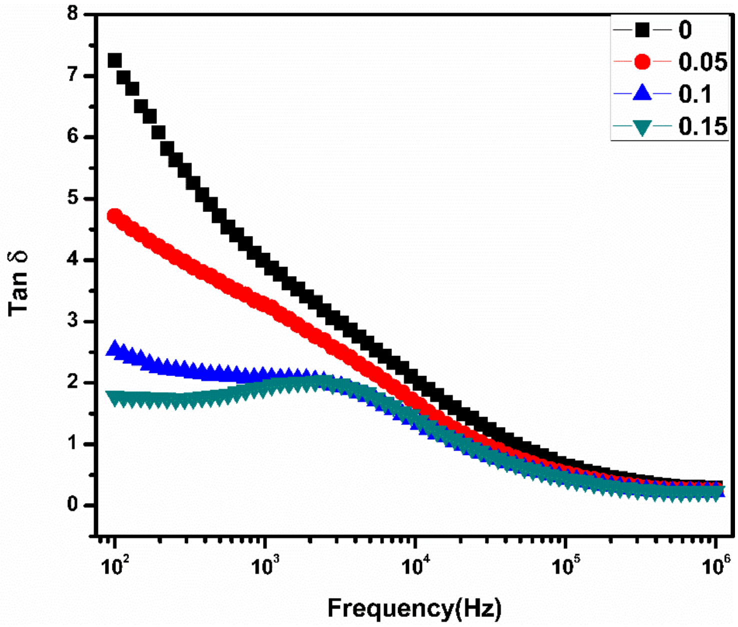

Fig 5.11 (b). The frequency dependence of dielectric loss of parent and Bi modified cobalt ferrite nanoparticles.

5.3.3. Dielectric properties

Dielectric constant variation with frequency at room temperature is shown in figure 5.12. The dielectric constant was measured in the interval of 100 Hz to 1MHz. The dispersion of real permittivity with frequency can be explained on the basis of various sources of polarization. The real permittivity in ferrites is due to results of four types of polarizations; surface polarization, dipolar polarization, atomic and ionic polarization [12]. This polarization mechanism is strongly frequency dependent. Sufficient time requires for surface and dipolar polarization so which are substantial at lower frequencies and remaining are significant at high frequencies. The electronic and ionic polarizations are major contributors for dielectric constant at higher frequencies and there is a sharp decrease in dielectric constant after certain frequency and becomes almost frequency independent. The same mechanism is responsible for polarization as well as conductivity in ferrites. Charge hoping between multi-oxidation states of the cobalt and iron in octahedral site is reasonable for the polarization in ferrites and after certain frequency they cannot follow the applied electric field thus resulting in the decrease in permittivity with increasing frequency [14]. Real permittivity decreases with increasing Bi substitution. It may be due to that the reduction of iron concentration in octahedral site which results in the decrease in hopping of charge carriers that leads to decrease in dielectric constant. The frequency dependence of dielectric constant was modeled with the modified Debye equation because more than one ion (O^{2-}, Co^{2+}, Fe^{3+}) contribute to the relaxation process [14].

$$\varepsilon' - \varepsilon_\infty = \frac{\varepsilon'_0 - \varepsilon'_\infty}{\left[1+(\omega\tau)^{2(1-\alpha)}\right]} \qquad 5.4$$

where ε_0 *and* ε_∞ are the dielectric constants at low frequency and high frequency respectively, $\omega=2\pi f$ is frequency τ is mean relaxation time and α is the spreading factor. From figure 5.12 it is observed that the experimental data (circles) is in good agreement with the Debye function (solid line) indicates more than one ion participating in the relaxation process of Bi substituted cobalt ferrite nanoparticles. The fitted values are τ = 3.10, 3.29, 3.44, 3.59 x10^{-3} s and α= 0.35, 0.23, 0.32, 0.27 for x = 0, 0.05, 0.1 and 0.15 respectively. Mean relaxation time increases with increasing Bi substitution. The existence of inertia to the charge movement would cause relaxation of polarization [30]. The increased mean relaxation time can be explained by using the structural analysis. The hoping length increases with the increasing Bi substitution and it may be a reason for decreasing relaxation time with Bi substitution. Electrode effect which plays important role for polarization of ferrites is marginalizing with the substitution of Bi^{3+}. This may be another cause for decreasing nature dielectric constant with bismuth doping.

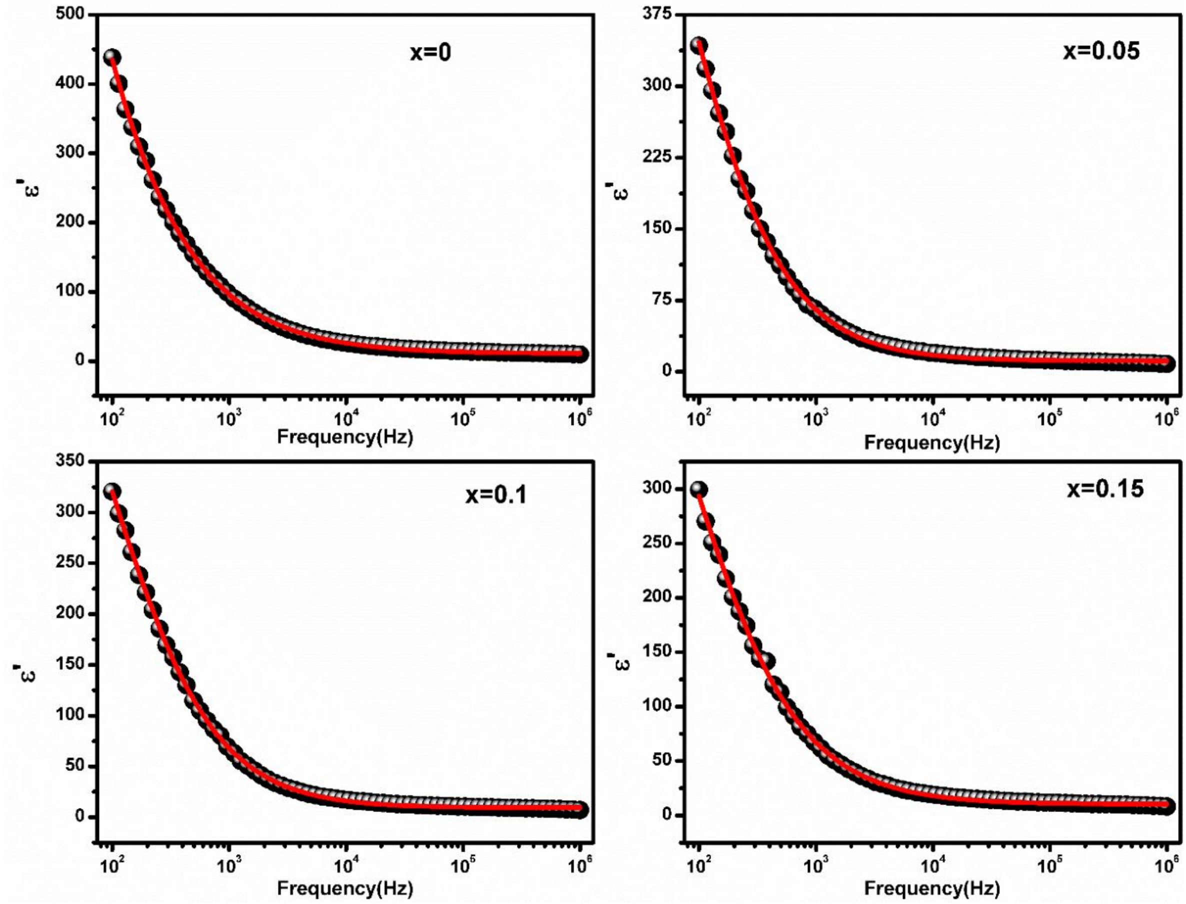

Fig 5.12. Frequency dependence of dielectric constant at room temperature and its modeling with modified Debye law

5.3.4. AC conductivity analysis

Ac conductivity of the bismuth substituted cobalt ferrite nanoparticles is shown in figure 5.13. Conductivity decreases with temperature and increases with frequency in all the samples which is natural behavior of the spinel ferrites. The same mechanism which is reasonable for the fall of dc resistance with temperature is responsible for the increase in conductivity with temperature. Frequency dependence of ac conductivity exhibits two types of behavior. The frequency independent region at lower frequency side and increasing trend with frequency at higher frequency side. Jonschers power law explains the frequency dispersion of ac conductivity. According to this law total conductivity is the sum of the dc and ac conductivity and is given by [31].

$$\sigma_t(\omega) = \sigma_{dc} + A\omega^n \tag{5.5}$$

where $\sigma_t(\omega)$ is the total conductivity, σ_{dc} is the dc conductivity, $A\omega^n$ is frequency dependent conductivity also known as ac conductivity and ω is the frequency, n (frequency exponent) and A are temperature and material intrinsic property dependent constants. It is known fact that the electrical properties are strongly depends on the concentration of iron atoms in the octahedral site [11].

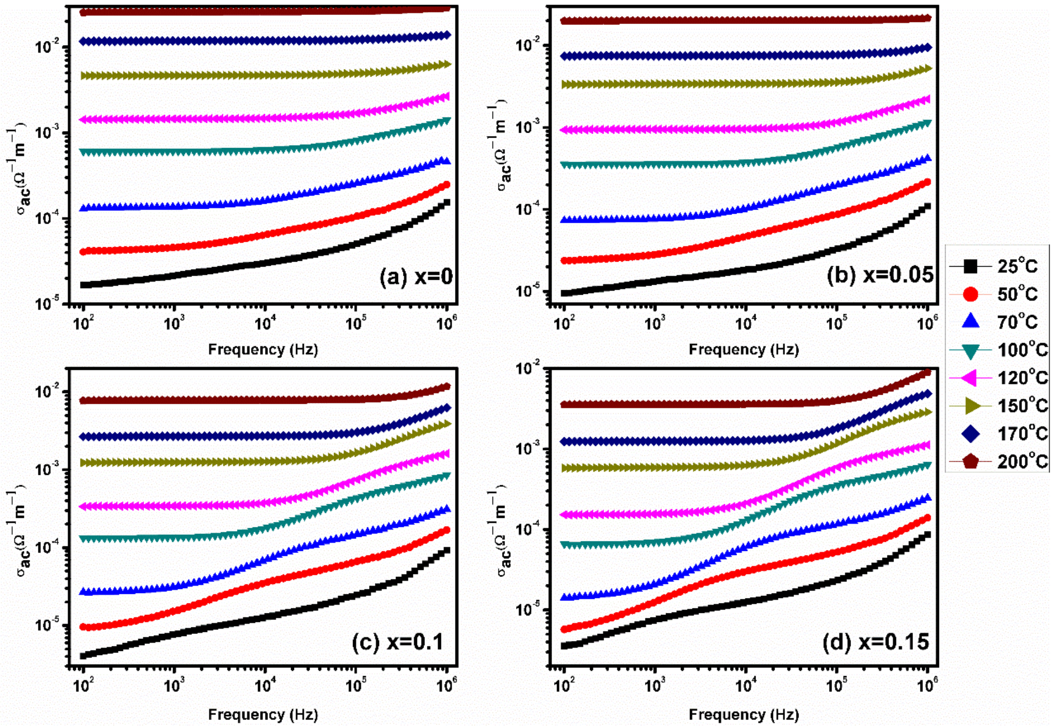

Fig 5.13. Frequency and temperature dependence of ac conductivity of Bi substituted cobalt ferrite nanoparticles

The conduction due to the electron exchange between multi-oxidation state of iron (Fe^{2+}-Fe^{3+}) and hole hoping between multi-oxidation sates of the cobalt ion in octahedral site but the contribution from the hole hoping is very much less compared to the electron hopping so that the conduction is mostly dependent on the iron concentration in octahedral sites [14]. The frequency independent region represents the dc conductivity part of the total conductivity due to the long range motion of the charge carriers [10]. The frequency dependent region results from the localized motion of the charge carriers due to short time availability and the frequency dependent represented by the frequency exponent n [10,32]. The total conductivity decreases with the Bi^{3+} substitution and agrees with the results of the dc resistance. Reduction of iron ions in octahedral site may be the reason for the decrease in total conductivity. From the conductivity plots it is observed that the behavior of frequency dependence of conductivity is changing with respect to the Bi substitution. For x=0 and 0.05 only two parts are frequency independent and frequency dependent. But for x=0.1 and 0.15 in addition to the frequency independent part, two dispersion regions appeared for the low frequency dispersion that belongs to grain boundary and the high frequency part related to grain conduction. This behavior is because of the appearance of grain relaxation in Bi substituted cobalt ferrite nanoparticles. This kind of frequency dependence of conductivity cannot be explained by single power law but with double power law and given by [32]

$$\sigma_t(\omega) = \sigma_{dc} + A_1\omega^{n_1} + A_2\omega^{n_2} \qquad 5.6$$

which explains the different contributions to conductivity. The first part σ_{dc} related to the dc conductivity, the second part is $A_1\omega^{n_1}$ related to the low frequency dispersion where $0 < n_1 < 1$ and third part $A_2\omega^{n_2}$ ascribes to the high frequency dispersion region where $0 < n_2 < 2$ [32]. The conductivity data fitted with the single power law and from the temperature dependence of the n value (shown in fig 5.14), it was observed that the overlapping large polaron tunneling (OLPT) is the most probable conduction process.

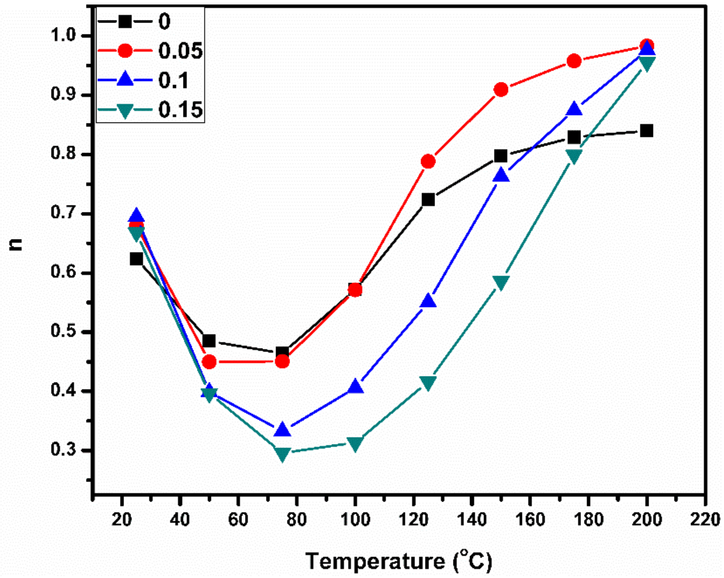

Fig.5.14. Temperature dependence of the frequency exponent ‘n’.

5.4. Magnetic properties

Figure 5.14 displays the field dependent magnetization study of CFO and its modified systems. The hysteresis loop shown in the plot indicates ferromagnetic ordering for all the samples. We have calculated magnetic moment per unit formula in terms of Bohr’s magneton from the following equations [17, 33-35]

$$\eta_B = \frac{M \times M_S}{5585} \qquad 5.7$$

where M is molecular weight of the composition, M_S is the saturation magnetization. All the magnetic parameters are tabulated below. Enhanced saturation (M_S) and remnant magnetization (M_r) and magneton number (η_B) is observed in modified CFO system accompanied with the reduced coercivity (H_c) shown in fig 5.15. The degree of enhancement depends upon the amount of bismuth content.

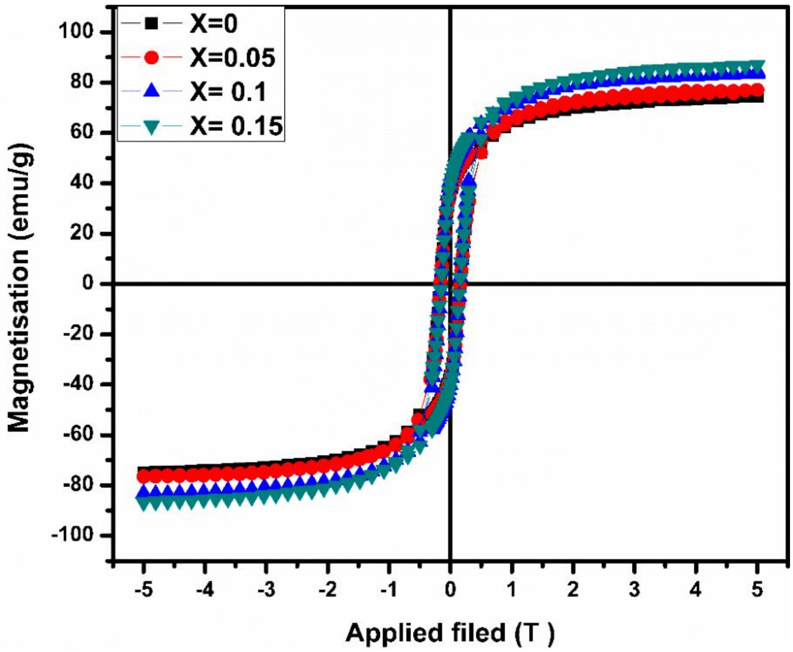

Fig 5.15. M-H loops of the cobalt ferrite and Bi substituted cobalt ferrite at room temperature.

Table 5.1. Magnetic properties of the $CoFe_{1-x}Bi_xO_4$

Composition (x)	M_S (emu/gm)	M_r (emu/gm)	H_C (Oe)	η_B (μ_B)
0.00	74.5	36.46	1633	3.13
0.05	75.8	36.92	1610	3.18
0.10	84.7	39.67	1539	3.55
0.15	86.5	41.04	1520	3.63

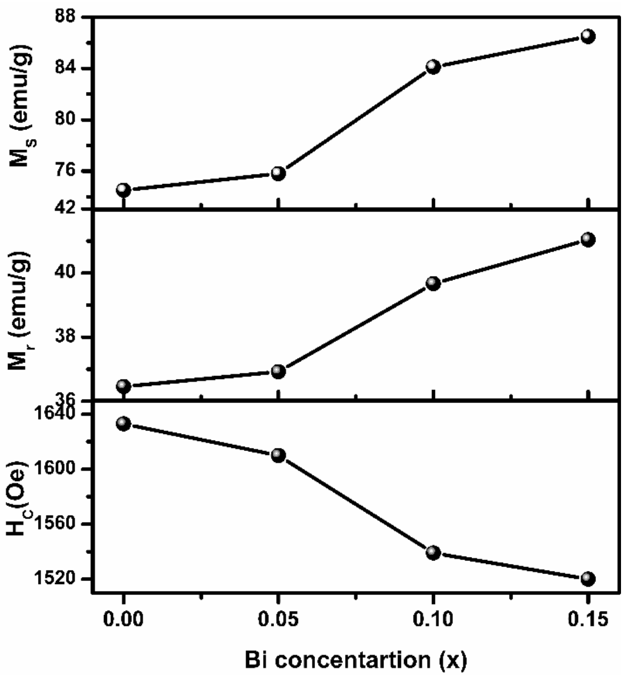

Fig 5.16. Effect of Bi on magnetic properties of the cobalt ferrite nanoparticles

The magnetic properties of the spinel ferrites are strongly dependent on the cation distribution between the tetrahedral (A) and octahedral (B) sites, as well as the interaction between them. Among the three existing exchange interactions such as AA, BB and AB, the antiferromagnetic AB interaction dominates over other interactions. Therefore, the resultant magnetic moment will be equal to $M_A \sim M_B$ where M_A is the total magnetic moment of thetetragonal site and M_B is the total magnetic moment of the octahedral site [26,36-39]. In CFO system, the structure transforms from partial inverse to inverse spinel as particle size changes from nano to bulk range. Therefore, the magnetic properties must change accordingly with the growth of particle size. Cobalt occupies the octahedral site in inverse spinel whereas it occupies both the sites in partial inverse spinel form [40, 41]. As bismuth substitution brings controlled particle growth therefore, there may be the migration of Co ion towards octahedral site with increases with bismuth content which leads to rise in saturation magnetization. In earlier investigations on size dependent study of magnetic properties in cobalt ferrite nanoparticles, it has been reported that the saturation magnetization increases and coercivity decreases with increasing particle size [42, 43]. Again, the increasing nature of saturation magnetization with increase in particle size is also reported due to the weakening of surface effects. The surface effects originated by distortion of the magnetic moments at the surface of nanocrystals and these effects weakened as particle size increases [44-47]. The coercivity of ferrite nanoparticles too strongly depends on the particle size [40,41]. It increases with decreasing particle size, gets maximum and then decreases to zero when superparamagnetism appears for extreme nanoparticles [26,46]. The coercivity depends upon the easy orientation of domain walls. When the domain size approaches particle size then domain orientation requires particle orientation. This creates large friction effect and hence large coercive field [16,48]. Number of domains in a particular particle changes with its size and therefore, coercivity also changes [26]. The relation [26] between the size and coercivity in a multi-domain region is given by

$$H_C = a + \frac{b}{D} \tag{5.8}$$

where D is diameter of the particle and a, b are constants. The controlled particle growth in bismuth modified system generates the possibility of multiple domains which are separated by domain walls. This ensures that the domain wall orientation is more preferable in modified CFO than particle orientation which reduces friction effect and hence, less coercivity appears.

Thus, bismuth modification in nano-cobalt ferrite system has successfully solved the problems to a large extent. The evolution of intrinsic behaviour *i.e.* grain effect and suppression of unwanted surface conduction makes it more versatile for application purpose. The increase in resistance of modified cobalt ferrite ceramic can be more suitably used as core of transformers as the induction of eddy current will be minimum. The enhanced saturation magnetization will be able to store more data for computer memory application. The suppression of dielectric loss at low frequency regime will meet the requirement for various electrical applications.

5.5. Conclusions

Single phase bismuth substituted cobalt ferrite was synthesized by auto combustion technique. Controlled particle growth brought interesting features in electrical and magnetic properties in the modified systems. Sufficient rise in resistance, evolution of grain effect, along with successfully suppressed the unwanted surface conduction as well as lowering the dielectric loss at lower frequency regime were the prominent observations. In addition, there was enhancement in saturation magnetization and reduction in coercivity in bismuth substituted cobalt ferrite nanoparticles.

References

[1] Y. Cedeno-Mattei, O. Perales-Pérez, O. N. C. Uwakweh, and Y. Xin, Journal of Applied Physics 107 (2010) 09A741.

[2] K. Khaja Mohaideen and P. A. Joy, Applied physics letters**101** (2012) 072405.

[3] A.B. Salunkhe, V.M. Khot, M.R. Phadatare, S.H. Pawar, Journal of Alloys and Compounds 514 (2012) 91-96.

[4] Atta ur Rahman, M. A. Rafiq, K. Maaz, S. Karim, Sung Oh Cho and M. M. Hasan, journal of Applied Physics 112 (2012) 063718.

[5] A. Franco, Jr. and F. C. e Silva, journal of Applied Physics 113 (2013) 17b513.

[6] I. C. Nlebedim, R. L. Hadimani, R. Prozorov, and D. C. Jiles, Journal of Applied Physics 113 (2013) 17A928.

[7] S. J. Lee, C. C. H. Lo, P. N. Matlage, S. H. Song, Y. Melikhov, J. E. Snyder, and D. C. Jiles, Journal of Applied Physics 102 (2007) 073910.

[8] R.K. Panda, D. Behera, Journal of Alloys and Compounds 587 (2014) 481-486.

[9] K. Kamala Bharathi and C.V. Ramana, Journal of Materials Research 26 (2011) 584-591.

[10] W. Chen, W. Zhu, O. K. Tan, and X. F. Chen, Journal of Applied Physics 108 (2010) 034101.

[11] R.K. Panda, R. Muduli, S.K. Kar, D. Behera, Journal of Alloys and Compounds 615, (2014) 899-905.

[12] N. Sivakumar, A. Narayanasamy, C. N. Chinnasamy, and B. Jeyadevan, J. Phys.: Condens. Matter 19 (2007) 386201.

[13] C. V. Ramana, Y. D. Kolekar, K. Kamala Bharathi, B. Sinha, and K. Ghosh, Journal of Applied Physics 114 (2013) 183907.

[14] Y. D. Kolekar, L. J. Sanchez, and C. V. Ramana, Journal of Applied Physics 115, (2014) 144106.

[15] Lijun Jia, Huaiwu Zhang, Xiaohu Wu, Tao Li, Hua Su, and Baoyuan Liu, Journal of Applied Physics 111, (2012) 07A326.

[16] A. Franco, Jr., F. L. A. Machado,V. S. Zapf and F. Wolff-Fabris, Journal of Applied Physics 109 (2011) 07A745.

[17] R. C. Kambale, K. M. Song, Y. S. Koo, and N. Hur, Journal of Applied Physics 110 (2011) 053910.

[18] R.C. Kambale , P.A. Shaikh , N.S. Harale , V.A. Bilur , Y.D. Kolekar , C.H. Bhosale and K.Y. Rajpure, Journal of Alloys and Compounds 490 (2010) 568-571.

[19] D.S.Nikam, S.V.Jadhav, V. M. Khot, R. A. Bohara, C. K. Hong, S. S. Mali and S. H. Pawar, RSC Adv.5, (2015) 2338–2345.

[20] Cameliu Himcins chi, Ionela Vrejoiu, Georgeta Salvan, Michael Fronk, Andreas Talkenberger, Dietrich R. T. Zahn, David Rafaja, and Jens Kortus, Journal of Applied Physics 113 (2013) 084101.

[21] Sagar E. Shirsath, R. H. Kadam, S. M. Patange, M. L. Mane, Ali Ghasemi, and Akimitsu Morisak, Applied physics letters 100 (2012) 042407.

[22] K. Vasundhara, S. N. Achary, S. K Deshpande, P. D. Babu, S. S. Meena and A. K. Tyagi, Journal of Applied Physics 113 (2013) 194101.

[23] R. Kannan, S. Rajagopan, A. Arunkumar, D. Vanidha, and R. Murugaraj, Journal of Applied Physics 112 (2012) 063926.

[24] Atta ur Rahman, M. A. Rafiq, S. Karim, K. Maaz and M. M. Hasan, J. Phys. D: Appl. Phys.44 (2011) 165404.

[25] A. Arunkumar, D. Vanidha, K. Oudayakumar, S. Rajagopan, and R. Kannan, Journal of Applied Physics 114 (2013) 183905.

[26] Razia Nongjai, Shakeel Khan, K. Asokan, Hilal Ahmed, and Imran Khan, Journal of Applied Physics 112 (2012) 084321.

[27] N. Sivakumar, A. Narayanasamy, K. Shinoda, C. N. Chinnasamy, B. Jeyadevan, Journal of Applied Physics, 102 (2007) 013916.

[28] N. Sivakumar, A. Narayanasamy, N. Ponpandian and G. Govindaraj, Journal of Applied Physics 101 (2007) 084116.

[29] O. Raymond, R. Font, N. Suarez-Almodovar , J. Portelles and J. M. Siqueiros, Journal of Applied Physics 97 (2005) 084107.

[30] K. Kamala Bharathi, G. Markandeyulu, and C. V. Ramana, J. Phys. Chem. 115 (2011) 554–560.

[31] A. Ghosh, Phys. Rev. B 47 (1993) 1537.

[32] N. Ortega, Ashok Kumar, P. Bhattacharya, S. B. Majumder, and R. S. Katiyar, Phys. Rev. B 77 (2008) 014111.

[33] R.C. Kambale, P.A. Shaikh, S.S. Kamble and Y.D. Kolekar, Journal of Alloys and Compounds 478 (2009) 599-603.

[34] Sonal Singhala and Kailash Chandra, Journal of Solid State Chemistry 180 (2007) 296-300.

[35] S. S. Jadhav, S. E. Shirsath, S. M. Patange, and K. M. Jadhav Journal of Applied Physics 108 (2010) 093920.

[36] Diego Gutierrez, Michael Foerster, Ignasi Fina, and Josep Fontcuberta, Physical Review B 86 (2012) 125309.

[37] C. E. Rodrıguez Torres, F. Golmar, M. Ziese, P. Esquinazi, and S. P. Heluan, Physical Review B 84 (2011) 064404.

[38] S. Soliman, A. Elfalaky, Gerhard H. Fecher and Claudia Felser, Physical Review B 83 (2011) 085205.

[39] Jeong Hyun Shim and Soonchil Lee, Physical Review B **73** (2006) 064404.

[40] A. Franco Jr., F. C. e Silva, and Vivien S. Zapf, Journal of Applied Physics 111 (2012) 07B530.

[41] M. Atif, R. Sato Turtelli, R. Grossinger, and F. Kubel, Journal of Applied Physics 113 (2013) 153902.

[42] K. Maaza, Arif Mumtaza, , S.K. Hasanaina, Abdullah Ceylan, Journal of Magnetism and Magnetic Materials 308 (2007) 289 – 295.

[43] Michal Sedlacik, Vladimir Pavlinek, Petra Peerd and Petr Filip, Dalton Trans.43 (2014) 6919.

[44] Yuqiu Qu Haibin Yang, Nan Yang, Yuzun Fan, Hongyang Zhu and Guangtian Zou, Materials Letters 60 (2006) 3548 – 3552.

[45] R. H. Kodama and A. E. Berkowitz, Physical Review Letters 77 (1996) 394-397.

[46] Yue Zhang, Yong Liu, Chunlong Fei, Zhi Yang, Zhihong Lu, Rui Xiong, Di Yin and Jing Shi, Journal of Applied Physics 108 (2010) 084312.

[47] C. Vazquez-Vazquez, M. A. Lopez-Quintela, M. C. Bujan-Nunez and J. Rivas, J Nanopart Res 13 (2011) 1663-1676.

[48] Ravi Kumar, S. K. Arora, I. V. Shvets, N. E. Rajeevan, P. P. Pradyumnan, and D. K. Shukla, Journal of Applied Physics 105 (2009) 07D910.

CHAPTER 6

Effect of Cr^{3+} on electric and magnetic properties of cobalt ferrite nanoparticles

This section describes the effect of incorporation of Cr^{3+} *into* $CoFe_2O_4$ *nanoparticles on its magnetic and electric properties, prepared by auto combustion method. The samples of* $CoFe_{2-x}Cr_xO4$ *(x = 0, 0.15, 0.3) series were characterized by x-ray diffraction and field emission scanning electron microscopy to find out the average particle size. The substitution of* Cr^{3+} *caused a significant reduction in particle size of the modified systems. Room temperature Mossbauer spectroscopy and magnetic characterization were performed. Analysis of extracted parameters concluded that* Cr^{3+} *replaced the* Fe^{3+} *at B-site (octahedral). The decrease in magnetization at B-site was found responsible for the observed reduced saturation magnetization and coercivity. Impedance spectroscopic analysis has revealed the suppression of electrode-sample surface conduction effect and enhancement of material resistivity. The latter was confirmed by dc resistivity measurement. All these results were explained on the basis of occupancy of* Cr^{3+} *at B-site, surface anisotropy potential and reduced particle size.*

6.1. Introduction

$CoFe_2O_4$ is one of the members of spinel ferrite family which has been extensively studied for its intrinsic properties of large spin polarization, good chemical stability, high resistance and high magnetic critical temperatures; typically well above the room temperature [1-3]. Number of modifications have been carried out to enhance on it both magnetically and electrically to make a potential material for wide range of applications such as magnetic recording and storage, spin filters, spintronics and phase shifters [4-6].

The general formula of spinel ferrite is AB_2O_4 which is accompanied by a cubic close packed arrangement of oxygen anions with A^{2+} and B^{3+} cations and the cations distribute themselves in two different sites of AO_4 tetrahedral and BO_6 octahedral with oxygen co-ordination. The resultant magnetic moment of unit cell in AB_2O_4 develops due to the uncompensated magnetic moments of A and B magnetic sub-lattice [7-9]. The ferromagnetic or antiferromagnetic nature of this type of material can be understood by studying the strength of exchange interaction among cations such as A-A or A-B interactions. Therefore, the magnetic properties of the spinel ferrites are strongly influenced by the distribution of cations among these tetrahedral and octahedral sites. The electrical properties also influenced by cation distributions in spinel ferrites. The modifications occurred by incorporating any dopant has effect on particle growth, A-A or A-B exchange interactions and subsequently on material properties [10-13].

$CoFe_2O_4$ assumes inverse spinel in its bulk form but gradually transforms into partial inversion spinel as the particle size approaches towards nano scale due to alteration in cation distribution [14-16]. In its bulk form, cobalt ferrite consists of two antiferromagnetically coupled sub-lattices [17,18]. Out of which, one of the sub-lattices is formed by ferromagnetically ordered Fe^{3+} ($3d^5$, magnetic moment ($M = 5\ \mu_B$) ions occupying the tetragonal A sites while the other one contains ferromagnetically ordered Co^{2+} ($3d^8$, $M=3\ \mu_B$) and Fe^{3+} ($3d^5$, $M=5\ \mu_B$) ions occupying the octahedral B sites of the spinel AB_2O_4 structure which provides net saturation magnetization of $3\mu_B$/f.u. [19-21]. Any change in distribution of cations among tetrahedral and octahedral site alters the spin order which strongly affects the magnetic and electric properties of cobalt ferrite. The incorporation of dopant at any preferable site not only brings change in magnetic moment but also controls on particle growth which can bring changes in cation distribution and ultimately controls material behaviors.

In our present work we have chosen Cr^{3+} as dopant to substitute Fe^{3+} in $CoFe_2O_4$ system. Similar modifications have also reported earlier by authors [22-24] on magnetic properties but limited discussion on electric properties. Here, we have performed a systematic and through investigation of electrical properties of Cr substituted $CoFe_2O_4$ system by complex impedance spectroscopy and magnetic properties from room temperature Mossbauer spectroscopic studies.

6.2. Materials and methods

$CoFe_{2-x}Cr_xO_4$ nanoparticles have been prepared by auto combustion method and using cobalt nitrate hex-hydrate ($Co(NO_3)_3.6H_2O$), Iron nitrate non-hydrate ($Fe(NO_3)_3.9H_2O$) and chromium nitrate ($Cr(NO_3)_3.9H_2O$) as initial precursors. The detailed procedure has been explained in our previous work [25]. The as prepared powder after combustion was calcined at 700^0 C for 4 hrs. Proper phase and structural identification and surface morphology were carried out by Rigaku Ultima-IV-X-ray diffractometer (Cu target) and Nova NanoSEM-450 Field emission scanning electron microscopy (FESEM) respectively. We have measured the dc electrical resistance by the Keithley electrometer (model 6517B) and ac electric properties of the nanoparticles by the HIOKI impedance analyzer (model IM3570) within the chosen frequency domain of 100 Hz to 1MHz and temperature range of 25^0 to 200^0 C the magnetic hysteresis loop at room temperature (RT) was measured by the SQUID magnetometer. Room temperature ^{57}Fe Mossbauer spectra for all the samples have been recorded in the transmission configuration with constant acceleration mode [26]. While a 25 mCi ^{57}Co isotope embedded in Rh matrix has been used as the Mossbauer source, a gas filled proportional counter has been used for the detection of the 14.4 keV Mossbauer γ - rays. The Mossbauer spectrometer has been calibrated with 95.16% enriched $^{57}Fe_2O_3$ and standard α-^{57}Fe foil. The Mossbauer spectra have been analyzed using a standard least square fitting program NMOSFIT [27].

6.3.Structural analysis

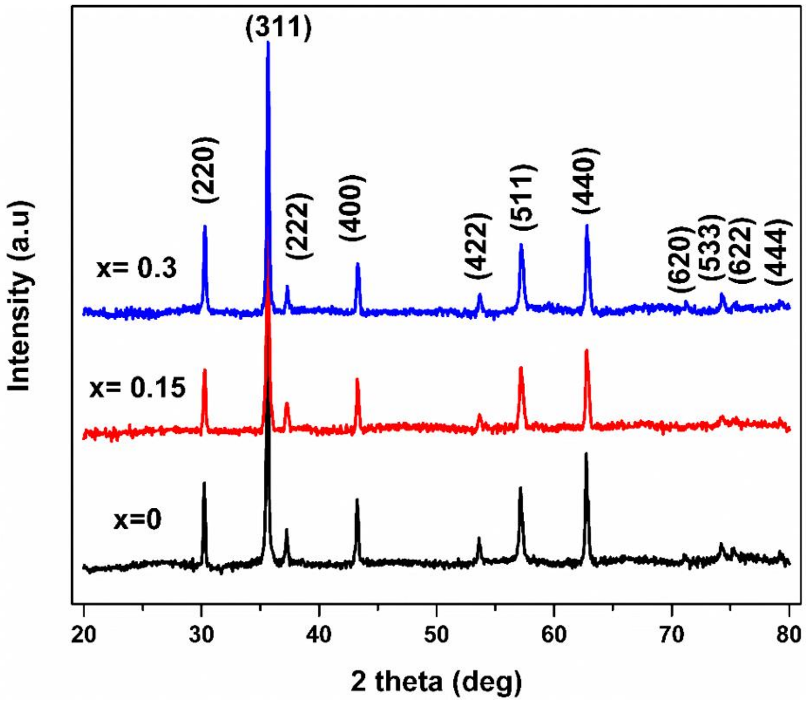

Fig 6.1. XRD pattern of the Cr substituted cobalt ferrite.

Figure 6.1 shows the XRD pattern of the $CoFe_{2-x}Cr_xO_4$, (x= 0.15-0.3). The position of the peaks match to the JCPDS card No22-1086 which belongs to the spinel symmetry with Fd3m space group. The strongest reflection comes from the (311) plane in all the samples. The broad XRD lines in the pattern indicate that the particles are in nano scale. We have calculated the particle size (S) by applying Scherer formula and taking the highest intensity peak (311) for consideration. The lattice constant (a), density (ρ_x) and hoping length for tetra (L_a) and octahedral (L_b) sites are calculated from the relations given below [28].

$$\left.\begin{aligned} a &= d(h^2+k^2+l^2)^{\frac{1}{2}} \\ \rho_x &= \frac{8M}{Na^3} \\ L_a &= 0.25a\sqrt{3} \\ L_b &= 0.25a\sqrt{2} \\ S &= \frac{0.94\lambda}{\beta cos\theta} \end{aligned}\right\} \qquad 6.1$$

Where d is spacing between the planes, (h,k,l) are the miller indices, M is molecular weight of the composition, N is Avogadro number, λ is wavelength of XRD, ‘θ’ is the Bragg’s angle and β is full width half maximum (FWHM) of (311) peak .

Table 6.1. Structural properties of the $CoFe_{1-x}Cr_xO_4$ (x= 0, 0.15, 0.3)

Compound (x)	Lattice constant a (A^O)	Density (g/cm^3)	Average Particle size (S) (nm) ~	L_a (A^O)	$L_b$$(A^O)$
0	8.3698	5.3186	54	3.6242	2.9591
0.15	8.3646	5.3117	43	3.6219	2.9573
0.3	8.3597	5.3079	35	3.6198	2.9556

From the table 6.1, it is observed that all the calculated parameters such as lattice constant a, x-ray density ρ_x, particle size S, tetrahedral and octahedral hoping length decreases with increase in mole percentage of chromium. Substitution of Cr^{3+} (0.615 Å), a smaller cation in place of Fe^{3+} (0.645 Å) having bigger ionic radius may be the possible cause of decrease in lattice constant. On the other hand, substitution of a heavier atom (Fe) by a lighter one (Cr) may reduce the x-ray density ρ_x as density of the formula unit decreases. Hoping length defines the distance between the magnetic ions and gives information regarding strength of spin interaction. The ionic radius difference between the impurity cations and the substituted cations may be the criteria for change in hoping length.

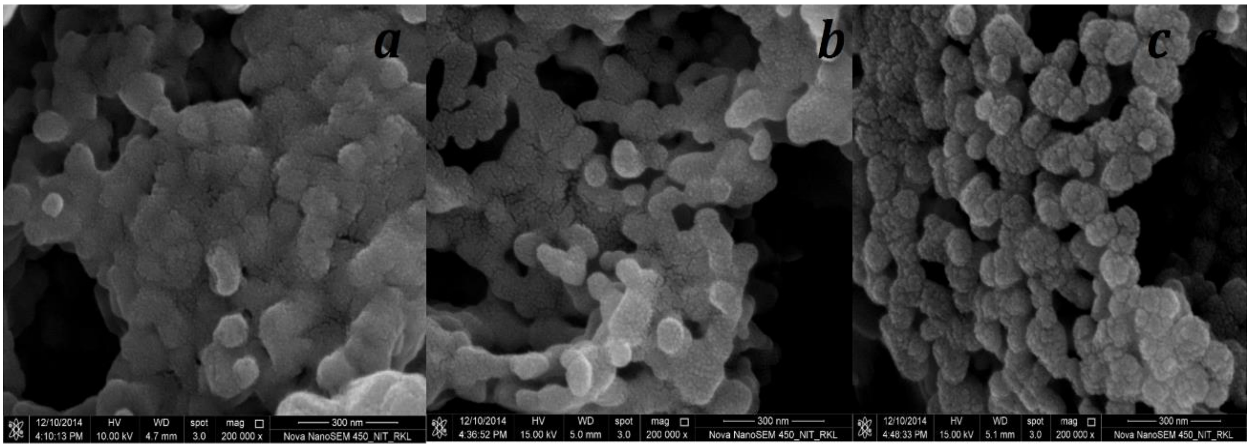

Fig 6.2. FESEM image of the $CoFe_{2-x}Cr_xO_4$ (x=0, 0.15-0.3)

Figure 6.2 shows the FESEM images of the prepared samples $CoFe_{2-x}Cr_xO_4$ (x= 0, 0.15, 0.3). The particles are found to be well distributed and agglomerated with spherical shape and the size decreases (~55 nm to ~35 nm) systematically with increase of Cr^{3+} content. It is reported that in case of a spinel ferrite, the particle size reduces when a chosen doping element has a strong site preference for which flexibility of substitution into the available sites reduces during the particle growth and that limits the nucleation process and size [29]. It has been an established fact that cobalt and chromium ions have a strong preference towards octahedral sites [22,29,30].

6.4. Magnetic properties

Room temperature Mossbauer spectra of $CoFe_{2-x}Cr_xO_4$ (x=0.1, 0.2, 0.3) nanoparticles recorded is shown in figure 6.3. The spectra exhibit two normal Zeeman spectrum which indicate that Fe^{3+} ion has occupied both the A- and B-site of spinel structure. The parameters derived from Mossbauer spectra such as (i) isomer shift, (ii) hyperfine field (iii) quadrupole splitting and (iv) line broadening provides information regarding occupancy of dopant, structure distortion, interaction among different cations etc. and we have discussed below the effect of Cr^{3+} substitution in cobalt ferrite nanoparticles.

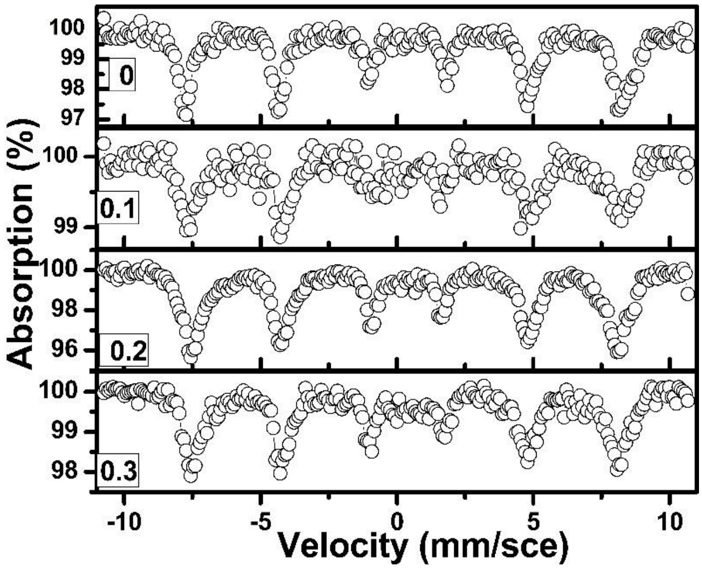

Fig 6.3. Transmission Mossbauer spectra of Cr substituted cobalt ferrite nanoparticles.

From the figure 6.4 it is observed that the value of isomer shift for B-site does not vary much with the addition of chromium. This indicates that charge distribution variation of Fe^{3+} remains unaffected by Cr^{3+} substitution in octahedral site. But the isomer shift for A-site shows a comparably variation and hence a possible change of charge distribution of Fe^{3+} may occurs in tetrahedral site. It is reported that Cr^{3+} has a strong octahedral site preference and hence not only substitutes Fe^{3+} in B-site rather, in effect, displaces Co^{2+} ion onto A-site [22].

The values of hyperfine field give two inferences: (i) the values of hyperfine field decrease with addition of Cr^{3+} content and (ii) the decrease in hyperfine field at B-site is faster than that of A-site. The first inference traces its root to reduction of Fe^{3+} ion at both sites. The second inference finds its cause in weakening of exchange interaction among A-B cations. Hyperfine field at nuclei is due to the super-transferred electron spin density. In other words, it represents the interaction among the magnetic cations [31]. The interaction between Fe^{3+}-O-Fe^{3+} is stronger than Cr^{3+}-O-Fe^{3+} because the magnetic moment of the Cr^{3+} (3 μ_B) is less than the Fe^{3+} magnetic moment (5 μ_B). The faster decrease in hyperfine field at B site can be explained on the basis of interactions involved at that site. The magnetic hyperfine field is related to the distortion in cubic symmetry as well as the nature of covalent bond at tetrahedral site [22,32]. There is no significant deviation of cubic symmetry and therefore, the net interaction among cations at tetrahedral site may be responsible. Two types of interactions A-B and B-B are prevalent at the B site. There is not a bigger change in hyperfine field of A-site and hence, the A-B interaction may not be a possible reason for faster reduction of hyperfine field of B-site. The next to nearest neighbor of B-site cation is another B-site cation. So the decrease in hyperfine field of B-site is due to the weakening of B-B interaction. The quadrupole shifting values are very near to the zero indicates Fe^{3+} is nearly cubic symmetry of the coordination of oxygen ions. The lattice strain arises due to the nano crystallinity of the material. This gives rise to an electric field gradient which contributes to quadrupole shift [32].

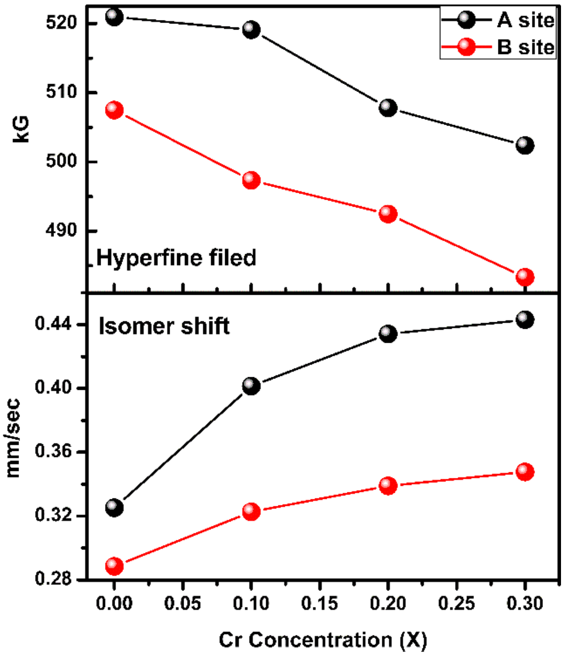

Fig 6.4 (a). Hyper field strength and isomer shift at A and B site as function of Cr content

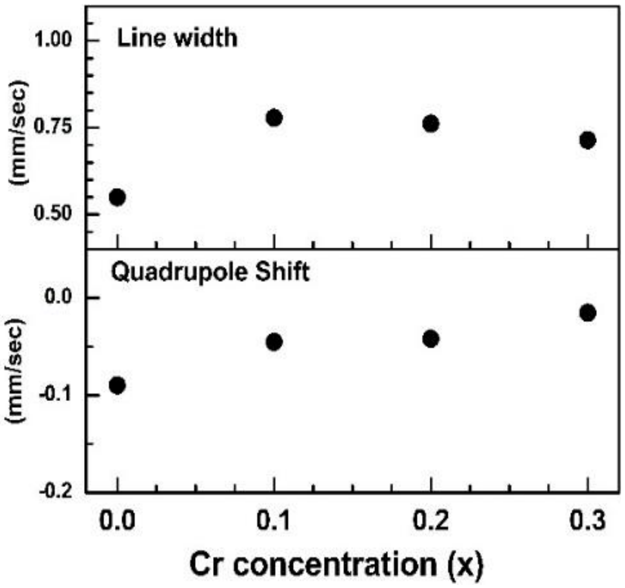

Fig 6.4 (b). Variation of line width and quadrupole shift with Cr content.

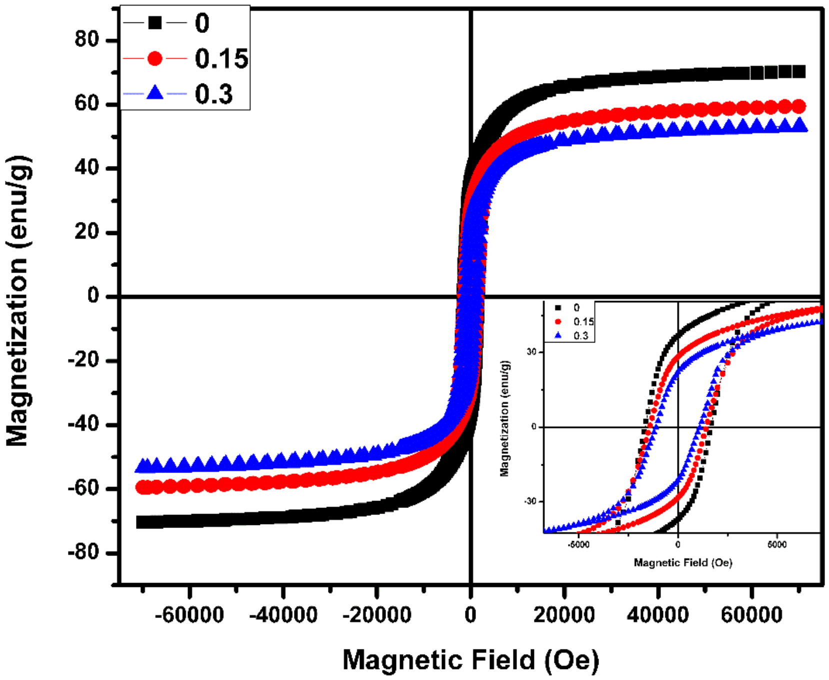

Fig 6.5. M-H loops of the Cr substituted cobalt ferrite nanoparticles.

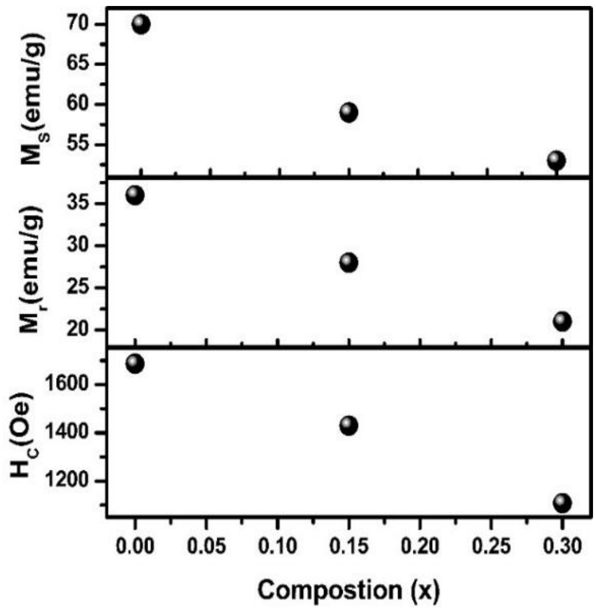

Fig 6.6. Effect of Cr on magnetic properties of the cobalt ferrite nanoparticles.

Figure 6.5 shows the room temperature M-H hysteresis loop of Cr substituted cobalt ferrite nanoparticles. The variation of saturation magnetization (M_S) and coercivity (H_C) with composition is shown in figure 6.6. Both the value of coercivity and saturation magnetization decreases with increase in Chromium content. The magnetic properties of the ferrites strongly depend on the particle size as well as cation distribution between the tetrahedral and octahedral sites [33].

Most of the literature on ferrite systems while studying magnetic properties has reported that the value of coercivity (H_C) increases and saturation magnetization (M_S) decreases with decrease in particle size [34-39]. The addition of chromium to CFO nano-system has reduced the particle size which varies further with dopant concentration. Though the effect of this reduced particle size matches with the results of saturation magnetization as a general behaviour but the results of coercivity goes contradictory by showing decreasing order. Similar results also reported by Toksha et al. on their work on Cr substituted cobalt ferrite system [40]. In addition, the similar effects on magnetic properties of Cr substitution in different spinel ferrite systems also have been reported [22-24]. It is supposed that the value of coercivity amounts to the magnetic field strength to overcome the potential barrier of anisotropy in order to shift the direction of magnetization with respect to external field [41]. This suggests that the lowering of the coercivity upon substitution of chromium might causes the reduction of the magnetization energy barriers and this may be due to magnetic coupling with a weaker magnetic moment of Cr^{3+} (3 μ_B). Mossbauer spectra of the samples reveal that the strength of interaction among the magnetic cations decreases with the Cr substitution. Even though Cr^{3+} possesses same number of unpaired electrons and theoretical orbital magnetic moment as Co^{2+} but the former produces weak L-S coupling compared to latter cation. Incorporation of Cr^{3+} in CFO system not only replaces Fe^{3+} at B-site but replace Co^{2+} onto A-site. This weakens the L-S coupling at B-site and hence less amount of magnetic field is required to change the magnetization direction. Additionally, this may happen that substitution of Cr^{3+} in parent compound has reduced the surface defects and anisotropy energy along with reduction in particle size [41]. The observed decrease in saturation magnetization and remnant magnetization can be explained by the increasing canting of magnetic dipoles due to the strong negative B-B exchange interaction as a result of replacing stronger magnetic moment of Fe^{3+} (5 μ_B) by weaker magnetic moment of Cr^{3+} (3 μ_B) . In order to support the above explanation, we have calculated the magnetic moment per formula unit in terms of Bohr magneton using the relation [33,42,43]

$$\eta_B = \frac{M \times M_S}{5585} \qquad 6.2$$

where M is molecular weight of the composition, M_s is the saturation magnetization. Magnetic moment per formula unit gradually decreases from 2.95-2.29 μ_B. This may be another reason for decreasing saturation magnetization with Cr^{3+} substitution.

6.5. Electrical properties

Figure 6.7 shows the dc resistivity vs. temperature for Cr substituted CFO nanoparticle. The value of resistivity marks a decreasing trend with increasing temperature and hence confirms the semiconducting nature of the systems. There are several reports which claim the semiconducting to metallic or metallic to semiconducting transition in cobalt ferrite system where particle size of nano scales strictly governs this transition mechanism [44,45]. Though in Cr substituted CFO nano systems, particle size reduces but no such transition behaviour is observed. Again with the increasing content of chromium the resistivity of the CFO nano systems also increases.

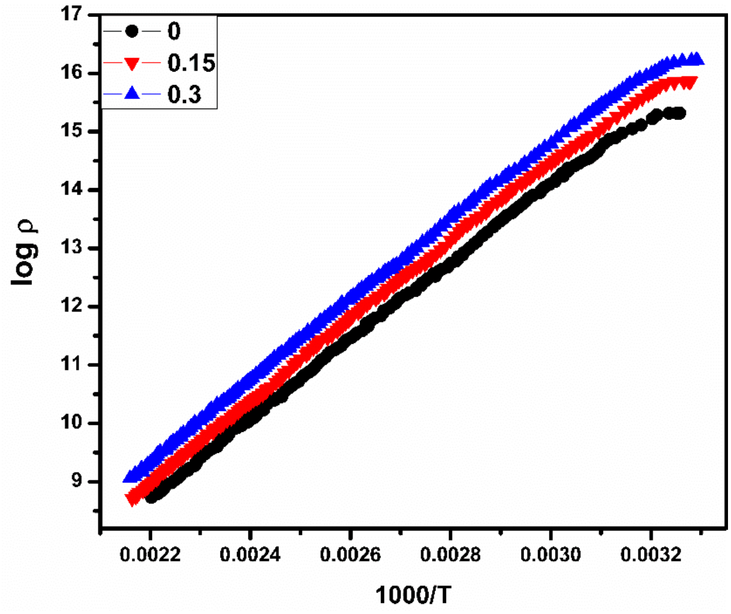

Fig 6.7. Temperature dependence of dc resistivity of $CoFe_{2-x}Cr_xO_4$ (x= 0, 0.15, 0.3)

In couple of the previous works on the substitution effect of Cr^{3+} on spinel ferrites, it is reported that the dc resistance increases with increase in chromium content [46,47]. In nano CFO system, Fe occupies both the tetrahedral as well as octahedral sites. In the present system, to substitute Fe by Cr, the probability for occupying both the sites holds for the dopant. But, it is already established that the Cr^{3+} occupies the octahedral sites as its most preferable place [22] and hence reduces the Fe^{+3} content in that site.

The conduction mechanism in ferrites is mostly governed by the electron and hole exchange among same cations having multi-oxidation states which are distributed randomly in the crystallographic sites. The hoping probability of charge carriers depends upon the separation of ions, activation energy and the temperature. In CFO system, the most prevalent conduction mechanism is due to electron exchange between Fe^{2+}-Fe^{3+} and additionally due to hopping of hole between Co^{3+}- Co^{2+} cations particularly in octahedral sites [48]. Therefore, the number of Fe ion in the octahedral site will determine the conductivity which ultimately reduces with the substitution of chromium and hence resistivity increases in the modified systems. Again it is a known fact that the electric and magnetic properties of ferrite are strongly dependent upon the particle size [46]. In ferrites, conducting grains are surrounded by grain boundaries which are insulating in nature. Previous reports claims that the increase in density of grain boundaries in ferrite system also increases the resistivity of the system[32]. From the XRD data and FESEM image it is confirmed that in Cr substituted CFO nano systems, particle size reduces with increase in Cr content and hence density of the insulating grain boundaries also increases. Therefore, resistivity of the modified CFO system also increases. We have also calculated the activation energy by fitting the temperature dependence dc resistivity data with the Arrhenius relation

$$\rho = \rho_o \exp(\frac{E_a}{k_B T}) \qquad 6.3$$

where ρ is resistivity, ρ_o is exponential constant, E_a is activation energy, k_B Boltzmann constant T is temperature in K. The activation energies for $CoFe_{2-x}Cr_xO_4$ are found to be 567 meV, 576 meV and 582 meV for x= 0, 0.15, 0.3 respectively. The activation energy values are comparable to the already reported values [44].

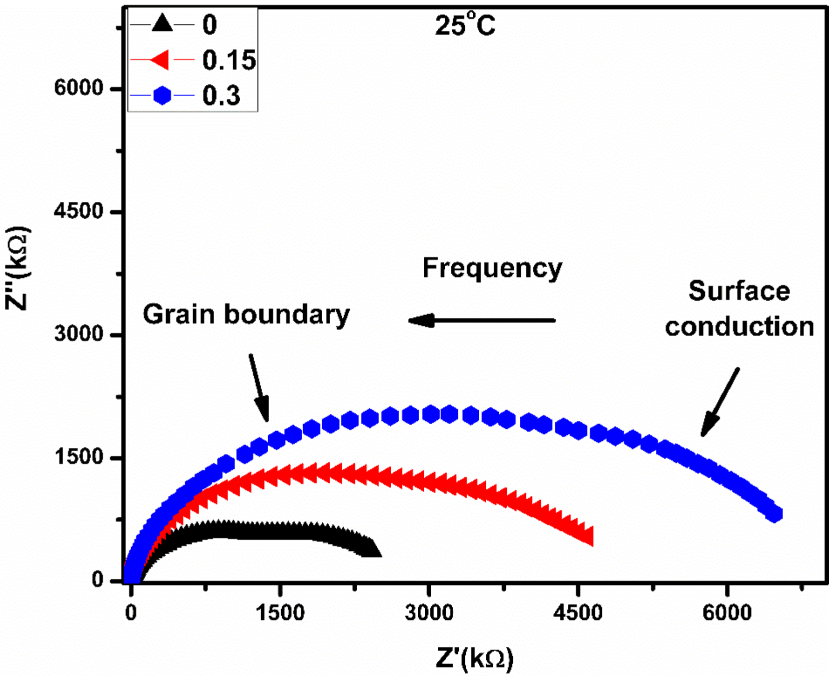

Fig 6.8 (a). Cole-Cole plots of $CoFe_{2-x}Cr_xO_4$ (x= 0, 0.15, 0.3)

The electrical properties of ferrites strongly depend on the microstructure, grain and grain boundary, defects, type of substitutional elements and amount of substitution [25]. Impedance spectroscopy is a good technique to investigate, analyze and differentiate the role of different microstructures in the conduction process as each region has their unique electrical response within the chosen frequency and temperature domain [49].

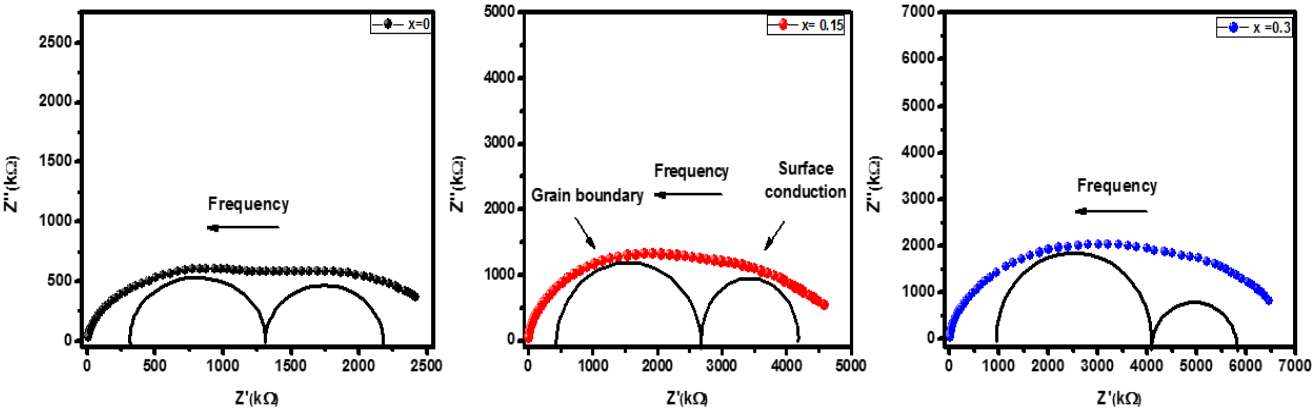

Fig 6.8 (b). Cole-Cole plots of CoFe$_{2-x}$Cr$_x$O$_4$ (x= 0, 0.15, 0.3)

Cole-Cole diagram plots real impedance (Z') against imaginary part of impedance (Z'') and the appearance of semicircles, their nature indicate the electrical relaxation corresponding to intrinsic (grain) conduction or extrinsic (interfacial) conduction. If three Cole-Cole semicircles appear within a chosen frequency and temperature domain then the one corresponds to higher frequency is identified as due to grain effect, the one corresponds to intermediate range belongs to grain boundary conduction and the semicircle at lower frequency regime attributes its appearance due to electrode surface conduction. For the center of the semicircle lying on the abscissa suggest for Debye type conduction and its radius measures the resistance of the material [50].

Figure 6.8 shows the Cole-Cole diagrams of the systems under study at RT. For CFO system, two semicircles of approximately equal radius appear in the plot. But with the substitution of chromium the semicircle at higher frequency end grows to bigger and that at lower frequency end reduces to smaller. The increase in radius of Cole-Cole semicircles indicates that the resistance of the material has increased which have already been confirmed from dc resistance study.

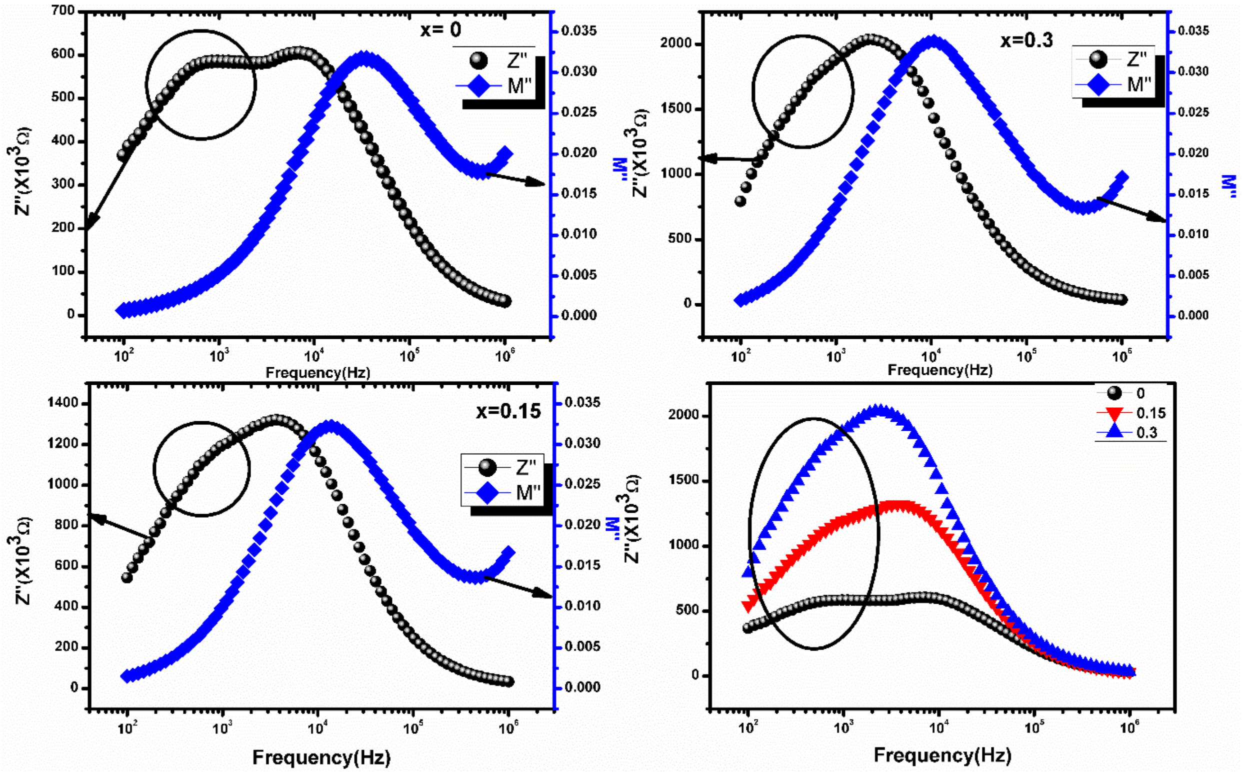

Figure 6.9. Combined plot of Z" and M" vs. frequency of $CoFe_{2-x}Cr_xO_4$ (x= 0, 0.15, 0.3) at room temperature. Surface conduction highlighted in the circle.

In order to identify the microstructures contributing to the distinct electrical relaxations, we have combined plot for the variation of imaginary part of impedance (Z") and the imaginary part of electric modulus (M") with frequency as is shown in Figure 6.9. Two relaxation peaks are clearly appeared in Z" in the parent CFO system at RT. It is observed that addition of chromium suppresses the lower frequency relaxation peak and the degree of suppression increases with the increase in chromium content. Again, it is noted that in M", the corresponding lower frequency relaxation peak also disappears. It is well known that M" inversely scales to capacitance and has the ability to suppress the conduction effect of highest capacitive region. Therefore, the lower frequency relaxation peak appears in Z" spectrum arises due to conduction of charge carriers in highest capacitive region and identified as due to the electrode surface contact effect [51]. In this respect we ascribe the appeared relaxation peak at higher frequency to grain boundary effect. In our previous report on cobalt ferrite nano particles we have already verified the absence of grain effect and dominant role of interfacial conduction process [25]. It is observed that the surface conduction is gradually suppressed with the addition of chromium and grain boundary conduction gradually dominates at RT.

The existing gap between the peak maximum of Z" and M" also increases with the increase in chromium content. This suggests that the effect of chromium substitution promotes localized motion of charge carriers over long range hopping and becomes more non-Debye type of conduction at RT [52]. We can assume that Cr^{+3} have effectively increased the grain boundary potential barrier for charge carriers which limits their escaping to surface for conduction. Iqbal et al. [53] have reported the increase in electrical resistance and decrease in dielectric constant because of the dominant B-B interaction over the A-B interaction due to rearrangement of the cations. The reports suggest that as particle size decreases B-B interaction becomes prominent over A-B interaction in ferrites [46,54]. This may be another reason for increment of resistance with Cr substitution.

Figure 6.10 shows the conductivity spectra of CFO and modified CFO systems at RT where we observe that the chromium substitution has reduced the conductivity. But to a large extent the nature of the plot matches each other. Figure 6.11 shows the conductivity spectrum of x= 0.3 Cr substituted CFO system at different temperatures. The plateau region expands with the elevation of temperature. The total conductivity is simulated properly to the Jonscher's power law is given as [55]

$$\sigma_t(\omega) = \sigma_{dc} + A\omega^n \qquad 6.4$$

Hence, it can explain the source of ac and dc conduction. A plateau region appears at low frequency side which is supposed to arise due to long range migration of charge carriers and contributes to dc conduction. This plateau region relaxes to a dispersive region at high frequency belt. The dispersive nature is moreover termed as ac conductivity and arises due to short range and localized hopping of charge carriers [55,56]. Here, σ_t (ω) is the total conductivity, σ_{dc} is the dc conductivity, $A\omega^n$ is frequency dependent conductivity also known as ac conductivity and ω is the frequency, 'n' (frequency exponent) and A is the temperature and material intrinsic property dependent constant.

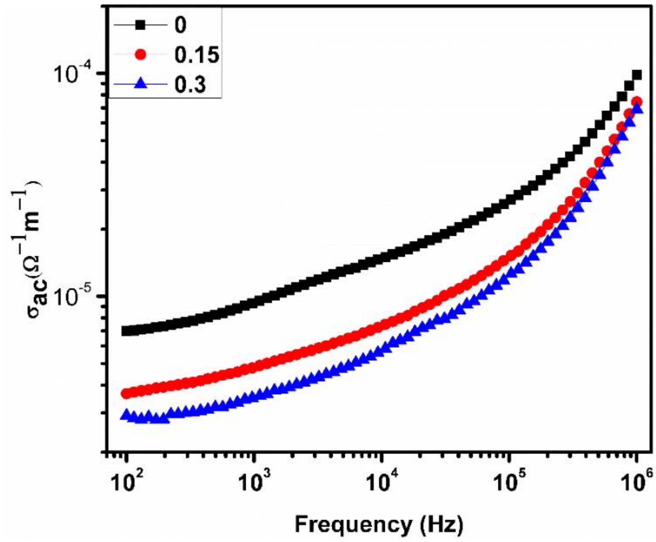

Fig 6.10. Frequency dependency of the ac conductivity of $CoFe_{2-x}Cr_xO_4$ (x = 0, 0.15, 0.3) at room temperature

It is established that in ferrites, the conductivity arises by a large extent due to the electron exchange interaction between Fe^{2+}- Fe^{3+} cations in the octahedral site. In cobalt ferrite system, additionally a minute contribution also comes from the hole hopping between Co^{2+} and Co^{3+} cations within octahedral site [57]. Therefore, the concentration of Fe cation plays an important role in determining the electrical properties of the ferrite systems. As it is already explained earlier that chromium as a dopant in place of iron substitutes the latter at octahedral sites for its preferable site. Therefore, reduction of electron exchange interaction between Fe^{2+}-Fe^{3+} drops the value of conductivity in the modified systems.

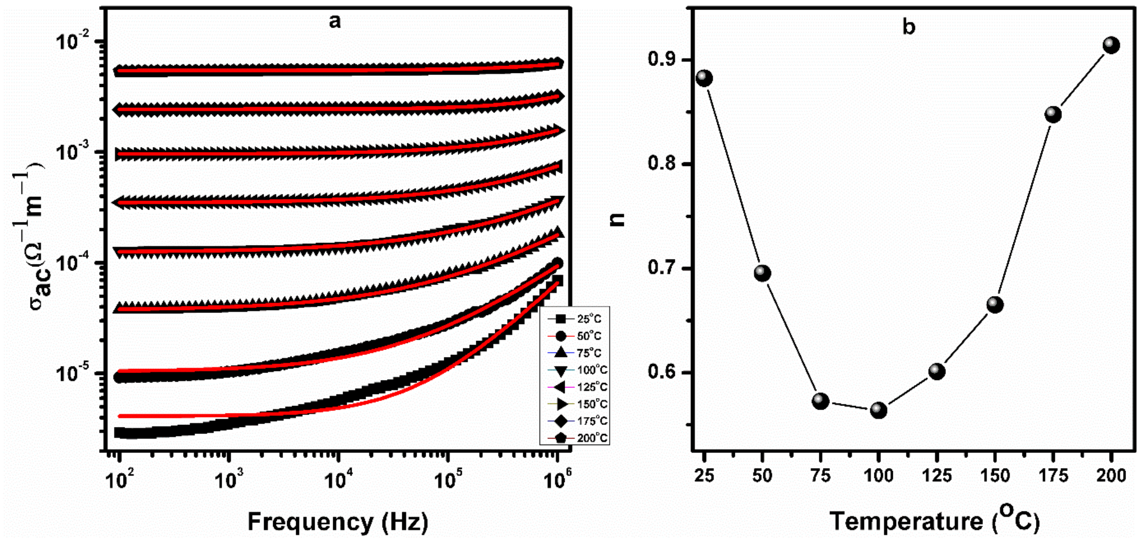

Fig 6.11. (a)Variation of ac conductivity with frequency at different temperature for substituted cobalt ferrite x = 0.3 and (b) variation of exponent with temperature at x = 0.3.

The variation of frequency exponent (n) with temperature is shown in figure 6.11. Initially it decreases with temperature, attains its minimum and thereafter increases with temperature. This behaviour suggests for overlapping large polaron tunneling (OLPT) type of conduction mechanism [25, 47]. The cations surrounded by close packed oxygen ions can be considered as isolated from each other due to minute overlap of the charge clouds which results the formation of the polarons and the charge transport may be considered between the nearest neighbors [57].

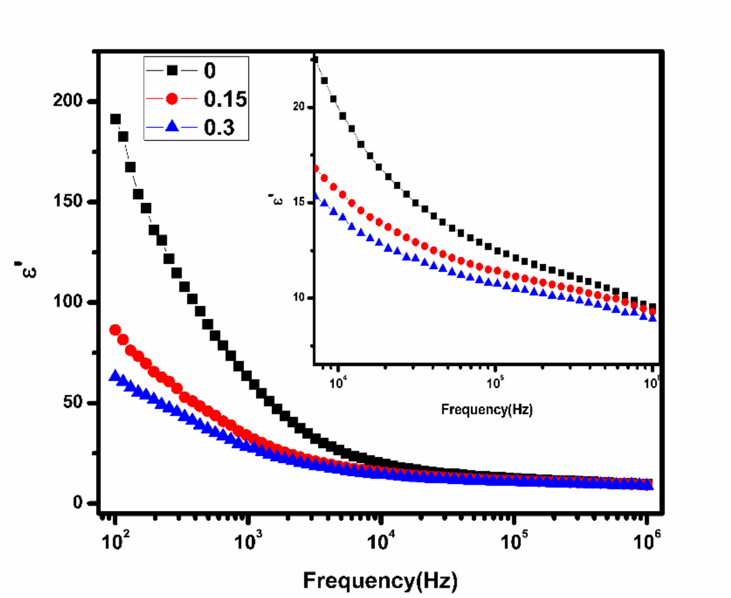

Fig 6.12. Frequency dependence of real permittivity of $CoFe_{2-x}Cr_xO_4$ (x= 0, 0.15, 0.3)

Figure 6.12 plots the variation of real permittivity with frequency at RT which shows two distinct regions: (a) a fast varying low frequency region of steep slope and (b) a slow varying high frequency region of mild slope. The real permittivity is the combined result of all sources of polarization like (i) space charge, (ii) dipolar, (iii) atomic/ionic and (iv) electronic polarization where the first two are temperature dependent and responds to low frequencies and last two are thermally independent and can respond to frequencies of all ranges [58].

It is observed that the low frequency permittivity value of the Cr substituted system has decreased a lot however, no significance difference is observed at high frequency regime. This clearly suggests that contribution from space charge/dipolar polarization has reduced. We have already verified that chromium substitution has suppressed the surface conduction effect i.e. has reduced the number of dipoles generated at surface. Though grain boundary effect grows more in modified systems but the capacitive effect of electrode surface is more prominent in grain boundaries. Therefore, the suppressed surface effect due to chromium substitution also may be the cause of reduced permittivity value in modified systems.

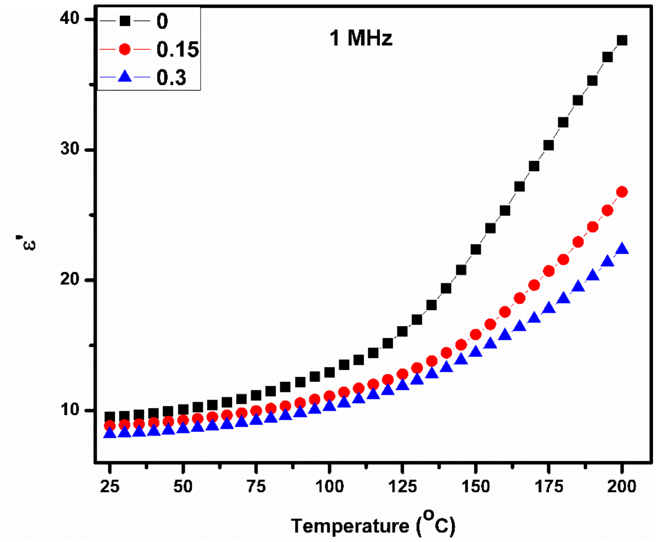

Fig 6.13. Temperature dependence of real permittivity of Cr substituted cobalt ferrite nanoparticles at 1 MHz.

We have also studied the temperature dependent relative permittivity plot as shown in Figure 6.13. The permittivity value gradually increases with increase in temperature and decreases with increase in chromium content. The permittivity of nano CFO system at high temperature shows a large difference from modified systems. At this temperature region the electrode surface effect of nano CFO system dominates the conduction process whereas that of the modified system has been suppressed to some extent due to chromium substitution. This confirms that the reduced dipole generation at electrode sample surface in the modified system is the factor behind the decrease in value of the relative permittivity.

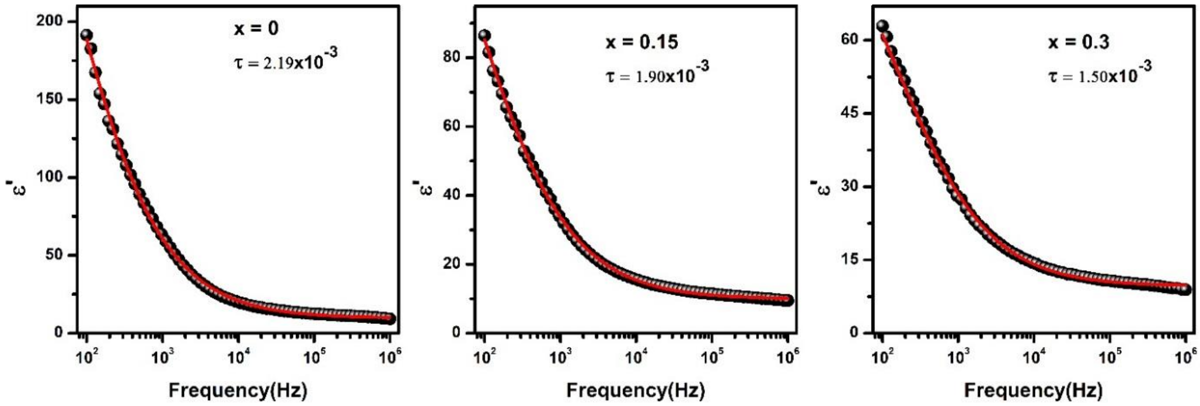

Fig 6.14. Simulation of the frequency dependent real permittivity of Cr substituted cobalt ferrite nanoparticles with the modified Debye law

The real part of relative permittivity is found to be well simulated to the modified Debye equation (shown in figure 6.14) and hence can explain the participation of more than one ions (Fe^{3+}, Co^{2+}, O^{2}) in the relaxation process accordingly [10].

$$\varepsilon' - \varepsilon_\infty = \frac{\varepsilon'_0 - \varepsilon'_\infty}{\left[1+(\omega\tau)^{2(1-\alpha)}\right]} \qquad 6.5$$

ε_o and ε_∞ re the dielectric constants at low frequency and high frequency respectively, $\omega = 2\pi f$ is frequency, τ is mean relaxation time and α is the spreading factor.

It is found that the mean relaxation time decreases with the Cr concentration. These results can be attributed to the existence of inertia to the charge movement which causes relaxation of polarization of charges [10]. This can be explained by considering the occurrence structural distortion due to modification. We found that the hopping length has decreased due to the addition of Cr^{3+} i.e. decrease in interatomic distance due to the smaller size of Cr^{3+} , which results in decrease of relaxation time.

Figure 6.15 exhibits the variation of dielectric loss with frequency and temperature. Dielectric loss represents the energy dissipation in a dielectric material. It develops on account of lagging behavior of polarization from the applied ac field due to impurities and imperfections in the crystal lattice of the materials [59]. With the increase in frequency and temperature the dielectric loss decreases and it increases respectively. Incorporation of chromium in the place of iron has been successful in reducing the dielectric loss as it is observed from the figure 6.15. Interfacial regions like the surface of material, grain boundaries contain more defects or imperfections comparably to intrinsic grain region. The suppression of surface conduction due to chromium addition in cobalt ferrite may reduce the dielectric loss overall in the spectrum.

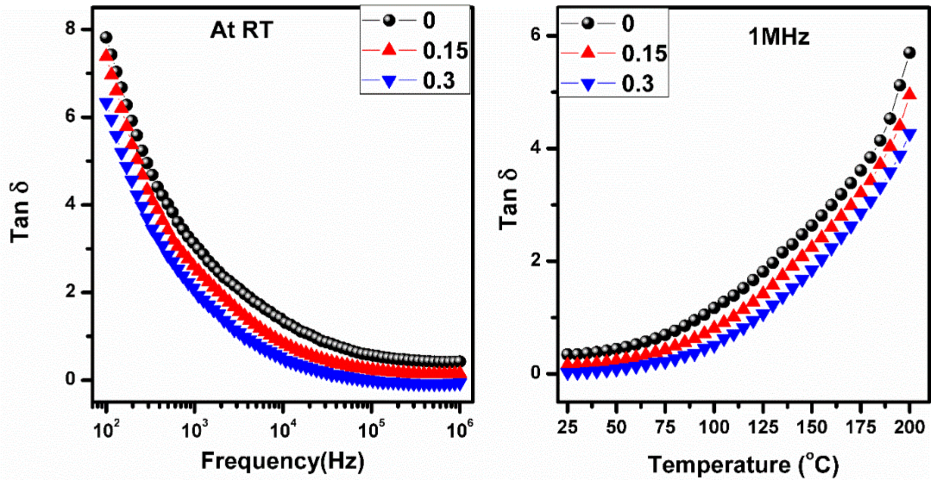

Fig 6.15. Frequency and temperature dependence of dielectric loss of $CoFe_{2-x}Cr_xO_4$ (x= 0, 0.15, 0.3)

6.6. Conclusions

Cr^{3+} substituted cobalt ferrite ($CoFe_{2-x}Cr_xO_4$, x = 0, 1.5, 3) nanoparticles were prepared by the auto combustion method. Average particle size was calculated from XRD and FESEM and reduction in particle size with chromium content was observed. Fe^{3+} was replaced at B-site (octahedral) by the dopant that weakened the magnetic interaction among cations and which caused decrease in saturation magnetization. The reduced surface anisotropy potential and particle size was found responsible for decrease in coercivity. The modification has resulted in increase in material resistivity and electrode-sample surface conduction was suppressed to a large extent. Ac conductivity analysis revealed that the OLPT mechanism takes place in Cr substituted cobalt ferrite nanoparticles.

References

[1] Y. Cedeno-Mattei, O. Perales-Pérez, O. N. C. Uwakweh, and Y. Xin, J. Appl. Phys. 107 (2010) 09A741.

[2] K. Khaja Mohaideen and P. A. Joy, Appl. Phys. Let. 101 (2012) 072405.

[3] A.B. Salunkhe, V.M. Khot, M.R. Phadatare, S.H. Pawar, J. Alloys Compd. 514 (2012) 91-96.

[4] Sateesh Prathapani, M. Vinitha, T. V. Jayaraman, and D. Das, J. Appl. Phys.115 (2014) 17A502.

[5] W. Chen, W. Zhu, O. K. Tan, and X. F. Chen, J. Appl. Phys.108 (2010) 034101.

[6] J. A. Moyer, C. A. F. Vaz, D. P. Kumah, D. A. Arena, and V. E. Henrich, Physical Review B 86 (2012) 174404.

[7] Diego Gutierrez, Michael Foerster, Ignasi Fina, and Josep Fontcuberta, Physical Review B 86 (2012) 125309.

[8] S. Soliman, A. Elfalaky, Gerhard H. Fecher, and Claudia Felser, Physical review B 83 (2011) 085205.

[9] N. Ponpandian and A. Narayanasamy, J. Appl. Phys.92 (2002) 2770.

[10] K. Kamala Bharathi, G. Markandeyulu, and C. V. Ramana, J. Phys. Chem. C 115 (2011) 554.

[11] K. Kamala Bharathi and C.V. Ramana, J. Mater. Research 26 (2011) 584591.

[12] A. Ar unk umar, D. Vanidha, K. Oudayakumar, S. Rajagopan,3 and R. Kannan, J. Appl. Phys.114 (2013) 183905.

[13] M. J. Iqbal, Z. Ahmad, T. Meydan, and Y. Melikhov, J. Appl. Phys.111 (2012) 033906.

[14] A. Franco Jr.,F. C. e Silva and Vivien S. Zapf, J. Appl. Phys.111 (2012) 07B530.

[15] Jeong Hyun Shim, Soonchil Lee, Jung Hye Park, Seung-Jin Han, Y. H. Jeong and Young Whan Cho, Physical Review B 73 (2006) 064404.

[16] S. J. Stewart, S. J. A. Figueroa, J. M. Ramallo López, S. G. Marchetti, J. F. Bengoa, R. J. Prado and F. G. Requejo, Physical Review B 75 (2007) 073408.

[17] I. C. Nlebed im, Y. Melikhov and D. C. Jiles, J. Appl. Phys.115 (2014) 043903.

[18] M. Atif, R. Sato Turtelli, R. Grossinger, and F. Kubel, J. Appl. Phys.113 (2013) 153902.

[19] K. Kamala Bharathi, K. Balamurugan, P. N. Santhosh, M. Pattabiraman, and G. Markandeyulu, Physical Review B 77 (2008) 172401.

[20] Ulrike Lüders, Manuel Bibes, Jean-François Bobo, Matteo Cantoni, Riccardo Bertacco, and Josep Fontcuberta, Physical Review B 71 (2005) 134419.

[21] T. Dhakal, D. Mukherjee, R. Hyde, P. Mukherjee, M. H. Phan, H. Srikanth, and S. Witanachchi, J. Appl. Phys. 107 (2010) 053914.

[22] K. Krieble, C. C. H. Lo, Y. Melikhov, and J. E. Snyder, J. Appl. Phys.99 (2006), 08M912.

[23] S. J. Leea, C. C. H. Lo, P. N. Matlage, S. H. Song, Y. Melikhov, J. E. Snyder, and D. C. Jiles, J. Appl. Phys. 102 (2007) 073910.

[24] Y.Melikhov, J.E.Synder, C.C.H Lo, P.N.Matlage, S.H.Song, K.W.Dennis and DC Jiles, IEEE Transact. Magnetics 42 (2006) 2861-2862.

[25] R.K. Panda, R. Muduli, S.K. Kar and D. Behera, J. Alloys.Compd. 615 (2014) 899.

[26] M. Chakrabarti, D. Sanyal and A. Chakrabarti, J. Phys.: Condens. Matter 19 (2007) 19 236210.

[27] E. V. Meerwall, Comp. Phys. Commun.9 (1975) 117.

[28] Dipali S. Nikam, Swati V. Jadhav, Vishwajeet M. Khot, R. A. Bohara, Chang K. Hong,Sawanta S. Malib and S. H. Pawar, RSC Adv.5 (2015) 2338.

[29] Ram Kripal Sharma, Varkey Sebastian, N. Lakshmi, K. Venugopalan, V. Raghavendra Reddy and Ajay Gupta, Physical review B 75 (2007) 144419.

[30] Carlos Fernan des, Clara Pereira, Marıa Paz Fernandez-Garcia, Andre M. Pereira, Alexandra Guedes, Rodrigo Fernandez-Pacheco, Alfonso Ibarra, M. Ricardo Ibarra,e Joao P. Araujo and Cristina Freire, J. Mater. Chem. C 2 (2014) 5818.

[31] G. A. Petitt and D. W. Forester, Phys. Rev. B 4 (1971) 3912.

[32] S. M. Patange, Sagar E. Shirsath, B. G. Toksha, S. S. Jadhav, and K. M. Jadhav, J. Appl. Phys. 106 (2009) 023914.

[33] R.K. Panda, R. Muduli, D. Behera, J. Alloys Compd. 634 (2015) 239.

[34] K. Maaza, Arif Mumtaza, S.K. Hasanaina, Abdullah Ceylan, J. Magn. Magn. Mater., 308 (2007) 289.

[35] Michal Sedlacik, Vladimir Pavlinek, Petra Peerd, Petr Filip, Dalton Trans.43 (2014) 6919.

[36] Yuqiu Qu, Haibin Yang, Nan Yang, Yuzun Fan, Hongyang Zhu, Guangtian Zou, Mater. Lett.60 (2006) 3548.

[37] R.H. Kodama, A.E. Berkowitz, Phys. Rev. Lett. 77 (1996) 394.

[38] Yue Zhang, Yong Liu, Chunlong Fei, Zhi Yang, Lu Zhihong, Rui Xiong, Di. Yin, Jing Shi, J. Appl. Phys., 108 (2010) 084312.

[39] C. Vazquez-Vazquez, M.A. Lopez-Quintela, M.C. Bujan-Nunez, J. Rivas, J.Nanopart. Res. 13 (2011)1663.

[40] B. G. Toksha, Sagar E. Shirsath, M. L. Mane, S. M. Patange, S. S. Jadhav, and K. M. Jadhav, J. Phys. Chem. C 115 (2011) 20905.

[41] Man Han, Christy R. Vestal, and Z. John Zhang, J. Phys. Chem. B 108 (2004) 583.

[42] R.C. Kambale, P.A. Shaikh, S.S. Kamble, Y.D. Kolekar, J. Alloys Comp. 478 (2009) 599.

[43] Sonal Singhala, Kailash Chandra, J. Solid State Chem.180 (2007) 296.

[44] A. Arunkumar, D. Vanidha, K. Oudayakumar, S. Rajagopan, and R. Kannan, J. Appl. Phys.114 (2013) 183905.

[45] Atta ur Rahman, M A Rafiq, S Karim, K Maaz, M Siddique and M M Hasan, J. Phys. D: Appl. Phys.44 (2011) 165404.

[46] P.P. Hankare , U.B. Sankpal , R.P. Patil , I.S. Mulla , P.D. Lokhande , N.S. Gajbhiye, J. Alloys Compd.485 (2009) 798.

[47] M J Iqbal and M R Siddiquah, J. Alloys Compd. 453 (2008) 513.

[48] C. V. Ramana, Y. D. Kolekar, K. Kamala Bharathi, B. Sinha, and K. Ghosh, J. Appl. Phys.114 (2013) 183907.

[49] M Idrees, M Nadeem and M M Hassan, J. Phys. D: Appl. Phys.43 (2010) 155401.

[50] R.K. Panda, D. Behera, J. Alloys Compd. 587 (2014) 481–486.

[51] H Mahamoud, B Louati, F Hlel and K Guidara, Ionics 17 (2011) 223.

[52] Jiagang Wu, John Wang, Dingquan Xiao and Jianguo Zhu, J. Appl. Phys.110 (2011) 064104.

[53] M. J. Iqbal, Z. Ahmad, T. Meydan, and Y. Melikhov, J. Appl. Phys.111 (2012) 033906.

[54] R. Kannan, S. Rajagopan, A. Arunkumar, D. Vanidha, and R. Murugaraj, J. Appl. Phys.112 (2012) 063926.

[55] N. Ortega, Ashok Kumar, P. Bhattacharya, S.B. Majumder, R.S. Katiyar, Phys. Rev. B 77 (2008) 014111.

[56] W. Chen, W. Zhu, O.K. Tan, X.F. Chen, J. Appl. Phys.108 (2012) 034101.

[57] M Younas, M Atif, M Nadeem, M Siddique, M Idrees and R Grossinger, J. Phys. D: Appl. Phys.44 (2011) 345402.

[58] N. Sivakumar, A. Narayanasamy, N. Ponpandian, and G. Govindaraj, J. Appl. Phys., 101 (2007) 084116.

[59] Y. D. Kolekar, L. J. Sanchez, and C. V. Ramana, J. Appl. Phys.115 (2014) 144106.

Conclusions

The electric and magnetic properties of bulk and nano cobalt ferrite and its modified systems have been investigated and the results have been analyzed. It is observed that the accompanied modifications are capable to control the electric and magnetic properties over a wide range. Some important observations of the research work are discussed below.

1) In bulk cobalt ferrite, grain effects found to be dominated at low temperature whereas interfacial polarization played important role in conduction mechanism at high temperature which witnessed the inter-competition between grain boundary and electrode effect within frequency windows.
2) The non-Debye type of relaxation behavior is confirmed from the stretched exponent parameter β value which is far away from unity, calculated from imaginary electric modulus spectra.
3) The space charge polarization near interfaces is responsible for dielectric behavior of CFO system. Apart from electron exchange interaction in Fe^{2+} - Fe^{3+}, the inverse spinel favours a conduction mechanism $Co^{2+}+Fe^{3+} \leftrightarrow Co^{3+}+ Fe^{2+}$ in which long range order of charge movement happens at high temperature belt at intermediate frequency regime along with short range hopping and localized relaxation hopping mechanism at high frequency.
4) Room temperature M-H loop indicates the orderedness of the ferrimagnetic cobalt ferrite. Temperature dependence of the magnetization exhibits maxima at 70^0 C due to its ferrimagnetic nature.
5) In cobalt ferrite nanoparticles, grain boundary conduction and surface polarization were the major contributors to its conductivity and dielectric properties.
6) OLPT type of conduction was responsible for ac conduction process as was confirmed from variation of frequency exponent ‘n’ with temperature.
7) Electron and hole exchange among Fe^{2+}- Fe^{3+} and Co^{3+}- Co^{2+} were found to be major contributor to dielectric constant value.
8) Room temperature M-H loop of cobalt ferrite nanoparticles indicates its ordered state and showed lower saturation magnetization value and higher coercivity compared to the bulk cobalt ferrite.
9) Single phase bismuth substituted cobalt ferrite nanoparticles were synthesized by auto combustion technique.
10) Controlled particle growth was observed in FESEM image with substitution of Bi^{3+}.

11) Sufficient rise in resistance, evolution of grain effect, along with successfully suppressed the unwanted surface conduction as well as lowered the dielectric loss at lower frequency regime were the prominent observations in Bi substituted cobalt ferrite nanopartilces.
12) There was enhancement in saturation magnetization and reduction in coercivity in bismuth substituted cobalt ferrite nanoparticles.
13) Cr^{3+} substituted cobalt ferrite ($CoFe_{2-x}Cr_xO_4$, x = 0, 1.5, 3) nanoparticles were prepared by the auto combustion method. Average particle size was calculated from XRD and FESEM and was observed reduction in particle size with chromium content.
14) Fe^{3+} was replaced at B-site (octahedral) by the Cr^{3+} that weakened the magnetic interaction among cations and which caused decrease in saturation magnetization. The reduced surface anisotropy potential and particle size was found responsible for decrease in coercivity.
15) The modification has resulted in increase in material resistivity and electrode-sample surface conduction was suppressed to a large extent. Ac conductivity analysis revealed that the OLPT mechanism takes place in Cr substituted cobalt ferrite nanoparticles.
16) K_2CrO_4 modified cobalt ferrite nanoparticles prepared by the auto combustion technique and due to the modification particle size was significantly reduced.
17) Unlike parent cobalt ferrite which behaves as semiconductor, modified cobalt ferrite nanoparticles exhibited metal to semiconducting transition. This transition due to the domination of direct cation-cation interaction than indirect cation-onion-cation interaction and the grain conduction was active at metallic region.

Future work

In this present work we have studied the electric and magnetic properties of bulk and nano system of cobalt ferrite and modified cobalt ferrite nanoparticles. Bulk cobalt ferrite prepared by the solid state method and cobalt ferrite nanoparticles synthesized by auto combustion method. Modified systems examined only in nano form in the same way these can be examined in bulk form and observe changes in electric and magnetic properties. The microstructural analysis using Transmission Electron Microscopy (TEM) will give better understanding about the particle size and structural analysis. Neutron diffraction would be the good source for understanding the spin structure. X-ray Magnetic Circular Dichroism (XMCD) examination needed to interpret the occupation of the ions in A and B sites and it would be helpful to understand the origin of magnetic properties.

List of publications

1) **R.K. Panda**, R. Muduli and D. Behera, Electric and magnetic properties of Bi substituted cobalt ferrite nanoparticles: Evolution of grain effect, Journal of Alloys and Compounds 634 (2015) 239–245.
2) **R.K. Panda**, R. Muduli, S.K.Kar and D. Behera, Dielectric relaxation and conduction mechanism of cobalt ferrite Nanoparticles, Journal of Alloys and Compounds 615 (2015) 899–905.
3) **R.K. Panda** and D. Behera, Investigation of electric transport behavior of bulk $CoFe_2O_4$ by complex impedance spectroscopy, Journal of Alloys and Compounds 587 (2014) 481–486.
4) R.Muduli, R.Pattanayak, S.Kumar, S.K.Kar, P.Kumar, S.Panigrahi, **R.K.Panda,** Journal of Alloys and Compounds 656 (2016) 33-44.
5) R.Muduli, R. Pattanayak, S.Raut, P.Sahu, Senthil.V, S.Rath, P.Kumar, S.Panigrahi, **R.K.Panda,** Journal of Alloys and Compounds 664 (2016) 715-725.
6) R.Pattanayak, R.Muduli, **R.K.Panda**, T.Dash, P.Sahu, S.Raut, S. Panigrahi, Physica B: Condensed Matter 485 (2016) 67-77.
7) A. Kujur, M. Sahoo, **R.K. Panda**, K. Asokan, D. Behera, The effect of 200 MeV swift heavy Ag ions on the transport property of $YBa_2Cu_3O_{7-\delta}$ thick films, Physica C: Superconductivity 492 (2013)168-173.
8) **R.K. Panda** and D. Behera, High Temperature Conductivity Study of Cobalt Ferrite, Advance Science Letters 20(2014) 683-685.
9) **R.K. Panda,** R. Muduli, D. Sanyal, D. Behera, Effect of Cr^{3+} substitution on electric and magnetic properties of cobalt ferrite nanoparticles. (Under review)

Conferences/Workshops/Seminars/Short Term Courses:

1) **R. K. Panda** and D. Behera, effect of Cr substitution on structural and magnetic properties cobalt ferrite nanoparticles, Indo-Japan conference on Nano magnetism, NISER Bhubaneswar 2015.
2) **R. K. Panda** and D. Behera, Effect of Cr substitution on structural, electrical and magnetic properties of cobalt ferrite nanoparticles, Research scholar week -2015, NIT Rourkela.
3) **R. K. Panda**, T.N. Giri and D. Behera, studies on dielectric relaxation behavior of cobalt ferrite, CMDAYS- 2013, 29-31 August 2013. NIT Rourkela.
4) **R. K. Panda** and D. Behera, synthesis and characterization high energy ball milled cobalt ferrite nanoparticles CMDAYS- 2012. BIT Mesra.
5) Awareness workshop on the facilities of UGC-DAE consortium for scientific research, march-2012, Utkal University Bhubaneswar.

Curriculum vitae

Ranjit Kumar Panda

Research Scholar

Department of physics and Astronomy

NIT Rourkela

Odisha

Email: physics.panda@gmail.com

Education

10th class, Board of Secondary Education, Andhra Pradesh	2001
78.5%, 1st class	
12th class, Board of Intermediate Education, Andhra Pradesh	2003
84.5%, 1st class	
Bachelor of Science in Physics, Andhra university, Andhra Pradesh,	2006
67%, 1st class	
Master of Science in Physics, Andhra university, Andhra Pradesh,	2008
68.8%, 1st class	
Master of Technology in Metallurgical and Material Engineering,	2011
NIT Rourkela, Odisha	
8.33 CGPA, 1st class	
Research Scholar and pursuing Ph.D.	2011-
Department of Physics and Astronomy	
NIT Rourkela	